Multimodal interrogation of cell type-specific transcriptional states and brain-wide activity profiles in maladaptive opioid use

Cassidy T. Burke

A dissertation

submitted in partial fulfillment of

the requirements for the degree of

Doctor of Philosophy

University of Washington

2026

Reading Committee:

Garret Stuber, Chair

Susan Ferguson

John Neumaier

Program Authorized to Grant Degree:

Neuroscience

University of Washington

Abstract

Multimodal interrogation of cell type-specific transcriptional states and brain-wide activity profiles in maladaptive opioid use

Cassidy T. Burke

Chair of the Supervisory Committee:

Garret Stuber

Departments of Anesthesiology and Pain Medicine, Pharmacology

Opioid use disorder is thought to arise from persistently dysregulated neural activity in brain regions associated with reward and motivation, but the precise molecular and circuit mechanisms underlying individual differences in susceptibility to escalated opioid use are not well understood. To address this gap, we have utilized a rat model of IV heroin self-administration in which rats display robust individual differences in self-administration. Multiple addiction metrics are collected throughout the paradigm and used to generate an addiction risk profile for each rat, which can then be classified as high or low risk. We compared brain-wide cFOS between rats with varying addiction risk histories, with and without re-exposure to a drug-paired cue, demonstrating brain-wide neural activity differences between high and low addiction risk rats after cued reinstatement. Using a generalized linear model, we tested for significant relationships between addiction metrics and cFOS z-scores in each brain region, revealing specific signatures of neural activity associated with unique behavioral patterns. High addiction risk rats were additionally found to be uniquely characterized by

a loss of correlated cFOS z-scores in cortical and parahippocampal brain regions during protracted withdrawal from heroin.

A central node in opioid addiction circuitry is the nucleus accumbens (NAc), which integrates glutamatergic input from diverse brain regions with dopaminergic input from the ventral tegmental area. To characterize the transcriptional state of neurons throughout this circuit, we conducted snRNAseq in prelimbic cortex (PL), NAc, and VP after self-administration and protracted withdrawal. We hypothesized that subsets of NAc medium spiny neurons (MSNs) would be significantly perturbed in rats with high addiction risk behaviors, while PL neurons were expected to display more uniform changes. Nuclei isolation and library prep were conducted using 10X Genomics Next GEM pipeline, and data analysis was completed using the R package Seurat. Data was integrated with high-quality mouse scRNAseq datasets to facilitate identification of shared and distinct neuronal subtypes for each brain region, producing an atlas of known and novel cell types. Analysis of each neuronal subtype revealed significant transcriptional alterations in multiple NAc D1 and D2 expressing MSN sub-clusters, as well as L2/3 and L4/5 IT neurons in PL, including a conserved response in genes associated with postsynaptic densities across these distinct cell types. In contrast, VP neurons were largely unchanged by heroin exposure, despite high expression of the μ-opioid receptor in VP. WGCNA analysis revealed neuronal subtype-specific modules of gene expression with differential expression by heroin addiction risk group and highlighted the importance of the metabotropic glutamate receptor mGluR5 in delineating high and low addiction risk gene expression patterns in all three brain regions. Using an intersectional CRISPR/Cas9 viral strategy, we knocked out mGluR5 from D1 MSNs in the NAc, which are known to alter their activity in acute opioid reward and during opioid withdrawal. Grm5 KO rats were less likely to engage in escalated opioid intake if they were classified as low risk before this intervention, and displayed signs of stabilization in their addiction risk phenotype if they were previously categorized

as high risk. In summary, we observed a brain-wide signature of altered neuronal activity in high-risk rats, as well as cell-type specific loss of correlated gene expression in PL and NAc. We hypothesize that the bidirectional changes detected in Grm5 (upregulated in PL, downregulated in NAc) may represent a protective homeostatic change induced after escalated opioid intake, accompanied by an opioid-use induced decline in NAc glutamatergic tone from higher-order cortical regions. Eliminating mGluR5 from D1 MSNs was sufficient to attenuate heroin escalation in both low-risk and high-risk rats. Thus, using a multi-modal approach, we have expanded our knowledge of the brain regions, circuits, and cell types that become dysregulated after escalated opioid use, and specifically identified a subtype of metabotropic glutamate receptor in the NAc as an important player in the regulation of neural plasticity across cycles of opioid use, abstinence, and relapse.

Table of Contents:

Acknowledgements

First, I would like to thank my scientific mentors. I was very fortunate to stumble into Ed Perez-Reyes's lab at the University of Virginia as an undergraduate, where I received extraordinary training in adeno-associated viral vector design, production, and utilization for mapping of hyperactive epileptic circuits. This experience led me to seek out an environment where I could combine my interests in genetic characterization of neuronal function with rigorous training in systems neuroscience: thus, I was thrilled to get the opportunity to join the Stuber lab for my graduate studies. Over the past four years, I have greatly benefited from Garret's strong passion for science, commitment to excellence, and impressive ability to remain unfazed by obstacles. I have also been supported, motivated, and encouraged by my fellow lab members, whose expertise and insight were essential to completing much of the work described here.

For as long as I can remember, my family's greatest priority has been to ensure that I can access the best possible education. Any milestone that I attain is a direct result of my parents' tireless hard work over many years. I am extremely grateful to them for their unwavering support and patience as I slowly work towards my goals. I would also like to thank my younger brother William, whose experience originally motivated me to pursue a career bridging basic neuroscience and clinical practice, and who has grown up to become the most resilient and compassionate person I know. This dissertation is dedicated to Bill, Sonya, and William Burke.

Introduction

Section I: On pain and pain-relief

In the natural world, pain has a vital role in shaping animal behavior to avoid circumstances which may lead to tissue damage and death. The utility and necessity of pain is obvious when considering the diverse dangers each animal may encounter throughout its life. Neural mechanisms underlying this process have been largely elucidated: nociceptive signals from peripheral sensory nerves are relayed to the brainstem and diverge into higher-order structures (somatosensory cortex, amygdala, insula), which integrate the pain signal within the larger environmental context. The general consequence of acute pain is initiation of movement away from the noxious stimulus, whether via a simple spinal reflex or a coordinated attempt to flee a dangerous environment for a safer one. Repeated or inescapable pain stimuli can lead to complete behavioral arrest, a state of mixed value while calculating odds of physical recovery and ultimate survival. A hypo-locomotive, injured mouse may benefit from a period of rest, but it also makes an easy target for an observant predator.

This hypothetical mouse has two conflicting evolutionary imperatives: first, to allow the injury to heal and avoid further damage, and second, not to be eaten. Thus, a system to temporarily oppose the aversive effects of pain is now required. The release of endogenous μ-opioid agonists (ex. enkephalin), in concert with faster-acting complementary neuromodulators in specific brain regions (ex. norepinephrine, dopamine) enables the mouse to briefly disregard the nociceptive input and engage in vigorous movement to run away from the circling hawk. A precise homeostatic balance of pain and pain-relief neural processes is crucial: too much pain, and the mouse is unable to move, but too much pain-relief can lead to additional injury and disrupt the encoding of pain-generating stimuli into memory.

The latter situation was near-impossible for most animals to achieve, until around 3,400 B.C.E., when Sumerians in Mesopotamia began cultivating the opium poppy.[1] In ancient Greece, the utility of opium as a painkiller and "sleep" inducer was well known to early physicians, as was the danger of drug tolerance, dependance, and overdose.[1] Despite the substantial risks associated with exogenous opioids, they have proved irresistible to physicians and patients alike for thousands of years. In 1915, a Johns Hopkins clinical instructor laid out the views of the medical establishment in JAMA: "If the entire materia medica at our disposal were limited to the choice and use of only one drug, I am sure that a great many, if not the majority, of us were choose opium; and I am convinced that if we were to select…half a dozen of the most important drugs in the Pharmacopeia, we should all place opium in the first rank."[2] Over a hundred years later, more modern tools have so far failed to supplant opioids, particularly when treating severe and intractable pain.

In humans, physical pain rarely occurs without some induction of emotional pain. Conversely, stress alone can be sufficient to induce hyperalgesia, particularly in those with a history of adverse experiences in early life.[3] From individual to individual, significant variability has been observed in both susceptibility to both the rewarding effects of opioids and to the potentially-aversive physical side effects of acute opioid intoxication (ex. nausea.)[4] As a result, the total population of people with opioid dependance represents a convergence of several groups: those with physical pain, those hoping to self-medicate emotional pain, distress, or anxiety, and those taking opioids recreationally for pleasure. All three groups have substantial degrees of overlap, and people in the "all of the above" category are likely most at risk for developing clinical opioid use disorder (OUD). A so-called "self-medication hypothesis" suggests that many cases of substance use disorder more closely resemble attempts to manage comorbid depression or anxiety conditions than uncontrolled instances of impulsive reward-seeking behavior.[5,6] OUD is distinguished from opioid dependence by out-of-control use and drug preoccupation, with both sharing the emergence of

negative symptoms during drug abstinence.[7] The stressors faced by modern humans in the developed world occasionally have parallels with the circling hawk (temporary and avoidable, with some luck), but often take more abstract and inescapable forms, particularly for populations without substantial social and economic resources. For those unable to alleviate their pain by other methods, opioids can provide short-term comfort and respite, but chronic exposure comes at the cost of long-term molecular and circuit-level adaptations, substituting a long-term dysphoric state that can potentiate future cycles of abstinence and relapse. Psychiatrists hoping to reset their patients' neural circuits to something resembling the opioid-naïve state are severely limited by the current pharmacological toolbox. While direct antagonism of the opioid system with naltrexone can partially alleviate cravings, it also often exacerbates negative physical and emotional symptoms during drug abstinence.[8] Partial opioid agonists are effective in reducing both drug cravings and withdrawal symptoms, but are generally prescribed in perpetuity to prevent relapse, maintaining some degree of opioid dependance. This status quo of "lesser" opioid treatment can be distressing to patients who desire complete freedom from drug use. Importantly, medical treatment of opioid use disorder symptoms has repeatedly been shown to be the superior approach from a total harm reduction standpoint.[9]

In summary, endogenous opioids serve an important evolutionary role in enabling organisms to temporarily ignore pain to facilitate action. Since the earliest recorded human history, the ubiquity of painful experiences has created a demand for exogenous opioids, which has grown exponentially in scale with the advent of more potent (and more easily obtainable) synthetic μ-opioid agonists. To move forward in supporting and treating people with opioid use disorder, and in developing safer and more effective pain treatments, it is imperative to improve our understanding of the precise neural mechanisms that drive and maintain maladaptive opioid seeking behaviors.

Section II: Adaptations to cortico-striatal circuits across the addiction cycle

Acute opioid reward circuitry: the ventral tegmental area and beyond:

Upon initial use, acute opioid-induced reward has been shown to be principally induced by a disinhibitory mechanism in the ventral tegmental area (VTA). Early mechanistic studies described concurrent hyperpolarization of GABAergic interneurons and increased dopamine (DA) neuron firing in response to μ-opioid agonists, for which expression of the G_i coupled μ-opioid receptor (MOR) in interneurons was required.[10] Primary projection targets of VTA dopamine neurons include the nucleus accumbens (NAc), prefrontal cortex (PFC), and amygdala.[11] NAc is principally composed of GABAergic projection neurons known as medium spiny neurons (MSNs), roughly divided into two major subtypes based on their expression of either the D1 or D2 dopamine receptor. The D1 dopamine receptor (D1R) is G_s coupled, inducing a pro-excitatory response to dopamine via cAMP/adenylate cyclase induction, whereas the D2 dopamine receptor (D2R) is G_i coupled and pro-inhibitory.[12] D1 and D2 MSNs also differ in respect to their projection targets, with D1 "direct pathway" MSNs largely projecting back to the VTA, and D2 "indirect pathway" MSNs targeting the ventral pallidum (VP).

Initial optogenetic studies comparing stimulation of D1 and D2 MSNs found that activating D2 MSNs alone in dorsomedial striatum induced a hypokinetic state, which could be reversed by activation of D1 MSNs, supporting roles for these neurons in driving a "go/no go" motor signal.[13] This finding was paralleled in ventral striatum by the observation of differing biases for each population in processing input with positive or negative affective value, with D1 MSNs shown to be activated by rewarding stimuli and D2 MSNs more likely to be activated by aversive stimuli.[14,15] Thus, a preliminary theory set out opposing roles for D1 and D2 MSNs, with D1 MSN activation induced by appetitive or rewarding stimuli and leading to immediate increases in behavior or

locomotion, and D2 MSN activation conversely induced by aversive stimuli and increasing anti-action inhibitory tone. However, recent work characterizing D1 and D2 MSN activity in bulk with fiber photometry has complicated this picture, demonstrating that D1 MSNs respond indiscriminately to salient stimuli (including rewards) and that both D1 and D2 MSN optogenetic self-stimulation can be reinforcing.[16] Single-cell miniscope 1p recordings in the NAc during appetitive and aversive conditioning produced similar results, showing predominant inhibition of D1 and D2s after sucrose delivery and excitation after shock.[17] Both D1 and D2 MSNs integrate the neuromodulatory DA signal from the VTA with glutamatergic input from mPFC, aPVT, basolateral amygdala, and ventral hippocampus, which may underly findings of highly correlated D1 and D2 MSN activity in response to various rewarding and aversive stimuli. Cell-type specific roles of these glutamate projections have partially been delineated: for example, chronic morphine potentiates PVT/D2 MSN circuits via enhanced expression of AMPARs.[18] D1 MSN projections to the VTA are not uniform, with medial shell MSNs inhibiting DA release directly, and lateral shell MSNs promoting DA release by inhibition of local GABAergic interneurons in the VTA.[19] This synaptic heterogeneity may explain some of the incongruity observed between studies measuring or manipulating MSN activity in varying behavioral contexts. Existing work characterizing MSN function generally focuses on their spatial location (NAc core vs. medial vs. lateral shell), rather than interrogating their cellular identity beyond the broad strokes of D1 and D2.

Given that MSN responses to VTA DA and other stimuli have been a major focus of many behavioral neuroscience subfields, the large body of work available to characterize them is not surprising, but the lack of congruity in the field about the role of these neurons in reward and motivation can be difficult to disentangle. This uncertainty is paralleled by ongoing debate about the role of VTA DA itself in learning, with the field still somewhat split about whether DA signals

reward/salience[20], reward prediction error[21] (RPE), or some combination of the two. A detailed discussion of DA's role in learning is somewhat out of the scope of this dissertation, but in short, it seems reasonable that much of the conflict about DA's role could be resolved by a more complete understanding of NAc MSNs themselves, who are likely the major effectors of the DA signal amongst the VTA's diverse projection targets. In self-administration studies, animals learn to self-administer drugs, which act either directly or indirectly to modulate DA, likely modifying current and future learning processes. When an animal does not engage in voluntary drug self-administration, there are at least two possible explanations for this: they may be neophobic and find the sensations induced by the drug more aversive than rewarding, or they may find the drug quite rewarding, but fail to make the association between the lever press and the drug reward. In the former case, we would hypothesize that rats would develop an avoidant response to the active lever, while in the latter they should continue to press both active and inactive levers occasionally and stochastically. Generally, we find that most rats with very low self-administration rates display patterns closer to the "aversive" category than the "poor learning" category. However, failed learners could still be considered valid members of the "low addiction risk" phenotype, as they may carry favorable genetic, epigenetic, or environmental factors which enable them to avoid acquiring a learned addiction-like behavioral response.

Nearly all D2 MSNs, and a subset of D1 MSNs, project to the ventral pallidum, a primarily GABAergic "limbic final common pathway."[22] Downstream targets of VP neurons include mPFC (cholinergic projection), NAc (GABAergic), basolateral amygdala (cholinergic/glutamatergic), VTA (GABAergic/glutamatergic), lateral habenula (GABAergic/glutamatergic), and mediodorsal thalamus (GABAergic/cholinergic.)[23] Within the VP is a "hedonic hotspot" of enriched MOR expression, which is sufficient to induce food-reward related behaviors upon direct delivery of MOR

agonists.[24] This hotspot may represent one potential mechanism of DA-independent exogenous opioid reward, a concept first explored after dopamine-deficient mice were shown to be capable of acquiring a conditioned place preference to morphine.[25] MORs are also abundant in the NAc, adding complexity to our model of opioid reward there, as MOR expressing MSNs must integrate glutamatergic, cholinergic, and dopaminergic relation with exogenous MOR activation. Meanwhile, non-MOR expressing MSNs "escape" MOR-mediated inhibition, possibly increasing their contribution to early opioid reward.

To recap the opioid reward circuit described thus far, MOR binding to VTA interneurons transiently increases DA neuron firing and local DA concentrations in the NAc. This increase is hypothesized to shift D1 MSNs to a pro-excitatory state, subsets of which project back to VTA interneurons, again promoting disinhibition, enhancing reward, and facilitating action. D2 MSNs are instead pushed in the opposite direction towards inhibition, leading to downstream disinhibition of VP neurons, whose firing is also strongly associated with reward and motivation for appetitive stimuli. However, for better or worse, both human and rodent behavior is not solely driven by basic sensations of rewarding and aversive stimuli. Instead, these inputs are integrated along with more neutral sensory information by higher cortical regions, with top-down inhibitory control over action largely associated with the medial PFC. Chemogenetic inhibition of prelimbic cortex (PL) pyramidal neurons is sufficient to block morphine-induced conditioned place preference (CPP), supporting a role for PL in the sensation and/or expression of opioid reward.[26] GABAergic local interneurons likely mediate much of the acute opioid response in PL, but in a cell-type and circuit specific manner, with parvalbumin (PV) neurons most likely to be inhibited immediately after morphine treatment.[27] In contrast, somatostatin (SST) neurons display enhanced inhibition of PVs, finally resulting in disinhibition of pyramidal neurons.[27] Universal blockade of AMPA receptors in PL (but

notably not in infralimbic cortex, another mPFC subregion) increased morphine CPP in a DA-dependent manner[28], confirming that PL DA release can modulate opioid reward-related behaviors. Differing levels of tonic PL DA are associated with distinct effects upon PL interneurons: in a low DA state, DA is principally bound by D1Rs, shifting these neurons towards excitation and increasing local GABAergic tone.[29] Conversely, high DA states bias the system towards D2R activation and decreased GABAergic tone.[29] On pyramidal neurons, activation of D1Rs can extend DA-induced long term potentiation, augmenting the high DA-induced disinhibition.[30] Taken together, the evidence reviewed here supports a primary disinhibitory mechanism of opioid reward, with exogenous opioids and DA acting in tandem to alter the balance of excitation and inhibition in diverse brain regions from the brainstem to the prefrontal cortex.

Chronic opioid self-administration sets the stage for withdrawal:

When does acute opioid exposure transition to chronic opioid use? In rodent models, the answer appears to be around five to seven days of opioid administration, or long enough to induce physiological drug dependance and withdrawal upon drug cessation. The great majority of mechanistic studies examine the brain either after acute opioid exposure or after opioid withdrawal, leaving the continuum of stepwise changes occurring during chronic opioid use largely mysterious. Acute or physiological signs of opioid withdrawal-induced autonomic dysregulation (wet dog shakes, chewing, GI upset, grooming, jumping, etc.) increase in the absence of drug up to the 48-hour mark, then gradually resolve.[31] They can also be induced more rapidly with naloxone treatment. An early study examining GABAergic VTA synapses in acute withdrawal found an enhancement in DA neuron IPSCs[32], which may contribute to the immediate negative physical and emotional effects observed in early stages of drug abstinence. After long-term or highly escalated opioid treatment or self-administration, symptoms of protracted withdrawal may emerge. For rodents, these include

decreased sociability and sucrose preference, as well as an increase in anxiety-related behaviors.[33] Both D1 and D2 MSNs have been implicated in driving opioid withdrawal phenotypes: long term depression induced in an anterior paraventricular thalamus (aPVT) to D2 MSN circuit ameliorated acute withdrawal symptoms but left protracted withdrawal unchanged, while dual D1 MSN LTP induction and norBNI pre-treatment reduced the severity of negative affective behaviors during morphine withdrawal.[34] The specific importance of the kappa opioid receptor (KOR) system in opioid withdrawal will be revisited in section III. D1 MSNs, but not D2 MSNs, display marked electrophysiological changes during fentanyl abstinence, with increased excitatory input and excitability despite reduced dendritic complexity.[35] Cell-type-specific adaptations are also observed in the VTA following chronic morphine exposure and withdrawal. GABAergic neurons in the rostromedial tegmental nucleus remain inhibited by opioids both in a drug-naïve state and in withdrawal, but only during withdrawal does their inactivation fail to induce DA neuron activity.[36] This loss of disinhibition co-occurs with reduced inter-VTA glutamatergic transmission, suggesting that the circuit has adapted to decrease the probability of DA neuron firing with or without opioids on board. Other neuropeptides also contribute to withdrawal phenotypes. For example, prodynorphin (pdyn) expressing serotonergic neurons in the dorsal raphe were found to mediate sociability deficits during abstinence by blocking 5-HT release in the NAc medial shell via KORs.[37] Just as opioid reward involves diverse brain regions, neurotransmitters, and circuits, so must the adaptations that occur over the course of chronic drug use and drug abstinence. However, if a single neuronal subtype had to be nominated as the most critical known node in protracted withdrawal circuitry, the D1R expressing MSNs of the NAc core and shell would make a reasonable choice. Comprehensive characterization of the transcriptional heterogeneity of these neurons will be a focus of Chapter 3, section IV.

Withdrawal-induced neural plasticity potentiates episodes of relapse:

In humans with opioid use disorder, periods of drug abstinence and protracted withdrawal are often followed by episodes of relapse. In the lab, "relapse-like" drug seeking behaviors can be induced after rodent opioid self-administration by restoring drug access, or even simply re-presenting a drug-paired cue. Whether true incubation of craving (defined as the development and potentiation of drug craving with increasing duration of abstinence[38]) occurs during opioid abstinence in humans is up for debate, with most clinical studies reporting a steady decrease in drug craving with increasing length of drug-free periods,[39] despite some evidence for opioid-induced incubation of craving in rats.[40] It is unclear whether this difference stems from an underlying alteration in neurobiology between rodents and humans, or instead reflects the much more limited environmental landscape and range of activities available to most laboratory rats and mice (if there is little opportunity for naturalistic behavior, can anything replace or blunt the pleasure of opioid reward?) Using an electric barrier, experimenters compared chosen abstinence with forced abstinence, and found that incubation of craving was substantially stronger in animals who voluntarily ceased drug-seeking due to painful consequences.[41] This finding emphasizes the vital importance of choice in drug-seeking and drug-taking when utilizing animal models. Although it is of course impossible to fully recapitulate human psychology in rats or mice, to come to a thorough understanding of a disorder that results from voluntary choice to consume a substance, that choice must be preserved in the selected animal model. Investigation of neural mechanisms of simple opioid exposure has provided a strong foundational understanding of early responses to opioid treatment, which is vital to the studies conducted here, but cannot fully illuminate the circuits that initiate and maintain maladaptive opioid use. However, incorporating choice into these studies does

raise the possibility that each rat will choose slightly differently, which can complicate rigorous statistical comparison between groups. This dilemma will be addressed in Chapter One.

Given that μ-opioid tolerance is pronounced in VTA DA circuits, it is likely that downstream reward and motivation hubs are more relevant for initiating and modulating the vigor of "relapse" behaviors. For example, glutamatergic drive to the NAc, particularly from mPFC, is thought to play an outsize role in determining reactivity to drug-related cues and environmental contexts. fMRI studies in humans repeatedly highlight the importance of mPFC in distinguishing people with OUD from healthy controls, with observations of disrupted default mode networks and decreased mPFC functional connectivity[42], dlPFC loss of gray matter[43], and reduced functional connectivity between PFC, OFC, and ACC.[44] These alterations are not as simple as sole loss of mPFC function in all opioid-experienced individuals: for example, a study conducted following heroin relapse found relapsed men had increased connectivity in dorsal ACC and dmPFC, but lower connectivity in dl and dmPFC than non-relapsed men.[45] A "hypofrontality" theory of addiction posits that loss of normal mPFC top-down control of behavior prevents individuals with drug use disorders from effectively self-regulating and maintaining abstinence, especially when faced with cues or environments that worsen drug cravings. Whether these individuals were also more likely than the general population to be impulsive prior to drug use remains unclear: in humans, evidence for this is very limited, and impulsive traits in rats are not associated with future heroin self-administration.[46] Decreases in activation in frontal brain regions in substance users have been associated with decreased D2R levels and DA release, supporting a potential link between striatal dysfunction and loss of coordinated prefrontal activity.[47] Concerningly, patients who underwent treatment with naltrexone during a brain imaging study showed decreased mPFC cortical thickness, with those who reported the most attenuation in drug cravings showing the greatest loss of

thickness.[48] These macro-structural side effects indicate that antagonizing the opioid system brain-wide, while effective in treating drug cravings, may also induce long-lasting alterations to circuits crucial for cognition, self-regulation, and general functioning. In one cell-type-specific investigation, authors identified hypoactive aPVT MOR-expressing neurons in heroin-experienced mice, along with loss of PVT synaptic innervation of NAc PV interneurons.[49] Notably, stimulation of the low-activity PVT population was sufficient to block reinstatement for heroin, introducing a possibility of restoration of behavioral inhibition via targeted recruitment of specific neural ensembles. Although excitation or inhibition of molecularly defined populations of neurons remains out of reach as a therapeutic tool in humans at this time, if we can better elucidate the intracellular mechanisms and signaling cascades which initiate and maintain the long-lasting neuroadaptations of addiction, we may find new druggable substrates that can be targeted to alleviate OUD symptoms and support drug abstinence.

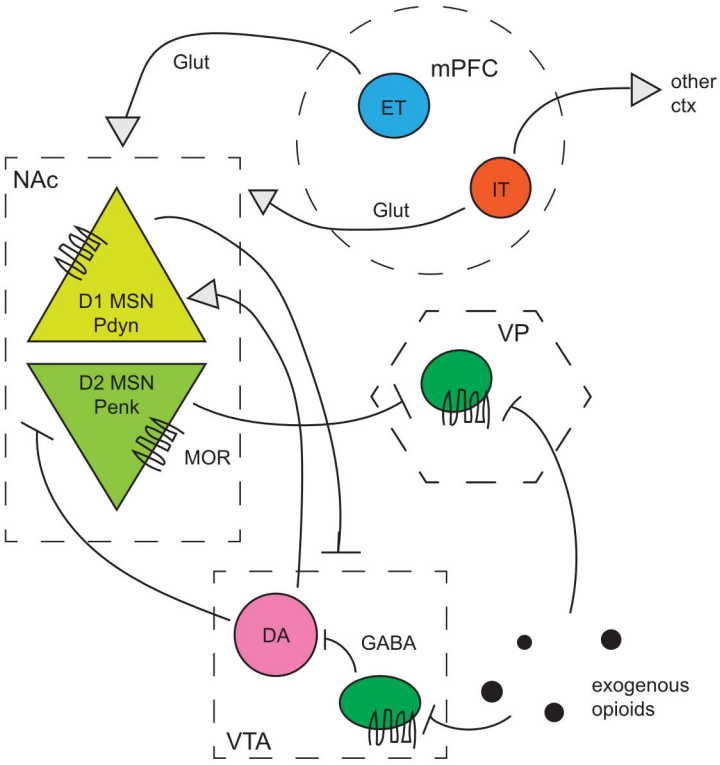

Schematic 1: (Very) simplified diagram depicting relevant circuits mediating acute opioid reward, plasticity in which is thought to reinforce future opioid-taking behaviors. NAc MSNs integrate dopaminergic, glutamatergic, and opioid (exogenous + endogenous) input, acting as a central node in this addiction circuit.

Section III: Molecular drivers of exogenous opioid-induced neuroplasticity

G protein coupled receptor-induced neuromodulation after acute opioid treatment:

Upon first administration, opioids facilitate enhanced VTA DA output to the NAc. There, DA induces the G_s signaling cascade in D1R MSNs, characterized by an increase in the second messenger cAMP and subsequent recruitment of protein kinase A (PKA) and cAMP-response element binding protein (CREB).[50] This signaling cascade can shift the D1 MSNs into a pro-excitatory state, which persists over a long timescale (minutes to hours.) The contribution of receptor desensitization and recycling via beta-arrestin to D1R signaling dynamics in varying DA concentrations is currently understudied, with limited characterization of D1R-beta arrestin binding to date, with or without drug exposure. Tolerance and desensitization is thought to be more physiologically relevant for exogenous opioid signaling at the MOR, with synthetic opioids inducing MOR phosphorylation and recycling much more rapidly than morphine and heroin.[51] However, the consequence of this pharmacological difference between agonists on reward and aversion circuitry (especially after repeated cycles of drug use) is also not particularly well understood. Cell-type-specific attenuation of GPCR-mediated signaling may also play a role in defining DA's capacity to excite MSNs: for example, the G-protein regulator Rgs9 is highly expressed in striatum, but its expression levels are differentially modulated after acute or chronic morphine exposure (increased after acute, but decreased after chronic.)[52] Complicating matters further, subsets both D1 and D2 MSNs express MOR and thus would be expected to shift to a pro-inhibitory state in the presence of exogenous opioids (assuming low levels of drug tolerance.) How these diverse G-protein coupled signaling cascades interact over short and long timescales of drug use is not well characterized, in the NAc or in other regions that simultaneously receive VTA DA input and express the MOR (one notable example being mPFC.)

D1 and D2 MSNs differ not only in the flavor of dopamine receptor that they express, (except for the ~10% that co-express D1R and D2R) but also in the endogenous opioid peptides that they produce. Proenkephalin (Penk), a μ-opioid agonist, is specific to D2 MSNs, while preprodynorphin is specific for D1 MSNs. When determining cell type from expression data, these peptides are generally more predictive of a given MSN's identity than their D1 or D2 expression levels, although not every putative MSN constitutively expresses them at high levels. Regions downstream of the NAc tend to express either or both of the MOR and KOR. Endogenous opioids can bind to multiple types of opioid receptors, but enkephalin is traditionally considered the archetypal MOR endogenous agonist, as is dynorphin for KOR. VTA KORs in particular are thought to play an crucial role in regulating neural responses to stress and aversive stimuli, as their activation by dynorphin potently inhibits DA neuron activity.[53] As previously discussed, the VP expresses MOR abundantly and is innervated densely by D2 Penk expressing MSNs. Here, exogenous opioids may transiently replace downregulated enkephalin release in VP, which would be expected to follow DA-induced inhibition in D2 MSNs. In the absence of exogenous opioids, tolerance in VP MOR-expressing neurons could blunt their ability to effectively sense and respond to endogenous opioids, contributing to anhedonia. Penk gene variants have been implicated in GWAS studies as associated with opioid dependence[54,55], implying that variation in baseline levels of endogenous opioids may modify one's risk of developing OUD. Otherwise, the peptide remains relatively unexplored in opioid addiction compared to its counterpart, dynorphin.

Transcriptional cascades associated with opioid use and withdrawal:

CREB is a robust transcriptional activator which can initiate the expression of both immediate early genes (IEGs), such as cFOS and Homer1, and neuropeptides (for D1 MSNs, dynorphin.)[56] cAMP/CREB induction does not occur exclusively with acute opioid administration:

precipitated withdrawal also is associated with elevated CREB in NAc and extended amygdala.[57] Canonically, genes designated as IEGs are expressed at very low levels until a cell becomes activated, after which their expression exponentially increases and peaks within one or two hours before returning to baseline levels.[58] Due to this tight temporal regulation, expression of IEGs (particularly cFOS, encoded by the Fos gene) has historically been used to identify subsets of drug-responsive neurons across the brain. Some IEGs are associated with more specific and coordinated synaptic adaptations: for example, Arc is trafficked to the synapse and strongly associated with induction of plasticity.[59] In certain cell types, chronic drug treatment can trigger induction of Fosb, which is spliced into ΔFosb, a protein unique among IEGs for resisting degradation and accumulating over extremely long intervals[60] (unlike its close relative, cFOS/Fos.) Comparison of ΔFosb induction in animals who underwent a variety of pharmacologic and behavioral interventions found that five days of morphine treatment induced ΔFosb expression in both D1 and D2 MSNs across the NAc core and shell.[61] The behavioral phenotype of ΔFosb overexpression in Pdyn/Substance P expressing D1 MSNs includes increased reward-related behavior after cocaine or opioid exposure and increased baseline locomotion.[60] This combination of effects makes it difficult to firmly ascertain whether ΔFosb is truly a specific "addiction circuit" splice variant, or if it instead promotes more general striatal hyperexcitability and thus enhances reward and locomotion in a stimuli-agnostic manner. The wide generalizability of ΔFosb induction across many types of drug exposures led to its proposal as a hypothetical "common molecular pathway" for addiction,[62] but since it can also be induced robustly by enriched environment or sucrose administration, it seems more reasonable to view it as a common pathway for striatal neuroplasticity (which certainly includes addiction.) Early proposed mechanisms for ΔFosb sensitization of drug responses include recruitment of GluR2 to reduce AMPA currents[63] and inhibition of dynorphin expression[64], in contrast to the enhancement of

dynorphin expression observed in CREB's signaling cascade. Traditional gene knockout experiments cannot easily target ΔFosb without also compromising Fosb function, which is required for normal mouse behavior and reproduction (Fosb KO mice fail to nurture their young, which is not a helpful trait in a laboratory mouse strain.)[65] As long as it remains impossible to remove ΔFosb from addiction circuits specifically, its unique mechanistic role in long-term synaptic adaptations will remain difficult to experimentally address. However, mapping of ΔFosb positive and negative neurons during protracted withdrawal may provide insight upon which MSN subtypes display prolonged dysregulation after voluntary opioid escalation.

A subset of IEGs induced by drug exposure are notable for their specific roles in modulating synaptic strength. One widely studied reinforcer of robust synapses is brain-derived neurotrophic factor (BDNF), direct application of which was sufficient to rescue chronic-morphine induced dendritic atrophy in VTA DA neurons.[66] Much of our knowledge of synapse-altering IEGs such as BDNF and Arc comes from the learning and memory field, where their roles in inducing long term potentiation and depression in hippocampal circuits have been thoroughly delineated. Compared to the quotidian experiences that the brain is usually tasked with encoding, the "memory" of pleasurable drug use can be exceptionally vivid and long-lasting, especially for a drug-naïve nervous system. Removing this memory is no simple task, as exposure to drug-related cues can rapidly recruit addiction circuitry even in patients who are many years removed from periods of drug use. fMRI-based comparison of cue-reactivity between individuals with heroin use disorder and healthy controls revealed significant increases in the nucleus accumbens, with vmPFC activity correlating directly with drug craving.[67] To broaden our understanding of where the memory of drug use is stored, we conducted a large scale whole brain cFOS experiment, using iDISCO whole-brain clearing, cFOS immunohistochemistry, and light sheet imaging in rats with varying levels of heroin

self-administration, with and without cue re-exposure prior to collection. Then, to investigate the molecular pathways disrupted during protracted withdrawal, we performed snRNAseq in three brain regions: prelimbic cortex, nucleus accumbens, and ventral pallidum. These experiments were made possible by a highly effective and valuable collaboration between three labs, each equipped with experts in rat self-administration behavior (Ferguson), whole brain light sheet imaging (Golden), and single nuclei RNA sequencing (Stuber). The following chapters will describe methods, analysis, and results obtained from each experiment, as well as ongoing follow-up and validation experiments. The overall goal of these studies was to develop a multimodal "atlas of opioid addiction," which we hope will serve as a resource for scientists working to better understand opioid use disorder and other psychiatric conditions.

Chapter One: Modeling opioid use disorder in mice and rats

Section I: What makes a rodent "high risk" for addiction?

Rodents, like humans, are not equally susceptible to maladaptive or escalated opioid use. As is the case with many other psychiatric conditions, genetic predispositions likely play a role in determining who is most susceptible to OUD. Twin studies suggest that up to 50% of opioid addiction risk could be hereditary, and genome-wide association studies (GWAS) have identified several "alleles of small effect", most notably variants in Oprm1.[68] Recent work has applied this technology to outbred rats, identifying several variants in microglial and neuroplasticity-related genes that were associated with vulnerability to heroin use.[69] Certain rat strains have previously been observed to display differing drug self-administration patterns, for example, naturally occurring genetic variation leading to loss of function in *Grm2* is associated with escalated alcohol intake in Wistar rats.[70] A "genetics-dominant" view of OUD may relieve some of the burden of responsibility placed on patients for their opioid use, and could lead to the identification of new therapeutic targets by illuminating relevant risk genes. However, genetic risk far from ensures a phenotype of drug use, and many patients with OUD have no family history of psychiatric disorders. To evaluate the spectrum of opioid intake in genetically homogenous C57B6/J mice, we adapted a system originally designed for delivery of oral oxycodone in the home cage.[71] Instead of oxycodone, we utilized pharmaceutical-grade fentanyl at a starting dose of 10 μg/mL. Both regular water and fentanyl-containing water were provided to each mouse, rendering any opioid consumption entirely voluntary, and interactions with both bottles were tracked via a lickometer.

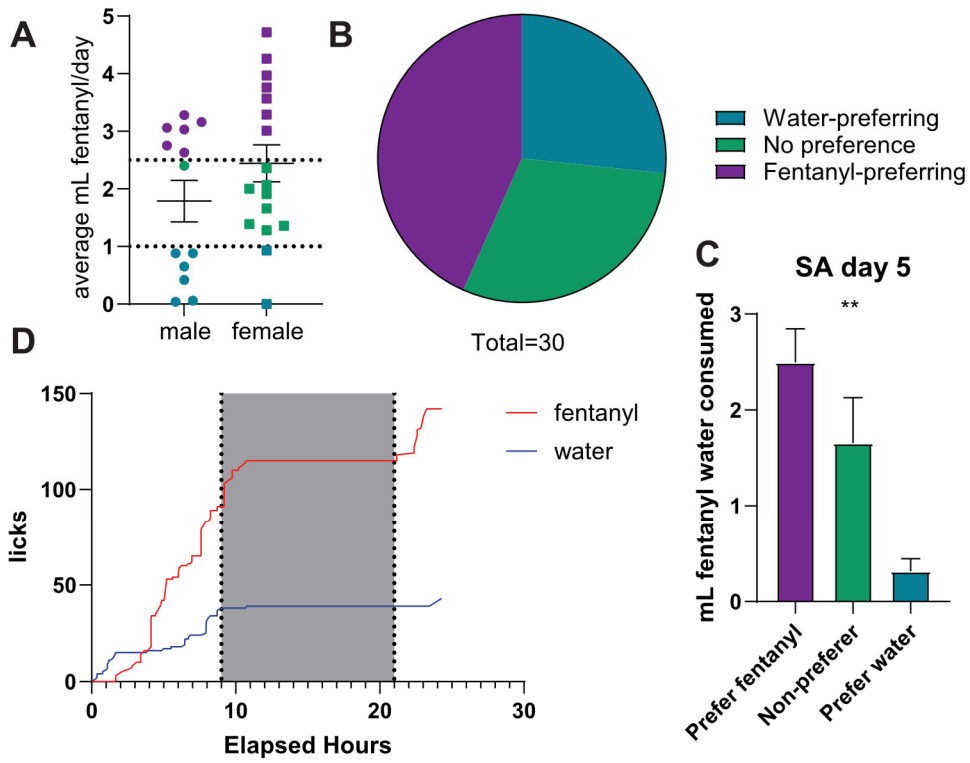

Figure 1: C57B6/J mice display divergent opioid-taking behavior in a new model of chronic oral fentanyl self-administration. (A) Average volume intake from fentanyl-containing bottle (10 μg/mL) during baseline phase, split by sex. (B) Distribution of preference between all mice, total n = 30. (C) Volume consumed from fentanyl-containing bottle on day five of self-administration, split by preference category. One-way ANOVA, p = 0.0011. Tukey's multiple comparison test: prefer fentanyl vs. prefer water p = 0.0007. (D) Representative lickometer trace depicting interactions with fentanyl-containing (red) and water bottles (blue.) Grey section represents inactive period (lights-on.)

Despite their homogenous genetic background, each cohort that was run during this pilot study (total n = 30) rapidly divided into three groups. Intake on day five of self-administration (Figure 1, panel C) was highly predictive of future preference group assignment. The first group drank almost exclusively from the water bottle, with very few interactions recorded by the lickometer at the fentanyl-containing bottle. The position of the two solutions was counterbalanced between mice, and all fentanyl-drinking mice consumed liquid from both bottles, suggesting that these water-preferring mice found the fentanyl solution aversive, and purposefully avoided it. Once this behavior was established, it did not change. One reason for utilizing fentanyl instead of oxycodone its increased potency, allowing for concentrations in the μg/μL range instead of the mg/mL range, and hopefully decreasing the number of mice that will avoid the solution because of taste alone. However, because the water-preferring mice had such limited interactions with the fentanyl bottle, it seems more likely that taste informed their aversion than the physiological effects of the drug.

On the other end of the spectrum, fentanyl-preferring mice rapidly developed a strong bias to the fentanyl-containing bottle. Instead of consuming exclusively from the fentanyl bottle (as did the water-preferring mice), these mice displayed a pronounced "loading" pattern of intake, with many interactions with the fentanyl bottle towards the beginning of the dark cycle, followed by more balanced consumption from both bottles (representative lickometer trace shown in Figure 1, panel D.) As a result, these mice consumed more total liquid per day than mice in the water-preferring group (~4.5 mL vs ~3 mL.) One surprising finding from this experiment was that even mice with a strong fentanyl preference seemed to max out around 4-4.5 mL of fentanyl-containing water per day, instead of continuing to escalate intake as is often observed in IV self-administration models. To test whether mice would self-administer higher doses, after four weeks of stable intake the dose of fentanyl-containing water was increased by 10 μg/mL a week, up to a maximum of 50 μg/mL.

This further subdivided fentanyl-preferring mice into two subgroups: dose-escalators and non-escalators. Escalators maintained stable drinking behavior at higher doses (n = 3), while non-escalators abruptly stopped drinking when the dose was increased beyond 10 μg/mL. Since escalators tended to display more stable and polarized drinking behavior than non-escalators, we hypothesized that some degree of opioid tolerance may be required to allow for escalation of oral fentanyl intake without aversive side effects. Over weeks of self-administration, escalators also developed a sensitized behavioral phenotype, with excessive chewing of the bottles and lickometer apparatus, rapid locomotion with frequently "popcorning" (abrupt vertical jumps), and a vertical tail position resembling Straub tail (a canonical behavioral response to acute opioid intoxication.)[72]

A third group, with strong female predominance (n = 8 females, 1 male), were labeled as non-preferers because they consumed similar volumes of fentanyl-containing water and unadulterated water on average. Unlike water and fentanyl preferring mice, who showed very stable drinking behavior at the 10 μg/mL dose, these mice generally maintained a preferred bottle for a few days to a week, then switched. In most cases, this began with a switch from a slight fentanyl preference to a slight water preference. One possible explanation for this pattern of mouse behavior is one of early opioid aversion and/or attenuation of reward: subsets of these mice consumed readily from the fentanyl bottle for limited periods, but unlike the fentanyl-preferring mice who reached a plateau of self-administration and stayed there, they decreased their consumption and switched to favor the water bottle. Importantly, even with very long admin periods (cohorts ran continuously for 8+ weeks), non-preferers maintained low to moderate fentanyl consumption, but always remained clearly separated from the fentanyl-preferring group. Viewing all three groups through the lens of addiction risk, non-preferers (rather than water-preferers, who had little to no opioid exposure and thus remain in an unknown risk group) likely represent a "low-risk" population, as they display what looks like self-regulation behavior at certain thresholds of fentanyl exposure. Whether their

voluntary opioid exposure was driven by reward or simply by chance was not assessed by this limited pilot study. In contrast, fentanyl-preferring mice represent at least "moderate-risk," with escalators surely in the "high-risk" category. These mice voluntarily consumed enough fentanyl to produce signs of physiological dependance, with further sensitization of their behavior and potentiation of fentanyl-drinking when drug access was removed. We hypothesize that acute or chronic stress would further alter each mouse's risk of displaying the escalating intake phenotype.

The diversity of voluntary opioid-intake behaviors we observed in these genetically homogenous male and female mice strongly suggests that non-genetic or epigenetic factors (early life stress, socialization, and likely many more) are equally if not more important in determining a rodent's total risk level for maladaptive opioid use. Many studies have previously examined individual risk for opioid addiction as a function of various traits, mostly in outbred rats. One obvious candidate is sensitivity to opioid effects, with analgesia being relatively easier to measure than hedonic reward. Rats that were initially less sensitive to the anti-nociceptive effects of morphine were more likely to display high levels of morphine self-administration[73], suggesting that some level of resistance to acute physiological drug effects (rather than heightened sensitivity) can result in increased opioid intake. Human fMRI studies have found a relationship between baseline reward circuit activity and opioid analgesia[74], demonstrating that enhanced susceptibility to anti-nociceptive opioid effects is highly likely to be coupled with increased engagement of the VTA and its downstream targets. Taken together, these findings are somewhat non-intuitive, as they imply that lower levels of initial engagement of reward circuitry by opioids is a "high-risk" trait. This also highlights one of the limitations of using operant behaviors alone as a readout for addiction risk: does more lever presses necessarily mean more addiction? Modern behavioral neuroscientists have addressed this problem by turning towards "addiction phenotypes," using additional metrics and novel statistical tools to more comprehensively characterize each animal's behavior.

Do rodents that move more (or more quickly) also move rapidly toward escalated drug intake? Surprisingly, locomotor activity in a novel environment was non-predictive of future morphine SA in Sprague-Dawley rats[75], but highly predictive of morphine SA in four other strains.[76] Complicating interpretation of these findings are the combination of two potential risk factors in the novel environment locomotion assay. Baseline locomotive vigor is known to differ among outbred rats and may reflect underlying differences in striatal circuitry, whereas exploration is more related to "sensation seeking," or the degree of drive each animal demonstrates for novel environments and experiences. In humans, measures of sensation seeking have been reported as predictive of drug use, and siblings with a drug use history were more likely to display similar degrees of seeking compared to non-drug using siblings.[77] This may not be universal across all OUD presentations, with prescription opioid users scoring lower on measures of sensation seeking but higher on impulsivity.[78] Both a rat that self-administers heroin and sits motionless, and a rat that does not administer heroin, but instead tirelessly explore its environment could be accurately characterized as sensation seeking. To address current limitations in our ability to identify and classify specific rat traits based on behavioral profiles, Section IV of this chapter will focus on novel methods for machine-learning based classification of rat behaviors during first opioid exposure, escalation, and withdrawal.

When animals are first exposed to opioids, only the immediate drug effects likely play a significant role in shaping their behavior. However, once they have experienced drug withdrawal, this new "memory" can alter behavior during future drug exposures. Rats that displayed lower motivation for rewards (measured by intracranial self-stimulation, or ICSS) during opioid withdrawal after experimenter-administered morphine injection displayed lower addiction-like behavior during subsequent morphine self-administration.[79] However, both the lack of a self-admin pre-test (instead

substituting noncontingent injections) and potential neuroplasticity induced by ICSS itself complicate evaluation of a causal relationship between severity of protracted withdrawal symptoms and future self-administration rates. Rats bred for low saccharin preference display increased ICSS during morphine withdrawal[80], and fail to develop a conditioned place aversion to opioid withdrawal[81], but again it is unclear whether this represents a true phenotype of high risk for opioid addiction, or rather is expected in rats with baseline relative anhedonia. These studies present a key question: is relative indifference to reward protective against opioid use, or can it worsen addiction by potentiating the negative effects of withdrawal? The answer is likely both, depending on an individual's specific level of addiction risk and prior history of opioid exposure.

Section II: General behavioral methods

The rat heroin IV self-administration paradigm utilized in this dissertation work was pioneered by UW Neuroscience graduate student Tim O'Neal, in the lab of Susan Ferguson. He found that long-access heroin SA reliably stratified rats into two risk groups, with addiction-related behavioral effects observed after chemogenetic modulation of specific MSN subpopulations in high-risk, but not low-risk rats.[82] This work provided two crucial jumping-off points for these studies: first, it demonstrated the feasibility of generating enough high and low addiction risk rats within each cohort to make comparisons, and second, it strongly supported a hypothesis of distinct neural mechanisms driving behavior within each addiction risk group.

Technical support for Med Associates boxes and their programmatic control was provided by Scott Ng-Evans. All catheter surgeries were expertly performed by the Ferguson lab's staff scientist, Nailyam Nasirova. Behavioral and surgical procedures were in accordance with National Institutes of Health (NIH) guidelines and approved by UW's Institutional Animal Care and Use Committee (IACUC.)

Subjects: Outbred male and female Sprague-Dawley rats, run in cohorts of 20 rats at a time (10 male, 10 female.) Rats were pair-housed in a housing room with a reversed 12 hr dark/12 hr light cycle, with all behavioral sessions occurring during the dark cycle.

Drugs: Heroin (diacetylmorphine HCl) was obtained through the National Institute of Drug Abuse's Drug Supply Program and diluted to a stock concentration of 5 mg/mL in sterile saline (0.9% NaCl.) Individualized heroin solutions were prepared for each subject based on their body weight for a final heroin dose of 0.075 mg/kg/infusion.

Catheter surgeries: Animals were anesthetized with isoflurane and catheters were introduced to the right jugular vein, exiting through a port midway between the shoulder blades. Metal caps were used to prevent debris from entering the catheter. All catheters were flushed daily with 0.2 mL of gentamicin sulfate, dissolved in sterile saline. Prior to starting self-administration, catheters were tested for patency using 0.2 mL of 10 mg/mL methohexital sodium, with ataxic behavioral responses within 5s of administration required before proceeding to self-administration.

Operant IV heroin self-administration: Med Associates rat operant chambers were utilized for all sessions. Each box contains two levers (each with a paired cue-light), a food-tray, and a light bulb ("house light.") Rats were each provided with one Nylabone to reduce the risk of opioid-induced self-injury behaviors. A syringe pump provided all heroin infusions via plastic tubing, which was attached to each rat's catheter before each session, and covered with a metal protective sheath.

Training: Initial cohorts (including all cFOS and RNAseq animals, n = 56) underwent five days of training, which consisted of a single drug available (DA) period 60 minutes in length. During DA periods, the house-light was turned off, and both levers were extended. Either the right or the left lever, counterbalanced between boxes, is designated as the "active" lever. When the active lever is pressed, the cue light was illuminated for 2.8s, during which the rat would receive a 50 μL heroin

infusion. Additional presses during the 2.8s are recorded, but do not result in additional infusions: these are designated as "excess" presses in downstream analysis. The food tray is unused throughout all sessions, but food tray head entries are logged by Med Associates software and utilized as a measure of off-target exploratory activity. Training sessions were capped at a maximum of 10 infusions, reaching this cutoff resulted in retraction of both levers. Later cohorts underwent 3-5 days of a modified training paradigm, which included three 45-minute drug available periods (drug periods), each followed by a 15-minute drug-unavailable period (nodrug periods.) Infusions were capped at a maximum of 10 per drug period: if rats reached 10 infusions before 45 minutes had elapsed, the program immediately proceeded to the next nodrug period. If the cap was reached during the 3rd drug period, the training session would end at that point. The goal of this change was to reduce the number of rats with low heroin exposure (<3 infusions) during the training sessions. Sufficient heroin exposure during training is important to ensure that low addiction risk rats display failure to choose to administer heroin, rather than failure to learn that heroin is available to them.

Intermittent self-administration: Following the training period, rats proceeded to ten days of long-access intermittent self-administration (IntSA.) These sessions consisted of 12 five-minute drug periods, each followed by a 25-minute nodrug period. Drug periods were as described above, while nodrug periods were distinguished by the house-light coming on. During nodrug segments, levers remain extended, but cue lights and infusions are no longer triggered by active lever presses, which are recorded as a readout of drug seeking.

Progressive ratio sessions: These sessions consisted of a single drug period with a progressive ratio (PR) schedule of reinforcement. Initial PR sessions used this schedule: (5, 10, 20, 45, 65, 85, 115, 145, 165, 185, 215, 245), with later cohorts adding an infusion after one press, otherwise keeping the

same pattern. If 30 minutes elapsed without a response, or if six hours passed in total, the session was terminated.

Extinction: After completing the PR test, animals underwent 8-10 days of extinction, consisting of at least 60 minutes in the self-admin apparatus with the house-light off and no reinforcers (no cue light, no drug delivery.)

Reinstatement test: Following the extinction phase, a subset of rats was noncontingently re-exposed to the cue light for four seconds. Subsequent active lever presses over 60 minutes would trigger the 2.8s cue light again, but no drug infusions were delivered.

Section III: Risk stratification: latent profile and principal component-based analyses of addiction metrics in rat IV heroin self-administration

To generate and test hypotheses about addiction risk, it is necessary to first define the groups that will be compared. When studying acute drug exposure, this is straightforward: the control group receives a sham injection of saline, and the experimental group receives the drug. Additional experimental groups may receive different concentrations of drug, or multiple doses of the drug over various time periods. To address the issue of tolerance, chronic noncontingent opioid studies can employ fixed escalating doses, which can more rapidly induce drug dependance and withdrawal upon drug cessation. Induction of tolerance creates complications when attempting to compare acute and chronic exposures: does the chronically opioid-exposed brain reflect the last dose, or the whole history of doses? (Of course, the answer must be both, but disentangling one from the other is not simple.) This issue can lead to confounds when attempting to make comparisons between rats with varying SA histories. One option to control for drug history alone is the use of yoked controls, where a control rat receives a noncontingent infusion whenever its paired experimental rat voluntarily earns one. However, the seemingly random nature of these infusions (from the

perspective of the yoked rat) would likely engage distinct and unique circuitry, especially for rats yoked to high addiction risk rats. Thus, we would likely need to classify the yoked controls as a separate experimental group, rendering their relative importance as a point of statistical comparison for the high addiction risk rats unclear. In an ideal world, we would have additional groups of yoked controls as well as saline-only controls, but given the limited number of behavior boxes, we have chosen to proceed with full cohorts of 20 experimental rats (10M, 10F.) This enables us to maximize the number of rats who are classified as high or low risk and include equal numbers of both sexes in each study.

IV self-administration has enormous value in recapitulating key features of human drug use, but there are myriad factors that can complicate its reliability: catheters can lose patency, equipment can break down, and animals can become disrupted by factors unknown to the experimenter. Given this inherent variability, especially over long paradigms, we hypothesized that an addiction risk profile that comprehensively spans multiple metrics collected over a sustained period would be more robust to stochastic variations in rat behavior than any single metric alone. These metrics can then be combined to form a profile, facilitating classification of rats into discrete addiction risk groups for classification. Two methods for establishing and cross-validating risk profiles are discussed below.

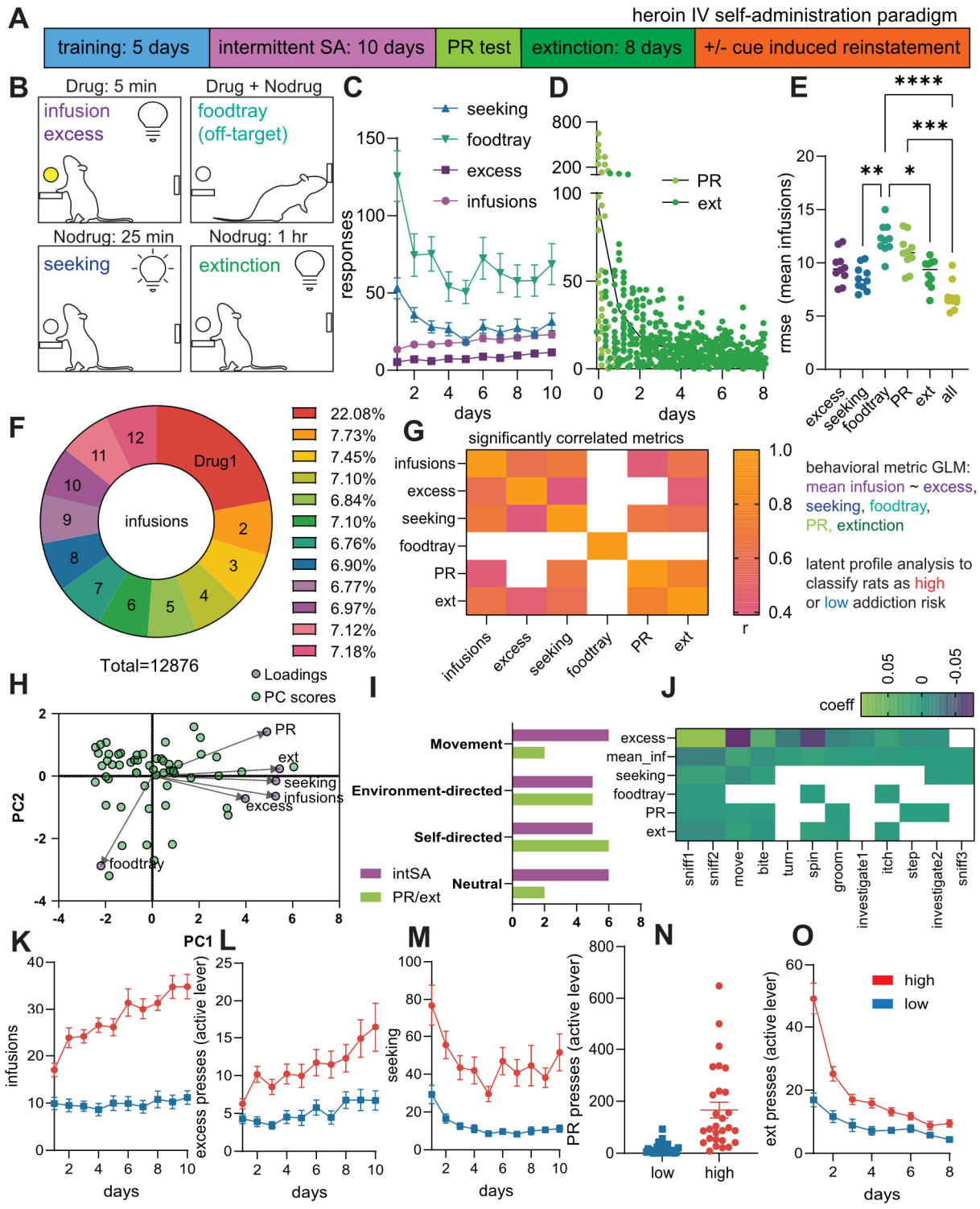
A
heroin IV self-administration paradigm
training: 5 days
intermittent SA: 10 days
PR test
extinction: 8 days
+/- cue induced reinstatement
B
Drug: 5 min
infusion
excess
Drug + Nodrug
foodtray
(off-target)
Nodrug: 25 min
seeking
Nodrug: 1 hr
extinction
C
seeking
foodtray
excess
infusions
responses
days
D
PR
ext
days
E
rmse (mean infusions)
excess
seeking
foodtray
PR
ext
all
F
Drug1
infusions
Total=12876
22.08%
7.73%
7.45%
7.10%
6.84%
7.10%
6.76%
6.90%
6.77%
6.97%
7.12%
7.18%
G
significantly correlated metrics
infusions
excess
seeking
foodtray
PR
ext
r
behavioral metric GLM:
mean infusion ~ excess,
seeking, foodtray,
PR, extinction
latent profile analysis to
classify rats as high
or low addiction risk
H
Loadings
PC scores
PC2
PC1
PR
ext
seeking
infusions
excess
foodtray
I
Movement
Environment-directed
Self-directed
Neutral
intSA
PR/ext
J
coeff
excess
mean_inf
seeking
foodtray
PR
ext
sniff1
sniff2
move
bite
turn
spin
groom
investigate1
itch
step
investigate2
sniff3
K
infusions
days
L
excess presses (active lever)
days
M
seeking
days
N
PR presses (active lever)
low
high
O
high
low
ext presses (active lever)
days

Figure 2: Latent profile analysis of addiction-related metrics reveals two distinct heroin-taking phenotypes. (A) IV heroin self-administration paradigm. (B) Self-administration block structure and addiction metrics. Each SA session consists of 12 drug-available periods and 11 drug-unavailable periods. (C) Addiction metrics over ten days of SA, n = 56 rats. (D) PR and extinction active presses over one PR session and eight days of extinction, n = 56 rats. (E) Root mean square error for each metric and all metrics combined. Data points reflect 10X bootstrapping of linear model with a 80% train 20% test data partition. Kruskal-Wallis test $p < 0.0001$, seeking vs. foodtray $p = 0.0038$, foodtray vs. ext $p = 0.0235$, foodtray vs. all $p < 0.0001$, PR vs all $p = 0.0002$. (F) Distribution of infusions across drug periods. (G) Correlation of addiction metrics, heatmap depicts Pearson r values where $p < 0.05$. (H) Biplot after PCA on addiction metrics. (I) Broad categories of behavioral syllables detected during training/SA, and during PR/extinction, n = 9 rats. (J) Syllables with significant variation in frequency during PR and extinction, as a function of specific addiction metrics. (K-O) Addiction metrics split by addiction risk group.

Generalized linear model (GLM) based analysis of addiction metric predictivity:

Med Associates software produces output files for each behavioral session, which contain text-based lists of events and timestamps. We developed an R-based pipeline for extracting these events, resulting in counts for the following values: active lever presses, inactive lever presses, food tray head entries, and infusions. We hypothesized that burst-like repeated pressing of the lever during the 2.8s infusion period might help distinguish more-addicted rats from less-addicted ones. To derive these "excess" lever presses, the number of active lever presses during drug periods was subtracted from the number of infusions. Nodrug period active lever presses were relabeled as "seeking." Initially, we did not plan to analyze food tray head entries, as there are no reinforcers in the food tray. However, after pre-processing of all behavioral output files was complete, it became

apparent that there was an unexpected degree of individual-to-individual variation in this behavior. It also seemed potentially useful to include a metric that was unrelated to drug-seeking, especially before we had access to a method for video recording the rats during their sessions. Both "excess" presses and "foodtray" are new metrics that were not analyzed prior to this dissertation work (at least in our hands.)

To investigate whether initial proclivity to self-administer heroin was predictive of future administration, we utilized linear regression to test whether maximum infusion count during training (number between 0 and 10) was predictive of average infusion across the ten days of SA. No significant linear relationship was found ($p = 0.5346$), suggesting that the factors that drive initial heroin SA may diverge from those that maintain and/or escalate SA throughout the paradigm. Based on this result, training maximum was dropped out of the addiction profile for each rat, which then consisted of mean infusion count (infusions), mean excess presses (excess), mean active presses during nodrug periods (seeking), mean food tray head entries (foodtray), active lever presses during PR session (PR), and mean active lever presses during extinction sessions (ext). We hypothesized that the remaining addiction metrics were likely to be correlated with one another. Statistical testing revealed that all metrics except foodtray (correlated with no other metric) and PR (correlated only with infusions, seeking, and extinction) had significant positive correlations (Figure 2G.) Of all the metrics, we selected mean infusion count as a proxy for the "ground truth" of each rat's addiction state, as all other metrics (progressive ratio responding, extinction responding, etc.) are not necessarily required for the rat to be validly designated as displaying a heroin addiction-like behavioral phenotype.

Using an 80% train 20% test partition, we trained a linear model to predict mean infusion from each metric separately, and from all the metrics together (Figure 2E.) After repeating this

process ten times, RMSE for each model was compared using one-way ANOVA. As expected, foodtray was the least predictive of mean infusion count. Utilizing all metrics was the most significant improvement over foodtray, followed by seeking alone, then extinction alone. Interestingly, testing two or three metrics at a time failed to produce improvements over a single metric: significant gains in predictivity were only observed when all metrics were combined. It is likely that a larger population of rats is required to definitively rank the contributions of each metric when predicting mean infusions.

```
train_index <- createDataPartition(data$Mean_infusion, p = 0.8, list = FALSE)
train_data <- data[train_index, ]
test_data <- data[-train_index, ]
model <- train(Mean_infusion ~ Excess, data = train_data, method = "lm",
trControl = trainControl(method = "cv", number = 5))
predictions <- predict(model, newdata = test_data)
results <- data.frame(Actual = test_data$Mean_infusion,
Predicted = predictions)
rmse <- sqrt(mean((results$Actual - results$Predicted)^2))
summary$Excess[i] <- rmse
```

Formula 1: Example code for data partitioning and testing predictivity of excess presses.

Latent profile analysis facilitates classification of each rat as high or low addiction risk:

Mean infusion count is normally distributed (D'Agostino and Pearson test, K2 = 2.375.) Since most of the values fall somewhere in the middle of the distribution, setting a high/low cutoff using mean infusion alone would likely be accurate for rats at the highest and lowest end of the spectrum, but relatively arbitrary for those towards the center. Prior work integrated other addiction metrics by z-scoring each metric within each cohort, then summing the z-scores for a final "addiction risk score."[82] However, this approach renders all metrics equal and cannot account for the observed differences in both intra-metric correlation and ground truth predictivity. Interpreting and assigning relative value to each metric as an experimenter is also not straightforward: for example, increased responding during extinction sessions could be viewed as indicative of increased

drug craving, or it could simply connote a failure to learn that the reward has been unpaired from the lever press. To develop an unbiased method for classifying rats as high or low risk, we turned to latent profile analysis (LPA), a statistical method that was originally developed for use in large human studies measuring multiple continuous variables. LPA utilizes a Gaussian mixture model to provide class designations for each subject, based on an experimenter-selected number of classes.[83] Users are encouraged to try multiple iterations with varying class numbers, and select an appropriate number of classes based on the entropy value computed (higher values of entropy are more desired, >= 0.8.) Higher entropy values tend to reflect lower levels of overlap across variables.

Working from the same comprehensive dataset of n = 56 rats, we used the tidyLPA R package to test varying numbers of classes. Two, three, and four classes each produced an entropy value > 0.8 (0.824-0.912.) Selecting two classes produced clear separation in the mean infusion variable, which has previously been established as most representative of addiction ground truth. This was paralleled by a high-low split with various degrees of noise in the other metrics, with PR active lever presses showing the most variability between high and low, and foodtray showing an inverse pattern (low risk rats trended towards more head entries.) Increasing the number of classes to four revealed new subclasses that were previously hidden: a high PR subclass (Figure 3B, blue) and a high foodtray subclass (Figure 3B, red.) Class four appeared to represent the lowest of the low heroin takers, and class three failed to distinguish itself across any metric. Throughout this dissertation, the two-class model is generally utilized when making comparisons or for visualization purposes (metrics split by class are shown in Figure 2, panels K-O.) However, the subgroups that were revealed with an increasing number of classes will be revisited and investigated when statistically feasible. Although limitations in number of subjects led us to select a two-class high/low classification system in most cases, entropy values for three and four classes improved over the two-

class model, suggesting that addiction risk in rats is more of a spectrum than a binary "evidence of addiction risk" vs. "no apparent risk" dichotomy.

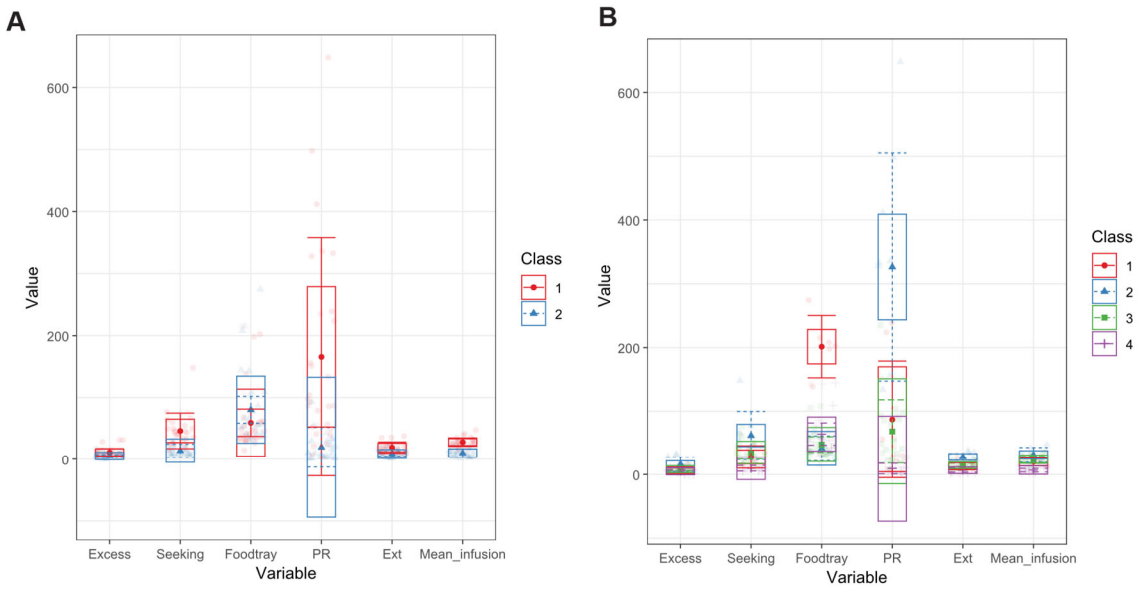

Figure 3: LPA-derived classifications of subjects with two (A) or four (B) classes selected. Entropy value is 0.824 for two classes and 0.912 for four.

Principal component analysis to further characterize the spectrum of addiction-related behaviors: Principal component analysis (PCA) is a widely used tool for dimensionality reduction of large and complex datasets. It facilitates identification of "principal components", or combinations of variables explaining percentages of the variance in the dataset, which are then ranked in numerical order based on the relative share of the variance that they explain. When selecting principal components for use in downstream analysis, it is generally recommended to choose PCs cumulatively explaining at least 80% of the variance in the dataset. Beyond 80%, the utility of additional PCs is often minimal, but an argument can be made for including them when analyzing

extremely large and complex datasets. Performing PCA on the addiction metrics for each rat resulted in the identification of six PCs. PC1 explained 53.73% of the variance and separated the rats via combinations of addiction metrics, with the largest contributions from extinction (0.233), mean infusion (0.219), and seeking (0.220). PC2 explained 16.3% of the variance and was primarily defined by food tray head entries (0.868), while PC3 explained 15.12% and was defined by excess (0.458) and PR (0.291). Taken together, both LPA and PCA demonstrate that binary separation of rats into high/low classifications is best accomplished with mean infusions, mean extinction presses, and seeking. High/low binary classifications made via class assignment (LPA) or directionality in PC1 (PCA) are nearly identical, with only 1/56 rats showing a mismatch between the two (LPA designates this rat as high, but its PC1 score is -0.116, trending towards the low rats.) Due to this broad cross-validity, we can simultaneously utilize LPA for classification and PCA for visualization and downstream quantification of changes in addiction risk state, which will become necessary in Chapter Four. Additionally, both methods also make apparent two subgroups of rarer behavioral phenotypes: high foodtray (Figure 3B, class 1), low foodtray (Figure 4A, bottom left quadrant), and high PR and excess (Figure 3B class 2, figure 4A top right quadrant.) These subgroups generated two new hypotheses: first, that increasing propensity for exploratory behavior during intSA sessions is associated with decreased addiction risk, and second, that measures of increased motivation for heroin (PR and excess) are only significantly increased in "ultra-high" addiction risk rats, not in the general population. If true, this may be accompanied by distinct adaptations to reward circuitry.

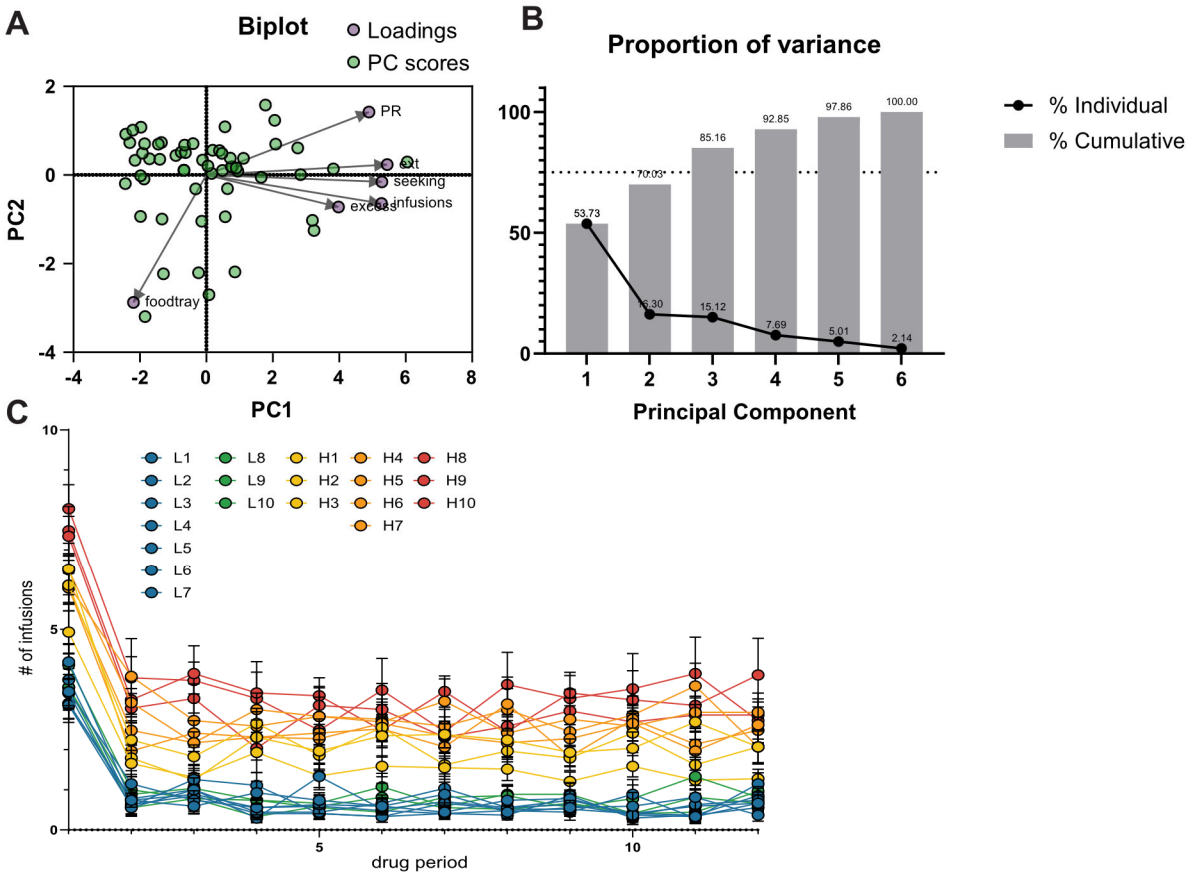

Figure 4: PCA illustrates contribution of each addiction metric to a full addiction phenotype. (A) Biplot depicting loadings (purple) and PC scores (green) for each subject. (B) Relative proportion of variance explained by each PC. (C) Distribution of infusions across drug periods for subjects in low "L" or high "H" addiction risk groups, separated by day of SA.

Section IV: Unsupervised machine learning approaches to capture a spectrum of naturalistic and opioid-induced behaviors during self-administration

Relatively little information is available to describe the effects of acute and chronic opioid self-administration on spontaneous rat behaviors (beyond locomotion.) To address this gap, we installed cameras into ten behavioral boxes and recorded male and female rats throughout all stages

of self-administration. To facilitate discovery of novel behavioral patterns, we chose to prioritize development of an unsupervised, machine-learning based behavioral analysis pipeline consisting of three stages: pose estimation and tracking, identification of stereotyped transition points of behaviors or "syllables," and downstream analysis of frequency, duration, and mean velocity of each syllable.

Pose estimation and tracking with SLEAP: Social LEAP Estimates Animal Poses (SLEAP) enables machine-learning based animal tracking via either top-down or bottom-up neural network based approaches.[84] SLEAP was optimized to allow accurate tracking of multiple animals in a single field of view, but also has single-animal tracking capability. We chose to proceed with SLEAP for pose estimation largely due to the sizeable quantity of input data to be tracked, as we found it to be the most efficient option for rapid training and testing of pose estimation models. Initial models utilized a complex skeleton and were limited by slow tracking speeds and low accuracy of keypoints (skeleton nodes.) After dropping out forelimbs and hindlimbs from the skeleton (which are frequently invisible in our top-down recordings), accuracy and speed in tracking dramatically increased, likely due to increased confidence in predictions for the remaining nodes.

Once a satisfactory model was trained, we next needed a high-throughput system for behavioral tracking. All sessions were recorded at 30 FPS, including 5h35 min daily SA sessions. Fully tracking each session created a bottleneck, as tracking time with the most accurate model took approximately 1.6x the video duration (~8.8 hrs to track one SA session.) The end goal of this project was to create an "in-the-loop" analysis pipeline, where behavior could be analyzed in real time after each session and used to generate a prediction regarding addiction risk. Thus, to assess which segments of SA sessions would be highest yield to include, we classified each infusion event recorded across all past cohorts by the DA period that it occurred in, based on the event's

timestamp (Figure 4C.) This analysis revealed that the highest-activity DA period for infusions was the first period, as expected, and that all other periods were statistically equivalent. After splitting rats by LPA class (low or high) and separating each day of SA, a stepwise trend of escalation in sum infusions became apparent in the high-risk rats, with a faint suggestion of a similar trend during days 8-10 in low-risk rats. Based on these observations, no strong argument could be made for the inclusion of any specific DA segment except DA1. We considered using a randomly selected second segment for each day, or using DA12, which would allow for maximal recovery from escalated DA1 heroin infusions, but for now have chosen to proceed with the first 30 minutes of each training, SA, PR, and extinction sessions. For SA days, this included DA1 (5 minutes) and DU1 (25 minutes.)

Identification of common behavioral syllables with Keypoint-MoSeq: Successful tracking results in a matrix of predicted skeleton node positions, or keypoints (neck/catheter, nose, left ear, right ear, and tailstart/centerpoint of rat rear), for each frame in each video. Although substantial effort has and is being placed on training accurate tracking models, for now the reality is that these datasets will always be vulnerable to error, especially in sub-optimal recording environments (which surely includes our behavioral apparatus.) Keypoint-MoSeq is a powerful tool for analyzing pose estimation data to make predictions about "syllables", or transitions from one behavioral state to another, while correcting for "jitter", or stochastic deviations of keypoints while the mouse is still due to tracking error.[85] This process begins with PCA-based analysis of keypoints, then is followed by iterative identification of syllables over a behaviorally relevant timescale. The length of time required for running MoSeq is dependent on the number of input prediction matrices: syllable identification based on four days of training and ten days of IntSA took approximately ~45 hours on a specialized analysis computer. To make statistical comparisons between animals, they must share a common syllable framework, making the choice of input data for syllable discovery quite an important one. Given that quality of syllables seems to improve with greater volumes of input data,

we chose to run all training and IntSA sessions through MoSeq together to obtain a "drug-on" set of syllables, then did the same for all PR and extinction sessions to detect "drug-off" syllables. We considered whether PR sessions should be instead grouped with IntSA, as animals can receive multiple infusions during PR if they are highly motivated, but qualitative assessment of high-addiction risk rat behavior during these sessions was more similar to early extinction than to late SA.

Each identified syllable was given a short label summarizing the common denominator of behavioral activity observed during representative videos generated by the MoSeq pipeline. For most syllables, clear patterns of rat movement were apparent: for example, syllables labeled "turn" connote a sudden change in head angle. "Investigate" was used to describe syllables in which the rat was actively moving throughout the enclosure, while "sniff" was more specific for a small, isolated head movement. Rats were very often initiating or emerging from grooming behaviors during syllables, which can look identical to sniffing the environment from the perspective of keypoints alone. As a result, a few syllables received the label "mixed" because the rats were performing a similar movement, but in diverse behavioral contexts (some sniffing, some grooming, some exploring.) Syllables were broadly classified into four categories: neutral (including turns and mixed syllables), self-directed (grooming, sniffing close to body), environment-directed (investigation, rearing, outward head movements), and movement (high-amplitude or abrupt movement, ex. running, jumping.)

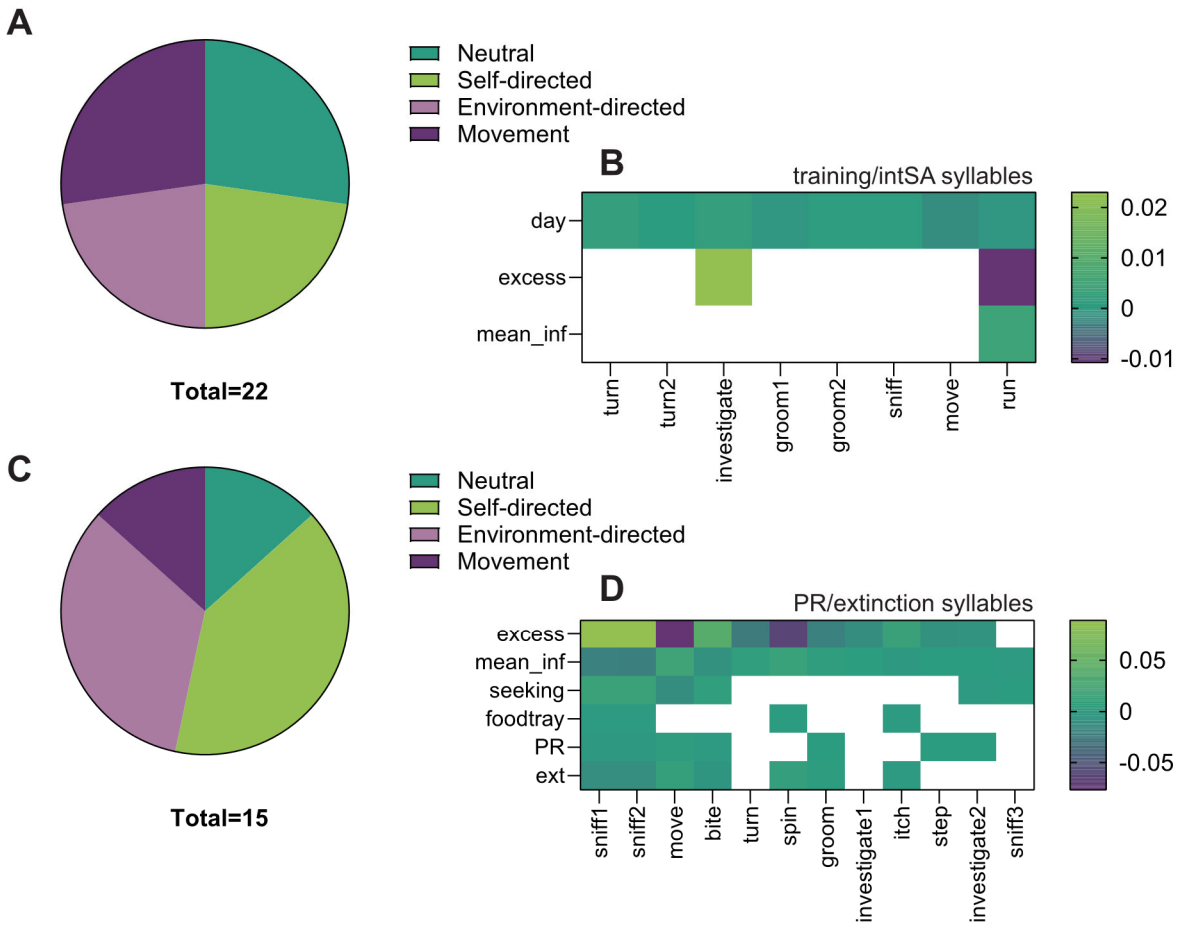

Figure 5: Machine-learning based keypoint analysis of behavioral syllables enables tracking of intSA-associated behaviors across days, with a distinct behavioral phenotype of high-addiction risk rats emerging primarily during drug-free sessions. (A, C) Qualitative classifications of each detected syllable during training/intSA (A) and PR/ext (C). (B, D) GLM coefficients from discovered significant relationships between syllable frequency, SA day, or behavioral metric.

Downstream analysis of keypoint and syllable data:

Two sets of syllables were produced from this cohort, the first based on training data from training day 1 to day 10 of intermittent SA (intSA syllables) and the second based on training data from the PR sessions and days 1-3 of extinction (post-SA syllables.) Whereas intSA syllables were

evenly distributed across the four categories (Figure 5A), post-SA syllables were biased towards self-directed and environment-directed behaviors (Fig 5C). First, we used a GLM to test relationships between syllable frequency/duration, day of SA, and addiction risk metric for a pre-selected subgroup of int SA syllables.

```
syllable frequency/duration ~ day + excess + foodtray + PR + ext + mean_inf
```

Formula 2: GLM for evaluating relationships between behavioral syllables, time, and addiction metrics for each animal.

This revealed a strong effect of day on most syllables tested, with investigative and self-directed behaviors becoming more frequent, and running and abrupt movements becoming less frequent (Figure 5B.) Longer running bouts during SA corresponded with higher PR and extinction responding, suggesting that animals that are hyperlocomotive during SA are more motivated for drug and more resilient against extinction. Post-SA syllables showed many more significant relationships with addiction metrics, but these relationships were more nuanced than expected (Figure 5D.) Rats with more excess presses (potentially the most addicted), showed much higher frequency of syllables 0 and 1, both self-directed syllables involving sniffing close to body. They also downregulated the environment-directed syllable 3 (investigating while moving about) and movement syllable 6 (rear/spin.)

Additionally, we used Moseq's built-in statistical model to test differences in frequency of each syllable between the four PCA-based behavioral groups: low investigative (low addiction metrics, high foodtray), low non-investigative (low addiction metrics, low foodtray), and high non-investigative (high addiction metrics, low foodtray.) High investigative animals were present in this cohort but were not represented amongst animals with cameras and will be assessed in later cohorts. Testing for differences in frequency in intSA syllables across all groups and all days resulted in no

significant changes, however, high rats tended to upregulate usage and transitions of syllables 8 and 9 (move2 and run, both "movement" syllables.) Given that these syllables became less frequent over days of SA, they may represent a hint of a hyperlocomotive high-risk phenotype, which later becomes blunted as the rats engage in SA and receive opioid rewards. Unsurprisingly, high addiction risk rats showed many differences in syllable frequency during PR and early extinction (Figure 6C). However, when comparing all three PCA groups present in this cohort, the observed alteration in high rat behavior looks less like a unique signature of addiction and more like a class switch between two different locomotor phenotypes. During SA, rats display homogenous behavior on the syllable level, with investigative rats identifying themselves only through rates of foodtray head entry. Since MoSeq is blind to everything in the behavioral apparatus except the rat itself, this is not surprising. In the post-SA period, separate behavioral profiles become appreciable, with the behavior of high-risk rats closely tracking along with the LN (low non-investigative) rats. As far as we can tell, these rats are characterized by relative behavioral arrest compared to their LI (low investigative) counterparts.

Section V. Summary

Leveraging cutting-edge machine learning behavioral tools, we have successfully tracked rat pose throughout the self-administration paradigm and generated two distinct lists of behavioral transitions associated with self-administration and early withdrawal. As most of our studies focus on the late withdrawal timepoint, we plan to analyze these sessions in the future but were stymied with this cohort by late technical difficulties. In the future, we plan to utilize these tools to observe differences in rat behavior before and after genetic intervention onto addiction circuits, one example of which is described below in Chapter Four. We also hope to implement drug-free recordings prior to the start of self-administration, as it would be helpful to get a baseline for each rat. This may

provide context for determining where future high-risk rats lie on the locomotion/investigation spectrum.

Despite these limitations, several observations from this work have provided actionable information about low and high-risk rats. First, we noted a subtle signature of hyperlocomotion in future high-risk rats, which fades as the rats become habituated to the behavioral apparatus and begin escalating their heroin intake. In early withdrawal, this pattern reverses, and high-risk rats engage in more self-directed behaviors, only distinguishing themselves from LN rats by a uniformly increased mean velocity across most syllables. Another remaining question is whether either LI or LN rats are more likely to represent a moderate risk level (that may engage in escalated heroin-taking after some insult): this topic will also be revisited in Chapter Four.

Chapter Two: Whole-brain activity profiling of high and low risk rats after protracted opioid withdrawal and reinstatement

Section I: Experimental design and hypotheses

The goal of this experiment was to assess whether high and low addiction risk rats differ in baseline and or cue-evoked neuronal activity, measured via whole-brain cFOS immunohistochemistry (IHC), after heroin IV self-administration and withdrawal. n = 18 male and female rats underwent heroin intSA as previously described, with a subset (n = 16) also undergoing a cue-induced reinstatement session at the end of the extinction period. This session occurred ~1 hr prior to paraformaldehyde perfusion and tissue collection, while all other rats were collected 1-2 days following their last extinction session. An additional group of four home-cage controls (2M, 2F) was added to facilitate normalization of cFOS to a drug-naïve baseline. cFOS IHC and whole-brain clearing was performed by the Golden lab utilizing iDISCO[86], which resulted in near-total tissue clarity and excellent signal:noise ratios in immunolabeling (Figure 7B.)

Since all animals were collected at a timepoint that is likely to correspond with protracted withdrawal symptoms (if they engaged in heroin SA), the non-reinstatement groups are labeled as high risk, withdrawal and low risk, withdrawal. High and low risk designations correspond to their LPA class assignments using a two-class model. It is important to stress that withdrawal severity is expected to differ between these two groups: as such, we hypothesized that high addiction risk rats were likely to display elevated cFOS in regions previously associated with negative affect in withdrawal, including amygdala, NAc, PVT, lateral habenula (LHb), and insular cortex. Groups that underwent cue-induced reinstatement are labeled high addiction risk, reinstatement, and low addiction risk, reinstatement. For these animals, we expected specific re-engagement of reward and motivation related circuitry, possibly to include VTA, NAc, and mPFC. That said, one major

rationale for this experiment was the opportunity to uncover new brain regions that were not previously known to play a role in mediating or driving symptoms of protracted withdrawal from opioids. When collecting and analyzing large and complex datasets like these, the potential for spurious findings can be high if not appropriately addressed at every step possible. Thus, to successfully analyze this dataset, we first needed to conceptualize and validate new methods with which we could rigorously test whether animal-to-animal fluctuations in cFOS in novel brain regions are related to their addiction risk status (rather than representing random noise.)

Section II: Computation methods for alignment and segmentation of volumetric rat whole brain imaging data

Registration of volumetric images to the rat brain atlas with ClearMap: For alignment of light sheet images to a rat reference atlas, we utilized the Waxholm Space Atlas, an MRI-based volumetric rat brain atlas,[87] in conjunction with ClearMap[88], a Python-based software platform for alignment and segmentation of whole-brain clearing data. No established framework previously existed for specific alignment of whole-brain data in rat. We substituted the mouse atlas for the rat atlas in ClearMap and adjusted parameters accordingly to maximize alignment accuracy. A hierarchal label file defining parent and leaf nodes for each brain region annotated in the Waxholm Space Atlas was provided to us directly by the team at eBRAINs, which was used to label each segmented neuron within each ROI delineated by the atlas. During alignment, a small subset of brains was noted to have mild to moderate areas of deformation or damage. Since these areas were always restricted to one hemisphere, damaged hemispheres were noted and excluded from further analysis. For brains with two undamaged hemispheres, one hemisphere was selected for analysis, counterbalanced between sex, addiction risk status, and experimental group. Non-selected hemispheres were never analyzed.

Machine-learning based segmentation of cFOS+ neurons with the Ilastik pixel classifier: ClearMap has a built-in cell segmentation algorithm, but results obtained by this method were highly variable between animals. We hypothesized that this variability was due to variation in signal:noise ratio between animals, which can occur both due to differences in cFOS density and in background, nonspecific antibody binding. To definitively address this issue, we trained a pixel classifier to count cFOS+ neurons using Ilastik[89], which uses a machine-learning based framework to rapidly classify pixels as either belonging to cells or to background. The pixel classifier was trained on images randomly selected from standardized z-ranges, with the goal of ensuring that all brain regions would be accurately segmented. All animals, including control animals, were included while training and testing the classifier (using the same number of images from each animal to avoid over or under-representation in the training pool.) The training process was deemed complete once the classifier had been tested on all animals and was able to accurately segment cFOS+ neurons in sparse and dense conditions alike, while reliably excluding artifacts. Extremely dense cFOS signal was likely undercounted, as it became impossible to train the classifier to capture clusters of cFOS+ neurons without clear borders without also allowing it to overcount elsewhere.

Alignment and segmentation were performed using two high-performance computational resources: UW's Hyak and PSU's Bridges system, made available via an NSF Access grant. Once alignment and segmentation were complete, each brain region within each subject was then z-scored to the mean of the home cage control group. All downstream analysis was completed using these z-scores (Figure 6C.)

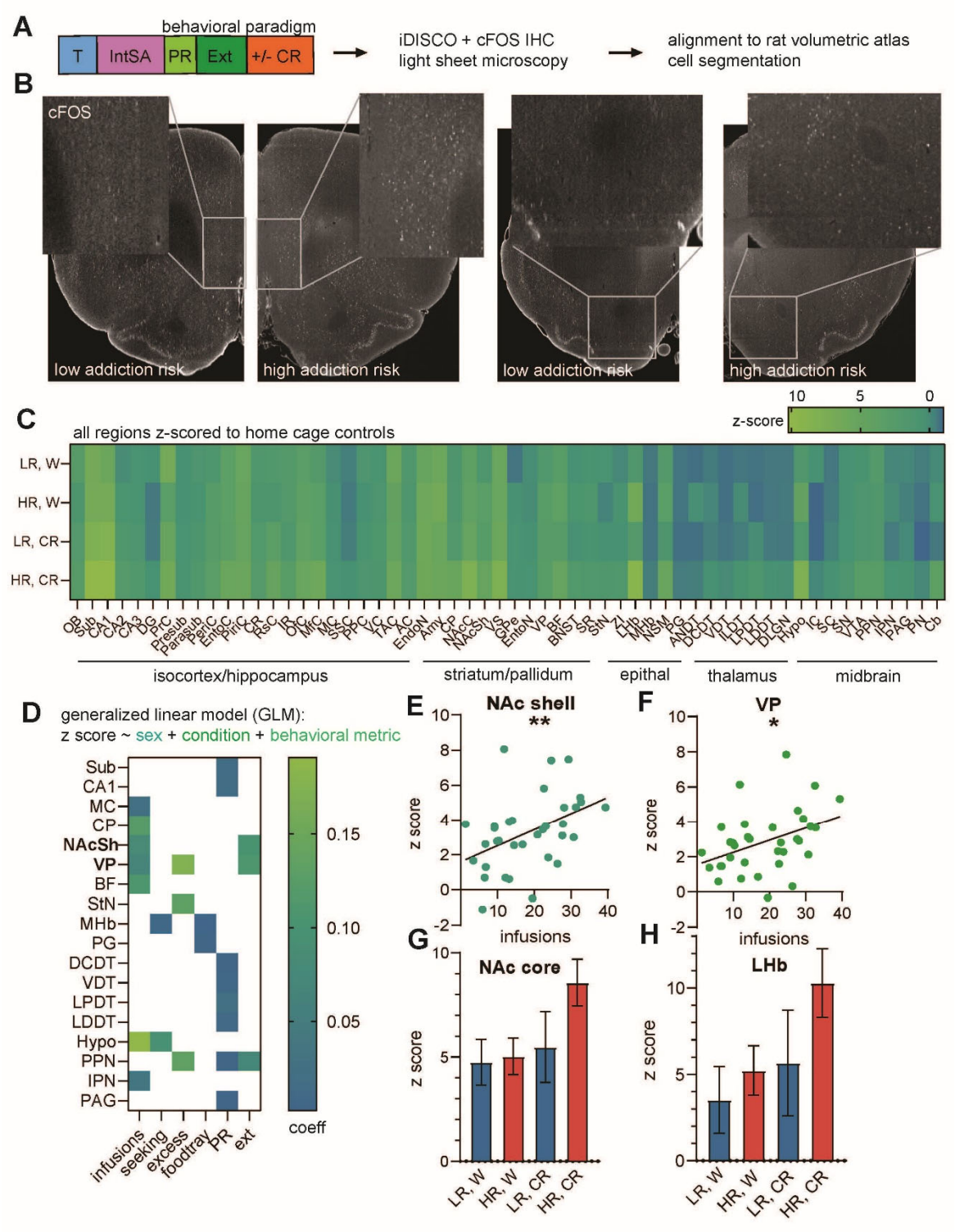
A
behavioral paradigm
T
IntSA
PR
Ext
+/- CR
iDISCO + cFOS IHC
light sheet microscopy
alignment to rat volumetric atlas
cell segmentation
B
cFOS
low addiction risk
high addiction risk
low addiction risk
high addiction risk
C
all regions z-scored to home cage controls
10
5
0
z-score
LR, W
HR, W
LR, CR
HR, CR
OB Sub CA1 CA2 CA3 DG PrC Presub Parasub PeriC EntoC PirC CR RsC IC OFC MFC MC SSC PPC VC TAC AC EndoN Amy CP NAcC NAcSh VS GPe EntoN VP BF BNST SR StN ZI LHb MHb NSM PG ANDT ADCDT VDT ILDT LPDT LDDT DLGN Hypo IC SC SN VTA PPN IPN PAG PN Cb
isocortex/hippocampus
striatum/pallidum
epithal
thalamus
midbrain
D
generalized linear model (GLM):
z score ~ sex + condition + behavioral metric
Sub
CA1
MC
CP
NAcSh
VP
BF
StN
MHb
PG
DCDT
VDT
LPDT
LDDT
Hypo
PPN
IPN
PAG
infusions
seeking
excess
foodtray
PR
ext
0.15
0.10
0.05
coeff
E
NAc shell
**
z score
infusions
F
VP
*
z score
infusions
G
NAc core
z score
LR, W
HR, W
LR, CR
HR, CR
H
LHb
z score
LR, W
HR, W
LR, CR
HR, CR

Figure 6: Alterations in whole-brain activity state as a function of addiction risk behaviors in protracted heroin withdrawal. (A) Experimental design and analysis pipeline. (B) Representative images of whole-brain clearing/cFOS IHC from high and low addiction risk rats. (C) Brain-wide z scores within each experimental group. 1-way ANOVA $p = 0.0013$. (D) Generalized linear model coefficients from regions with significant correlations between cFOS z scores and addiction risk metrics. (E-F) Uncorrected correlations between infusions and cFOS z scores in the nucleus accumbens shell (E) and ventral pallidum (F.) (G-H) Selected regions (NAc core, G, lateral habenula, H) with significant differences after 2-way ANOVA with multiple comparisons. NAcC HR, W vs. HR, CR $p = 0.0078$. NAcC LR, CR vs. HR, CR $p = 0.0458$. LHb HR, W vs HR, CR $p = <0.0001$. LHb LR, CR vs. HR, CR $p = 0.0006$.

Section III: A generalized linear model facilitates statistical testing for relationships between addiction risk metrics and brain-region-specific induction of cFOS

The first step in downstream analysis of this data required choosing a level in the rat atlas hierarchy. Immediately, it became clear that this was not a simple task, as some regions were highly parcellated (dozens of subregions for thalamus) and others were not parcellated at all (instead of basolateral and central amygdala, we have only "amygdaloid area unspecified.") Due to the lack of consistency in which regions received multiple leaf nodes, we decided to proceed at an experimenter-selected atlas level containing 58 regions with no overlap, spanning from the olfactory bulb to the cerebellum.

Next, we performed a 1-way ANOVA between all experimental groups with multiple comparisons. As expected, this indicated significant differences between all groups ($p = 0.0013$.) Out of all possible multiple comparisons, three were significant: HR vs LR in reinstatement ($p = 0.0114$), HR reinstatement vs HR withdrawal ($p = 0.0132$), and HR reinstatement vs LR withdrawal

($p = 0.0022$.) These findings illustrated a few crucial points: first, high addiction risk rats display increased brain-wide cFOS compared to LR rats, but only following re-exposure to the drug related cue stimulus. Within addiction risk group, only high-risk rats displayed a stepwise increase in cFOS after reinstatement. Additionally, the HR reinstatement group encapsulated the most polarized average cFOS z scores in most brain regions (Figure 6C.) As we had hypothesized that protracted withdrawal would be associated with activity in specific regions, not brain-wide cFOS induction, it was not surprising that HR and LR rats failed to differentiate themselves in the withdrawal condition. In summary, reinstatement is associated with increased cFOS, but only in high addiction risk rats. This nicely validated the previous findings from the Ferguson lab and supports the hypothesis that high addiction risk rats have distinct and long-lasting engagement of motivational circuitry.

But which specific regions are most important in driving these between group brain-wide differences in cFOS? To address this, we utilized a 2-way ANOVA to compare cFOS z-scores within each brain region. This test revealed a relatively short list of regions with significant differences between groups, including retrosplenial cortex, caudate/putamen, nucleus accumbens core (Fig 6G), lateral habenula (Fig 6H), dorsal thalamus, and hypothalamus. Hypothalamus was particularly notable for being the only region with a high/low difference in the withdrawal condition. Visual evaluation of the spread of the data points within each region quickly made it apparent why so few regions displayed between-group differences: cFOS z-scores from high and low rats in every brain region analyzed rarely separated in a binary pattern: instead, they looked much more like a spectrum. As we learned in Chapter One, although it is possible to validly divide each experimental group of rats using a two-class model, a multi-class model fits better and more completely reflects the wide behavioral variability found within those groups. For advice on how best to proceed, we reached out to the Witten group at UW, who have previously collaborated with the Stuber lab on

several challenging statistical dilemmas. Statistics grad student Ethan Ancell recommended a generalized linear model for testing relationships between addiction risk metrics and cFOS z-scores. After some adaptation, the final model we utilized was as follows:

```
cFOS z score ~ sex + condition + behavioral metric
```

Formula 3: Generalized linear model setup. Condition was specified as E (extinction, or protracted withdrawal timepoint alone) or R (protracted withdrawal + cue-induced reinstatement.) Behavioral metrics were tested individually due to high levels of correlation between most metrics.

This approach assigned each region for each animal a coefficient and a p-value. After filtering for p-values < 0.05, we compared the scale and directionality of coefficients (Figure 7D.) Significant regions for each metric are listed below:

Infusions: Motor cortex, caudate putamen, NAc shell, VP, basal forebrain, hypothalamus, and interpeduncular nucleus

Seeking: Medial habenula, hypothalamus

Excess: VP, subthalamic nucleus, peripeduncular nucleus

Foodtray: Medial habenula, pineal gland

PR: Subiculum, CA1, dorsal-caudal midline group of the dorsal thalamus, ventral nuclei of the dorsal thalamus, lateral posterior nuclei of the dorsal thalamus, laterodorsal nuclei of the dorsal thalamus, periaqueductal gray

Extinction: NAc shell, ventral pallidum, peripeduncular nucleus

The first pattern we noted was the specific engagement of canonical reward and motivation circuitry with increasing infusions (NAc shell, VP, basal forebrain, hypothalamus) and extinction

responding (NAc shell, VP.) The conservation of NAc shell and VP as related to both infusion history and extinction responding could represent specific recruitment of the indirect D2 MSN-dominated striatal-pallidal pathway in high-risk rats. Cue-induced reinstatement responding was also tested in the model and surprisingly was only significantly correlated with paw somatosensory and motor cortex. Although this provides striking face validity for the use of cFOS as a proxy for neural activity (as cFOS in those regions rose significantly with increasing recent history of lever presses), the lack of any other correlated regions indicates that increased responding during reinstatement is not necessarily indicative of increased engagement of addiction-related circuits. Conversely, it is possible that these circuits (particularly mPFC) become inhibited during this "uncontrolled" responding, which we are not powered to detect with cFOS: we will specifically address this question in Chapter Three.

Due to the lack of significant relationships between increasing reinstatement responding and cFOS, we chose to pool withdrawal and reinstatement rats but kept condition as a variable in the GLM. This allowed us to correct for any small effect of reinstatement outside what was previously noted in somatosensory and motor cortex, while increasing our statistical power to assess relationships with the other addiction metrics. Even after doing so, some motor regions still came out as significantly related to increasing infusions, which likely reflects the increased motor activity of HR rats during reinstatement. Another surprise uncovered by the model was the appearance of medial habenula and its projection target, the interpeduncular nucleus, as significantly correlated with infusions and off-target activity (foodtray). This circuit has been highly studied in the context of nicotine use disorder, as the IPN is highly enriched in nicotinic receptors and receives cholinergic input from the MHb.[90] IPN cFOS is increased after anxiety-provoking environments, and silencing IPN-Drd3 neurons that receive MHb-Substance P inputs reduces anxiety behaviors in mice.[91] Additional validation is needed to determine whether this circuit may become dysregulated during

protracted withdrawal from opioids. In Chapter Two, we found that rats with increased exploration or investigative activity (i.e. foodtray head entries) were more likely to be low-risk, suggesting a potential protective role for the MHb-IPN circuit against escalation of heroin intake.

Progressive ratio responding was associated with a unique signature of regions, including multiple groups of dorsal thalamic subregions. The four-group LPA model selects high-PR responding animals as their own group, separating themselves via their high motivation for heroin. They also tend to score highly on the other metrics, making a strong case for designation of these rats as the "most addicted." CA1 and subiculum are nodes in the hippocampal tripartite circuit, which aids in recruitment of cortical and subcortical areas to support learning and memory. This circuit, along with PVT, may be providing enhanced glutamatergic input to the NAc in these potentially super-high risk rats. Periaqueductal gray (PAG) is notable for its high native expression of the μ-opioid receptor, and has been previously well-characterized for its role in top-down pain processing[92], but the specific mechanistic connection between PAG μ-opioid agonism and pain regulation has not been fully eludicated.[93] Out of all the regions with a significant cFOS z score correlation, only PAG fits the criteria for a "negative affect" or "pain" related, which we had hypothesized would make up the majority of regions with elevated cFOS in protracted withdrawal. An additional group collected during acute withdrawal would have been a helpful comparator to ascertain whether lack of cFOS in amygdala, insula, and LHb was related to true lack of physical withdrawal symptoms at this late timepoint.

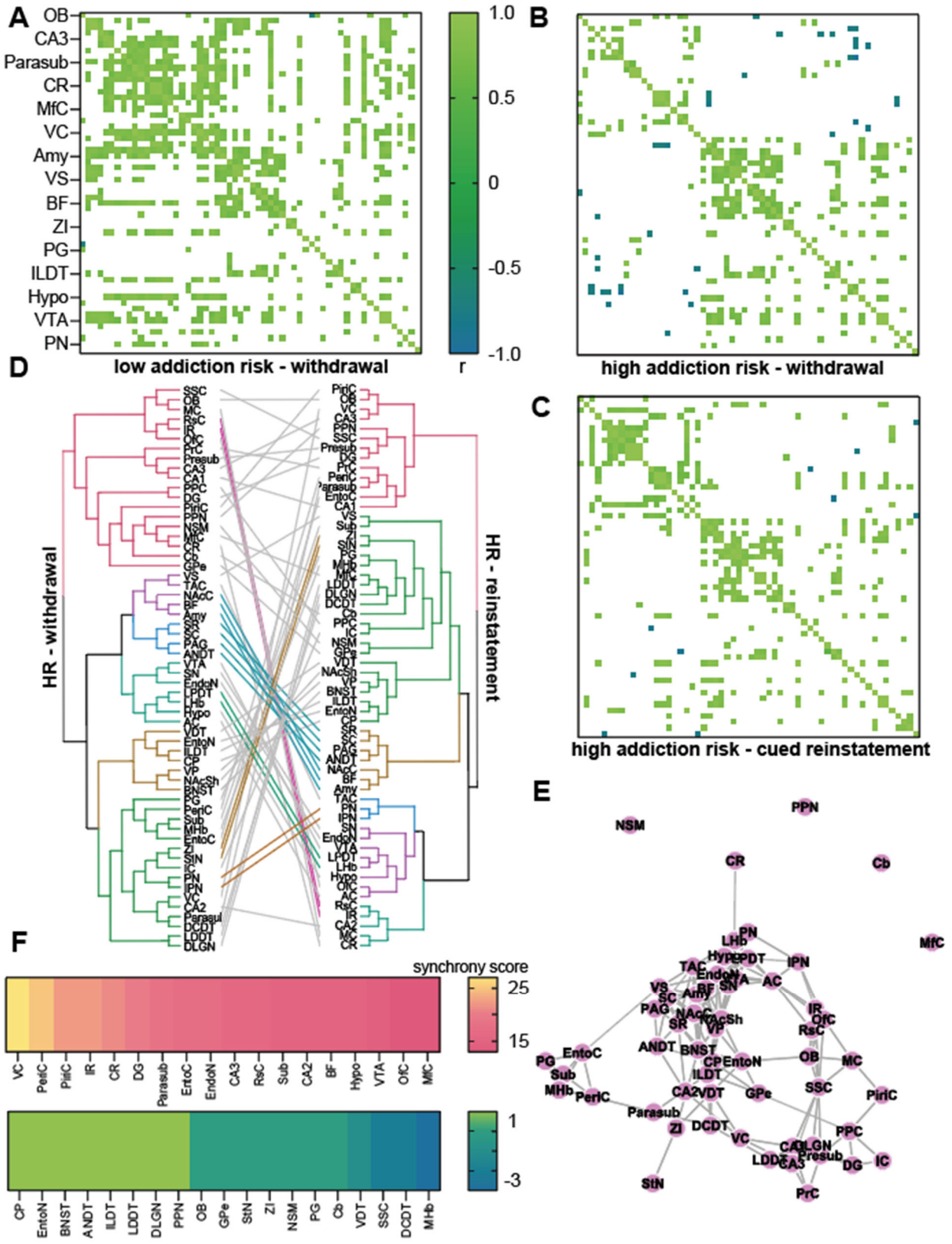
A
OB
CA3
Parasub
CR
MfC
VC
Amy
VS
BF
ZI
PG
ILDT
Hypo
VTA
PN
low addiction risk - withdrawal
1.0
0.5
0
-0.5
-1.0
r
B
high addiction risk - withdrawal
C
high addiction risk - cued reinstatement
D
HR - withdrawal
HR - reinstatement
E
F
synchrony score
25
15
1
-3

Figure 7: High addiction risk rats are uniquely characterized by loss of correlated cFOS z-scores in frontal and parahippocampal brain regions. (A-C) Significant ($p < 0.05$) r scores for each brain region in low risk and high-risk rats in withdrawal (A, B) and high-risk rats after cue-induced reinstatement (C). (D) Hierarchal clustering on significant r values in high-risk rats. Colored lines highlight conserved positions between withdrawal and reinstatement groups. (E) Network constructed from correlations in high addiction risk group, withdrawal. (F) Brain regions ranked by synchrony score (# of correlated brain regions in low addiction risk, withdrawal - # of correlated brain regions in high addiction risk, withdrawal.)

Section IV: Network analysis reveals loss of correlated cFOS z-scores in high addiction risk rats

To assess brain-wide coordination of neuronal activity in each condition, we tested for significant within-group correlations in cFOS z-score in each brain region. In low addiction risk animals, these correlations were generally positive ($r > 1$) and were most concentrated between cortical and parahippocampal regions (Figure 7A). Strikingly, these correlations were almost entirely lost in high addiction risk rats, with only subtle re-engagement of cortical and subcortical regions in the cue-induced reinstatement group. Hierarchal clustering of high addiction risk rats in the protracted withdrawal (Figure 7D, left) and cue-induced reinstatement (right) conditions revealed well-preserved clusters of brain regions with similar brain-wide cFOS correlation profiles. One cluster, consisting of NAc core, basal forebrain, amygdala, septal region, superior colliculus, PAG, and the anterior nucleus of the dorsal thalamus, is particularly notable for its enrichment of negative affect/withdrawal-related brain regions. Although cFOS was not significantly increased in each of these regions as a function of increasing addiction metrics (just BF and PAG), their similar correlation profiles suggest that these regions may be involved in a co-regulated withdrawal circuit.

Specific visualization of connectivity of each node in the high addiction risk, protracted withdrawal group revealed four regions with zero significant correlations: nucleus of the stria medullaris, peripeduncular nucleus, cerebellum, and mediofrontal cortex (which contains prelimbic and infralimbic cortex as lower leaf nodes.) This pronounced loss of correlation between mediofrontal cortex and the rest of the brain seems to mirror what was observed in human fMRI studies characterizing "hypofrontality," or loss of coordinated brain activity in mPFC with prior history of escalated opioid use. Finally, to rank brain regions based on their relative correlated-ness, we computed a "synchrony score" for each region by subtracting the number of regions it was positively correlated with in the high addiction risk group from those it was positively correlated with in the low addiction risk group. Close to orbitofrontal and mediofrontal cortex in the "medium synchrony score" category was the VTA, which like PFC was conspicuously absent from the GLM output of significant relationships between cFOS z scores and addiction metrics. We cannot directly detect inhibition with cFOS, but the pronounced loss of correlated cFOS z scores observed in high synchrony score regions can be inferred to be due to loss of relative activity, suggesting that VTA and MfC may enter a net-hypoactive state in high addiction risk rats during protracted withdrawal. The MHb was one of only a handful of regions with a negative score (gains correlations in high addiction risk group) despite clustering together with regions with high synchrony scores, again implying that it may play a unique role in opioid addiction risk.

Section V: Summary

The differences in cFOS signatures quantified here were roughly consistent with our hypotheses, with several significant exceptions. Considerable evidence supports the idea that high-risk animals with escalated opioid intake will have distinct neuronal activity profiles, as reviewed in Chapter One. However, all rats compared in this experiment underwent surgery and weeks of

operant behavior, during which they all self-administered heroin, rendering them much more similar than subjects in studies comparing acute drug treatment to a sham injection. Furthermore, all rat brains were collected for the study during protracted withdrawal, without any opioid drugs on board. After considering these factors, it seems logical that subtle differences in behavior would result in only subtle differences in cFOS, which needed to be carefully uncovered via alternative analytical methods. However, there was one crucial deviation from this pattern: the striking loss of correlated z-scores in cortical and parahippocampal regions of high-addiction risk rats. Another surprising result was the failure of the cue-induced reinstatement session to re-engage reward and motivation circuitry, despite being associated with a broad increase in brain-wide cFOS. This may in part be due to overall limited responding during these sessions, as some rats robustly reinstated their pressing, but many were relatively indifferent to the cue stimulus (Figure 2D.) Evidence exists to support a role for PL inactivation in potentiating cue-induced reinstatement of cocaine seeking, as inhibition of PL-RMTg projections specifically disrupted cue-induced reinstatement, but not drug-induced reinstatement.[94] Thus, after future cue-induced reinstatement tests it may be more prudent to assess neuronal inhibition rather than excitation, at least in mPFC. If this experiment were expanded upon in the future, additional time points during early withdrawal (48-72 hours post last session) and very late withdrawal (day 14+) would further clarify the trajectory of the alterations we observed (is cFOS within each region turning on, fading away, or staying consistent as physiological withdrawal transitions to protracted withdrawal?)

Three brain regions that emerged from this analysis as compelling enough to stand alone were NAc shell, VP, and mediofrontal cortex. NAc shell and VP showed significant correlations with both infusions and extinction responding (Figure 6, E-F), while MfC showed a complete loss of correlation with cFOS z scores in all other brain regions in the high risk, withdrawal condition (Figure 8E.) To interrogate which neurons become most perturbed in each of these regions, and to

better understand the local "balance of power" amongst projection neurons, interneurons, and glia between low and high-risk rats, we went on to perform snRNAseq in NAc, VP, and PL (the MfC subregion of greatest interest.) Analysis of this data illustrated which neurons may be most crucial in contributing to a "hypofrontality-like" phenotype.

Chapter Three: Identifying and comprehensively characterizing opioid-perturbed cell types with single nuclei RNAseq

Section I: Rationale, experimental design, and hypotheses

The development and gradual technical streamlining of single nuclei RNA sequencing (snRNAseq) technology over the past ~10 years has massively expanded the ability of neuroscientists to explore and characterize a wide variety of cell types in the mammalian brain, as well as to characterize alterations in these cell types following various insults. The Stuber lab was an early innovator in this field, using single cell RNAseq technology to characterize subsets of lateral habenula neurons responsive to shock[95], lateral hypothalamus neurons projecting to the VTA and LHb[96], and in collaboration with the Palmiter lab, neurons of the parabrachial nucleus.[97] More recently, this approach has facilitated the discovery of lateral septum GABAergic neurotensin-expressing neurons as crucial modulators of acute opioid withdrawal symptoms[98], and revealed cross-species conservation of VP cell types.[99] Reproducibly identifying cell types in snRNAseq data has become gradually more straightforward due to the wealth of data available, although exponentially increasing granularity in cell types can also complicate statistical comparison, creating a dilemma (should we parcellate cells down into the most homogenous possible groups, limiting our power to make comparisons across conditions, or should we lump together heterogenous cells, perhaps diluting biological effects?) It is also important not to over-interpret snRNAseq results. When sampling nuclei for sequencing instead of capturing whole cells, some degree of error or "dropout" is inevitable, although computational tools are now available to partially address this while batch-correcting and normalizing samples for analysis.

By sequencing PL, NAc, and VP, we hoped to capture three critical nodes within the addiction circuit: top-down inhibitory control over action (PL), integration of sensory information

and affective states in motivation and learning (NAc), and homeostatic regulation of action and pleasure (VP). Other regions we considered included VTA and LHb, which were passed over due to technical concerns, but may be re-visited in the future. Previous Stuber lab members Yoshiko and Koichi Hashikawa had collected a pilot multiomic LHb snRNAseq/ATACseq dataset in mice after morphine escalation +/- withdrawal, which we utilized to develop, test, and refine the basic snRNAseq analysis pipeline for these experiments.

Technical and cost-related considerations required us to pool at least two rat samples together for each single-nuclei isolation and sequencing run. Due to this limitation, we selected only the highest-high (n = 5) and the lowest-low (n = 6) rats for inclusion in the study. Rats were pooled into two technical replicates per addiction risk group and region: high A and B, and low A and B. All rats were collected at the protracted withdrawal timepoint, 1-2 days after their 8th extinction session.

In prelimbic cortex, we hypothesized that interneurons and pyramidal neurons would display differential levels of perturbation between the two opioid-risk groups, with interneurons more likely to be altered. One potential explanation for the loss of within-group cFOS correlation (which could also be summarized as loss of organization in PL activity patterns between subjects) could be dysfunction of local PL interneurons, leading to disorganization of the normally tightly regulated mPFC pyramidal neuron activity. In NAc, due to the NAc shell-VP cFOS signature previously observed, we expected D2 MSNs to be relatively more perturbed than D1 MSNs. For both NAc and VP, we hypothesized that MOR+ neurons would be more likely to vary in expression of neural activity-related genes between addiction risk groups when compared to MOR- neurons. Agnostic of region, an induction of inflammatory or cell-stress related transcriptional responses by glia was expected. Acute morphine has been noted to cause disproportionate transcriptional glial activation responses in early snRNAseq studies of responses to acute opioid administration[100], with additional

reports of morphine withdrawal-induced microglial cytokine signaling in LHb[101], and opioid-induced recruitment of peripheral T-cells driving persistent neuroinflammation.[102] In humans, white matter pathologies have occasionally been associated with opioid use, particularly heroin.[103–105] Findings such as these have been used as supporting evidence for the "substance use as brain disease" hypothesis, which makes particular note of changes to neurons and glia that resemble those observed in more "traditional" (i.e. non-psychiatric) CNS disease states. Proponents of this view emphasize the need for more definitive medical treatments for OUD and other substance use disorders, rather than simply hoping that any pathology-like changes will reverse if patients achieve long-term abstinence from drug use. On the other hand, concerns have been raised regarding characterization of drug-exposed brains as "diseased" or "damaged," as this designation may lead to loss of agency in OUD patients, which is not particularly helpful in the current medical and sociological landscape for patients or physicians. Further unbiased characterization of the molecular, transcriptional, and circuit-level adaptations in OUD models is needed to provide additional information about the scale and potential reversibility of any changes found to be associated with escalated opioid use.

Section II: snRNAseq methods and analysis pipeline

Tissue collection and purification of nuclei: Rats were deeply anesthetized with a terminal dose of sodium pentobarbital and intracardially perfused with artificial CSF (NMDG buffer, pH 7.35-7.4). Brains were rapidly extracted and sectioned at 300-400 μM on a vibratome. Bilateral tissue sections from prelimbic cortex, nucleus accumbens, and ventral pallidum were dissected and flash frozen. Frozen tissue sections were pooled into four groups (low risk A/B, high risk A/B) and dissociated in lysis buffer (10 mM Tris-HCl, 10 mM NaCl, 3 mM $MgCl_2$, 0.1% Igepal, 0.2 U/μL RNAse inhibitor) using a 2 mL dounce homogenizer on ice. After filtering and centrifugation (500xg, 10

minutes, 4C), the nuclear pellet was resuspended in homogenate solution (0.25M sucrose, 25 mM KCl, 5 mM $MgCl_2$, 20 mM Tris-HCl, 0.2 U/μL RNase inhibitor, pH 7.8-8) and re-spun in an OptiPrep gradient solution (50% OptiPrep over 30% OptiPrep, 3000xg, 15 minutes, 4C). Following centrifugation, the OptiPrep solution was carefully removed, and the nuclear pellet was resuspended in 100 μL wash buffer. Nuclei yield and quality was inspected using a fluorescent Apotome microscope after staining with propidium iodide, and samples were diluted to target 10,000 nuclei per 10X sequencing reaction (one reaction per group in each region.)

Nuclei preparation, cDNA library prep, and sequencing: We utilized 10X 3' NextGem technology for all samples. Purified nuclei are loaded into a microfluidic chip, which facilitates delivery of a unique barcode to each nuclei via a NextGem bead. Barcoded nuclei then undergo reverse transcription. After additional cDNA amplification, library quality control, and cleanup steps, cDNA libraries were sequenced using the NovaSeq X Plus platform (Novogene) to a depth of 750 million paired reads.

Alignment of reads to the rat reference atlas: 10X's CellRanger software was used to build a rat reference atlas based on the mRatBN7.2 genome assembly, the most up-to-date assembly for *Rattus norvegicus*.[106] FASTQ sequencing files were uploaded to 10X's Cloud Analysis service for genome alignment, resulting in the generation of matrix files containing counts for each gene for each individual barcoded nuclei.

Quality control, normalization, and integration: All downstream snRNAseq analysis was completed using the R package Seurat, version 4.2. Samples were filtered to exclude nuclei with fewer than 1000 or greater than 40,000 reads, or with greater than 3% of reads from mitochondrial genes (which is often associated with low quality in snRNAseq.) The SCTransform algorithm was utilized to normalize each sample prior to and after integration, which we have found to produce

superior results when compared to log-normalization strategies. This method uses a GLM-based approach in which sequencing depth for each nuclei is a covariate, improving our ability to make comparisons between samples that were run separately and likely contain technical variation.[107] We utilized percentage of mitochondrial reads as an additional regression variable to further control for discrepancies in cell quality between samples. Normalization is followed by PCA, which identifies PCs from the gene expression data for each sample, 20 of which were used to generate a UMAP. After nearest-neighbor analysis is completed, each cell is classified into a putative cluster. Clustering resolution can be adjusted upwards or downwards to produce more or fewer clusters respectively, but we observed satisfactory results with resolution = 0.3 for most samples. Doublets were identified and removed using the R package DoubletFinder, after which samples were re-normalized. 11/12 samples had excellent quality control metrics and clear separation of clusters, but one NAc sample had a large cluster consisting of MSN-like cells of lower quality and unclear cellular identity. Although these cells passed our stringent QC threshold, we remained concerned about technical variation in this sample and ultimately chose to fully exclude this cluster from downstream analysis. Per-sample QC metrics (% of mitochondrial reads, # of reads, and # of genes) for each cell type are available in the supplement. Samples for each region were integrated together using Seurat's SCT-based integration strategy. We also tested integration of all samples but noted that subsequent normalization steps produced different results when all brain regions were included compared to individually. For example, L2/3 IT neurons clustered together with MSNs, presumably due to underlying transcriptional similarity. However, it appeared that normalization with all cell types was introducing a degree of over-correction, removing biological variation due to missing information about cell types that would normally provide an intermediate state between, for example, cortical pyramidal neurons and striatal MSNs. Due to this uncertainty, we decided to use the fully integrated

Seurat object primarily for visualization, with all DEG and module analysis completed on separate objects for each region.

Cell type identification: One persistent problem in the single-cell analysis field is the issue of "double-dipping", which occurs when sequencing data is used to generate clusters (presumably with differential gene expression), then cells assigned to different clusters are statistically compared. Without correction, the p value produced by this test does not account for the initial usage of the data to generate the groups for comparison. In general, this dissertation work escapes the double-dipping problem by only making statistical comparisons for differential gene expression discovery between high and low animals within the same cell type or cluster, instead of between cell type A and cell type B. However, accurate cell typing is crucial to ensure the validity of these tests, as we want to maximize the odds that any significant findings are related to experimental variation, rather than technical drift in clusters or cell types. Luckily, the Allen Brain Institute has made monumental progress in recent years by sequencing and characterizing cell types throughout the mouse brain.[108] Although our studies have been completed in rats, in most cases we find that the Allen mouse cell types map well onto the dataset, with relatively few cells left without a clear identity. However, we have taken additional steps to integrate our data with pre-existing mouse and rat datasets in the same regions, with the goal of fully characterizing the diversity of cell types within and across species for each region, rather than automatically adapting the mouse brain labels.

In NAc and VP, we encountered some challenges with the mouse-derived cell type labels due to relative homogeneity in NAc labeling (the majority of neuron are simply labeled as D1 or D2 MSNs by the Allen MapMyCells algorithm, despite significant transcriptional differences between them based on clustering patterns) and extreme diversity in VP (often <= 200 neurons per individual cell type label.) The Allen mouse database provides sub-cell type labels achieved via

increasing clustering resolution on major cell types, but we preferred to maintain a consistent position in the cell type hierarchy to avoid experimenter-induced bias in cell typing and to simplify communication of results. Given recent findings showing cross-species cell type preservation between mouse and primate in VP[109], we decided to try the new Allen "consensus" basal ganglia taxonomy, which is based on single-cell sequencing data from human, macaque, and marmoset.[110] We found that these cell type labels aligned more closely with the clustering patterns observed in our data in both NAc and VP, and thus subsequently chose to adopt the consensus primate-based cell types for downstream analysis in striatum and pallidum. PL data continues to utilize mouse brain-derived cell type labels. When UMAPs of all regions integrated are shown, those labels reflect mouse cell types. Counts for each cell type in each region and sample are summarized in Supplemental Figure 1.

Differential gene expression analysis: Within each cell type in each region, differential gene expression testing was performed between cells from high risk and low risk animals, respectively, using a Wilcoxon rank sum test. Genes with an adjusted p value of less than 0.05 were classified as differentially expressed (DEGs.) For each cell type, we calculated a "perturbation score" by subtracting its DEG ratio (DEGs from cell type/sum DEGs for region) from its cell type ratio (number of nuclei in that cell type/number of nuclei in the region.) The number of DEGs detected tends to be roughly proportional to the number of nuclei tested: thus, if a cell type's share of the DEGs is greater or less than this expected proportion, it suggests that this cell type is relatively more or less perturbed compared to other cell types in that region. Perturbation scores for all major cell types are shown in Figure 8 and will be further discussed in the following sections. To determine whether specific molecular functions, pathways, and cellular structures were significantly over-represented in these lists compared to what would be expected by chance, we utilized the R package Enrichr to query lists of upregulated and downregulated DEGs against three gene ontology (GO)

databases: Molecular Function, Cellular Component, and Biological Process (2025 versions for all.) Each GO "hit" is assigned an adjusted p value based on the number of matches, the number of terms in the GO set, and the number of input genes, providing a readout of which molecular pathways are most significantly altered between high and low addiction risk rats.

Weighted gene correlation network analysis: As previously discussed in the cFOS section, we are comparing high and low addiction risk rats who both self-administered heroin, at a protracted withdrawal timepoint with no drug on board. Consequently, we expect that any "signature" of high addiction risk would be subtle and cell-type dependent, which aligns with the results we observed from DEG analysis (to be covered in subsequent sections.) To further characterize the transcriptional landscape in each region between the two conditions, we need to move beyond DEG identification and analysis alone. Fortunately, our samples showed remarkable technical consistency: the cell-type distribution within-region was well-conserved between the four samples for each region, with no major cell types over or under-represented (Supplementary Figure 1.) This preservation of cell-type proportion between samples enables us to turn to weighted gene correlation network analysis (WGCNA) to identify correlated gene sets and test for differential expression of these sets across conditions. As WGCNA was originally designed for use in bulk sequencing analysis, we accomplished this using the R package hdWGCNA, which is specialized for single-cell data.[111]

As a first step, the dataset is parcellated into "metacells" consisting of nuclei with similar gene expression. From these metacells, correlated gene expression analysis leads to the identification of co-expression networks, which are then hierarchically clustered to form modules (in a similar workflow to the network analysis pipeline we developed for whole-brain cFOS in Chapter Two.) The single cell normalization tool Harmony[112] was utilized during this process to provide additional

between-sample batch correction, maximizing the odds that identified gene modules represent biological variation. Each module is described by a "module eigengene" (ME), the first PC of the gene expression matrix for that module. Every gene assigned to a certain module was ranked by a kME score, providing a measure of how closely aligned that gene's expression pattern is with the overall ME for the module. Genes with the highest kME scores for each module were designated as "hub genes." Often, hub genes are also DEGs (resembling "master regulators" of both defining addiction risk status and describing cell-type-wide expression patterns), but not always. To identify differentially expressed MEs (DMEs), a Wilcoxon rank sum test was used to compare MEs in all cells derived from high-risk animals with those from low-risk animals, separately for each region. DMEs were further characterized using gene set enrichment analysis as described above. We found that most DMEs were specific for one or two cell types. DEG and WGCNA analysis results for each region will be discussed in detail below.

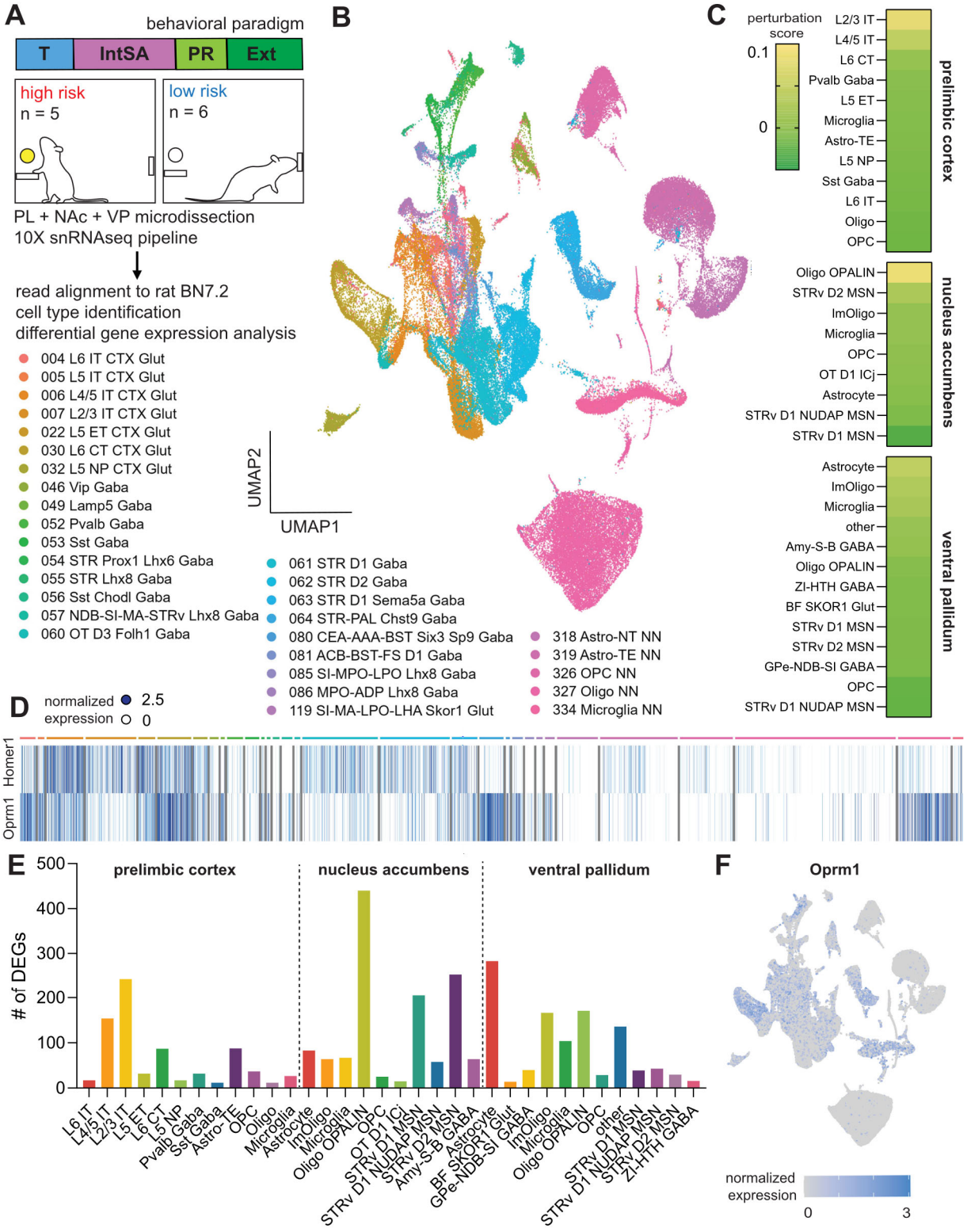
A
behavioral paradigm
T
IntSA
PR
Ext
high risk
n = 5
low risk
n = 6
PL + NAc + VP microdissection
10X snRNAseq pipeline
read alignment to rat BN7.2
cell type identification
differential gene expression analysis
004 L6 IT CTX Glut
005 L5 IT CTX Glut
006 L4/5 IT CTX Glut
007 L2/3 IT CTX Glut
022 L5 ET CTX Glut
030 L6 CT CTX Glut
032 L5 NP CTX Glut
046 Vip Gaba
049 Lamp5 Gaba
052 Pvalb Gaba
053 Sst Gaba
054 STR Prox1 Lhx6 Gaba
055 STR Lhx8 Gaba
056 Sst Chodl Gaba
057 NDB-SI-MA-STRv Lhx8 Gaba
060 OT D3 Folh1 Gaba
B
UMAP2
UMAP1
061 STR D1 Gaba
062 STR D2 Gaba
063 STR D1 Sema5a Gaba
064 STR-PAL Chst9 Gaba
080 CEA-AAA-BST Six3 Sp9 Gaba
081 ACB-BST-FS D1 Gaba
085 SI-MPO-LPO Lhx8 Gaba
086 MPO-ADP Lhx8 Gaba
119 SI-MA-LPO-LHA Skor1 Glut
318 Astro-NT NN
319 Astro-TE NN
326 OPC NN
327 Oligo NN
334 Microglia NN
C
perturbation score
0.1
0
L2/3 IT
L4/5 IT
L6 CT
Pvalb Gaba
L5 ET
Microglia
Astro-TE
L5 NP
Sst Gaba
L6 IT
Oligo
OPC
prelimbic cortex
Oligo OPALIN
STRv D2 MSN
ImOligo
Microglia
OPC
OT D1 ICj
Astrocyte
STRv D1 NUDAP MSN
STRv D1 MSN
nucleus accumbens
Astrocyte
ImOligo
Microglia
other
Amy-S-B GABA
Oligo OPALIN
ZI-HTH GABA
BF SKOR1 Glut
STRv D1 MSN
STRv D2 MSN
GPe-NDB-SI GABA
OPC
STRv D1 NUDAP MSN
ventral pallidum
D
normalized expression
2.5
0
Homer1
Oprm1
E
# of DEGs
500
400
300
200
100
0
prelimbic cortex
nucleus accumbens
ventral pallidum
L6 IT
L4/5 IT
L2/3 IT
L5 ET
L6 CT
L5 NP
Pvalb Gaba
Sst Gaba
Astro-TE
OPC
Oligo
Microglia
Astrocyte
ImOligo
Microglia
Oligo OPALIN
OPC
OT D1 ICj
STRv D1 MSN
STRv D1 NUDAP MSN
STRv D2 MSN
Amy-S-B GABA
BF SKOR1 Glut
GPe-NDB-SI GABA
ImOligo
Microglia
Oligo OPALIN
OPC
other
STRv D1 MSN
STRv D1 NUDAP MSN
STRv D2 MSN
ZI-HTH GABA
F
Oprm1
normalized expression
0
3

Figure 8: snRNAseq of prelimbic cortex, nucleus accumbens, and ventral pallidum of high and low risk rats uncovers cell-type and region-specific gene expression signatures. (A) Behavioral paradigm for snRNAseq experiment. (B) UMAP generated from cross-region integrated data, neurons color-coded by subclass label after mapping to Allen Institute mouse brain atlas. n = 110,095 cells after QC. (C) Perturbation score (DEG ratio – cell type ratio, DEG ratio = # of cell type DEGs / # of total DEGs for that region, cell type ratio = # of nuclei of that cell type / total # of nuclei in sample) for PL (top), NAc (center), and VP (bottom) cell types. (D) Relative expression of Homer1 and Oprm1 in all nuclei, sorted by Allen cell type. (E) # of DEGs for each major cell type within each region. F: Feature plot depicting normalized expression of Oprm1 across all nuclei.

Section III: Divergence in IT and PT neuron transcriptional state by addiction risk group in prelimbic cortex

Cell-type specific differences in relative perturbation and gene set enrichment of DEGs:

Prelimbic cortex contains at least three major categories of long-range pyramidal projection neurons: intratelencephalic (IT) neurons, which project primarily to contralateral cortex and striatum, corticothalamic (CT) neurons, which project to thalamus and subcortical structures including VTA[113], and extratelencephalic (ET) neurons, which project to striatum and lower-order structures including lateral hypothalamus, VTA, and substantia nigra. Of these three, IT neurons were by far the most perturbed when comparing DEG ratio between cell types (Figure 8C), L2/3 > L4/5. L2/3 neurons are thought to be biased towards intra-cortical signaling[114], but relatively little is known about their function in the mPFC, particularly in the context of opioid addiction. Specific inactivation of IT neurons, but not PT neurons, impaired mouse performance on a delayed match to sample task[115], demonstrating the importance of these neurons in self-regulation during active behavior. In motor cortex, L2/3 neurons directly innervate L5 projection neurons and alter their

activity with visual stimuli during movement, suggesting a primarily integrative role in the motor circuit.[116] Chemogenetic inhibition of anterior cingulate cortex IT neurons reduced the aversive effects of cocaine, in contrast to PT neuron inhibition, which enhanced the rewarding effects of the drug.[117] If a similar bidirectionality in mediating drug responses applies in PL, it may explain the divergence in perturbation between IT and ET neurons at the protracted withdrawal timepoint (with CT neurons somewhere in the middle.) Rarer pyramidal cell types include L5 NP (near-projecting) and L6 IT neurons, both of which were comparatively less perturbed than the other cell types found in layer 5 and 6.

Within the most-perturbed cell type of L2/3 IT neurons, the gene with the greatest fold change between high and low addiction risk rats was the IEG *Homer1* (Figure 10B.) This gene is notable for its role in modulating glutamatergic synapses via binding to metabotropic glutamate receptors,[118] and has been additionally implicated as a regulator of synaptic strength in concert with NMDAR activation and induction of synapse-associated proteins (i.e. Shank.)[119] More recently, *Homer1* was implicated as a genetic risk factor for individual differences in regulation of attention, with lower *Homer1* levels associated with increased GABA receptors and an enhancement of inhibitory tone in mPFC.[120] This pronounced upregulation of *Homer1* in L2/3 IT neurons of high addiction risk rats was accompanied by upregulated gene set enrichment of Ca^{2+} mediated signaling genes (Figure 10D.) However, the second-most upregulated gene was *Plcg2*, which is associated with an auto-inflammatory phenotype and cell stress responses in the CNS.[121] This gene was non-specifically increased in high addiction risk rats across almost all cell types with significant DEGs. Thus, the overall L2/3 IT transcriptional state in high-risk rats appears to be one of both increased neuronal activity (*Homer1*, Ca^{2+} response) and cellular stress (*Plcg2*, Ca^{2+} response.) Accompanying the upregulation in *Homer1* was a more modest ~0.10 $\log_2$ fold change increase in the metabotropic

glutamate receptor 5 (mGluR5, encoded by the *Grm5* gene.) Homer1 and mGluR5 are known to interact, with increased expression of Homer1 resulting in removal of mGluR5 from postsynaptic densities.[122] mGluR5 is G_q coupled, with activation leading to Ca^{2+} release and recruitment of phospholipase C. Thus, the modest upregulation of mGluR5 may be contributing to the observed Ca^{2+} response pathway enrichment observed in L2/3.

L4/5 IT neurons, although relatively less perturbed, partially mirror the transcriptional state observed in L2/3 IT, with *Homer1* and *Plcg2* conserved as the highest fold-change DEGs. However, gene set enrichment analysis on L4/5 upregulated DEGs revealed a more well-rounded list of altered functions than L2/3, including genes associated with learning, LTP, and synaptic transmission in addition to the common Ca^{2+} signaling response observed in both cell types. Specific genes of note include a 0.175 $\log_2$ FC upregulation in *Grin2a*, an NMDAR subunit known to play a role in schizophrenia risk via modulation of mPFC neuronal activity[123], and a 0.129 $\log_2$ FC upregulation in *Camk2a*, supporting a hyperactive phenotype for these neurons. Complicating this picture somewhat, layer 4/5 neurons also have significant downregulations in IEGs *Npas4* (~0.1 $\log_2$ FC decrease) and *Fosb* (0.16 $\log_2$ FC decrease.) Given that not all IT neurons displayed *Homer1* induction, these bidirectional changes in IEGs may reflect diverging activation states within cell type (some cells excited, others inhibited.) Also downregulated (0.17 $\log_2$ FC) was the G-protein modulator *Rgs4*, which acts to modify G_i coupled alpha subunits[124] and has been implicated as a schizophrenia risk factor associated with structural alterations in human dlPFC.[125] The most obviously relevant G_i-coupled GPCR in PL during opioid withdrawal is *Oprm1* itself, which displays cell-type specific expression patterns roughly inverse to *Homer1* (Figure 8D.) L6 CT neurons are a significant exception to this rule, showing robust *Oprm1* expression (Figure 8D) and polarized but strong *Homer1* induction (best appreciated in Figure 11E.) Relative to other PL cell types, IT

neurons display relatively low levels of *Oprm1* expression (L4/5 >> L2/3), which may be contributing to their apparent hyper-excitability/enhancement in Ca^{2+} signaling in high addiction risk rats.

Most GABAergic neurons in the dataset were either parvalbumin+ (Pvalb) or somatostatin+ (Sst.) More uncommon interneuron types, including Pvalb chandelier neurons, VIP Gaba neurons, and Sncg Gaba neurons were also captured, but their numbers were generally too low to facilitate meaningful high:low comparisons. Among these two major subcategories, Pvalb neurons were more perturbed than Sst, and displayed upregulation of *Homer1* (0.18 $\log_2$ FC, with an additional 10% increase in the number of Pvalb neurons expressing the gene.) This finding is consistent with recent observations from the field: for ex., a new mechanistic study of PL circuits in cocaine withdrawal showed enhancement of GABAergic tone from Pvalb interneurons onto L5 ET neurons.[126] Overall, the emergence of L2/3 IT, L4/5 IT, and Pvalb neurons as specifically altered in high addiction risk rats supports a phenotype of dysregulated intra-cortical circuits. This finding is consistent with our observations from the cFOS experiment, in which there was no dramatic increase or decrease in total cFOS in mediofrontal cortex, but instead a lack of correlated intra-cortical neural activity as observed in low-risk rats.

PL glia displayed a split phenotype, with microglia and astrocytes appearing more perturbed than oligodendrocytes and OPCs. DEGs from both microglia and astrocytes paralleled the Ca^{2+} mediated stress-like response that was observed in neurons. However, aside from this similarity, there was no clear signature of neuroinflammation in PL. Among glia, microglia were the only population to uniformly express *Oprm1*, but expression levels did not differ between high and low animals.

Broad downregulation of correlated gene modules in high addiction risk rats: To further characterize the gene expression landscape in PL, we turned to WGCNA, which identified eight modules in PL, all of which showed significant differences between the two addiction risk groups. Modules are labeled with a color, which we have maintained for visualization purposes. A network plot depicting the top hub genes for each module is shown in Figure 9B. As colors may be repeated across regions and have no relationship to the module's actual gene expression, we have labeled each module with its most relevant gene ontology term and with cell type showing most enriched expression of that module. Only one module, expressed primarily in astrocytes, was upregulated across the dataset in high addiction risk rats, all others were downregulated. Most modules were specific for one or two cell types, except for the "axonogenesis" module, which was highly expressed in all glutamatergic neurons except L5 near-projectors (Figure 10C.) As the name implies, L5 NP neurons are distinguished by their short projection range, perhaps requiring less axonal maintenance than the other cell types. The hub gene for this module is *Tenm2*, which is known to play a role in axon guidance, but appears unexplored in studies of PFC specifically.

A "synaptic transmission"-related module best characterized by the hub gene *Syt1* was most enriched in L6 CT neurons. *Syt1* downregulation has previously been observed in the PL of alcohol-dependent rats, and projection specific knockdown of *Syt1* in PL-BLA synapses was sufficient to enhance alcohol drinking.[127] Despite the name, CT neurons can project outside the thalamus, including to the VTA. Thus, the downregulation of both "axonogenesis" and "synaptic transmission" related gene modules in these neurons may directly contribute to decreased glutamatergic drive from the PFC to the VTA. The consequence of this hypothetical decrease would depend on the exact projection targets of these neurons, as PFC-VTA afferents can contact DA neurons and interneurons alike.

Two modules related to "RNA splicing" were enriched in L2/3 IT neurons but displayed relatively limited gene set enrichment compared to the other modules and thus are thought more likely to represent lower-quality or less specific gene expression patterns. The remaining three modules encapsulated and expanded upon the high:low differences already discussed above: a "synapse organization" module enriched in L4/5 IT neurons and two modules related to neural activity enriched in L2/3 IT neurons, "positive regulation of Map kinase/Jun kinase" and "positive regulation of transcription." The hub gene for the "synapse" L4/5 module is *Arpp21*, a cAMP-modulated transcriptional regulator implicated in dendritogenesis[128], also not previously characterized in PFC. The L2/3 IT "positive regulator" modules had more familiar hub genes: *Homer1* (+ regulation of transcription) and *Grm1* (mGluR1 or metabotropic glutamate receptor 1, + regulation of mapk/junk.) As previously discussed, Homer1 is known to bind mGluRs to modulate excitability at the postsynaptic density.

How is it possible that upregulated DEGs (ex. *Homer1*) could also be hub genes for downregulated gene modules? DEGs emerged from tests within matched cell types, while the directionality of DMEs depends on their expression throughout the dataset. Aside from *Homer1*, IEG expression throughout the dataset in PL not particularly high, especially for L5 ET, L5 NP, and Pvalb neurons. This finding aligns with what we would expect based on the brain-wide cFOS study, in which mediofrontal cortex cFOS was not correlated within-group specifically in high-risk rats, but not significantly decreased or increased in high risk compared to low risk. The loss of correlation implies a more stochastic dysregulation of PFC activity in high-risk rats, rather than either widespread activation or inhibition. On a region-level, high-risk rats were found to display broad downregulation of genes associated with axonogenesis, synaptic transmission, and synaptic maintenance. However, within cell-type, L2/3 and L4/5 neurons are disproportionally altered in high-risk rats, with profound and specific induction of *Homer1* and *mGluR1/5*. Enhancement of this

pathway is congruous with synaptic weakening in PL, given that high levels of Homer1 can lead to removal and recycling of mGluRs. These observations led us to question whether high addiction rats may display widespread neuronal inhibition in PL.

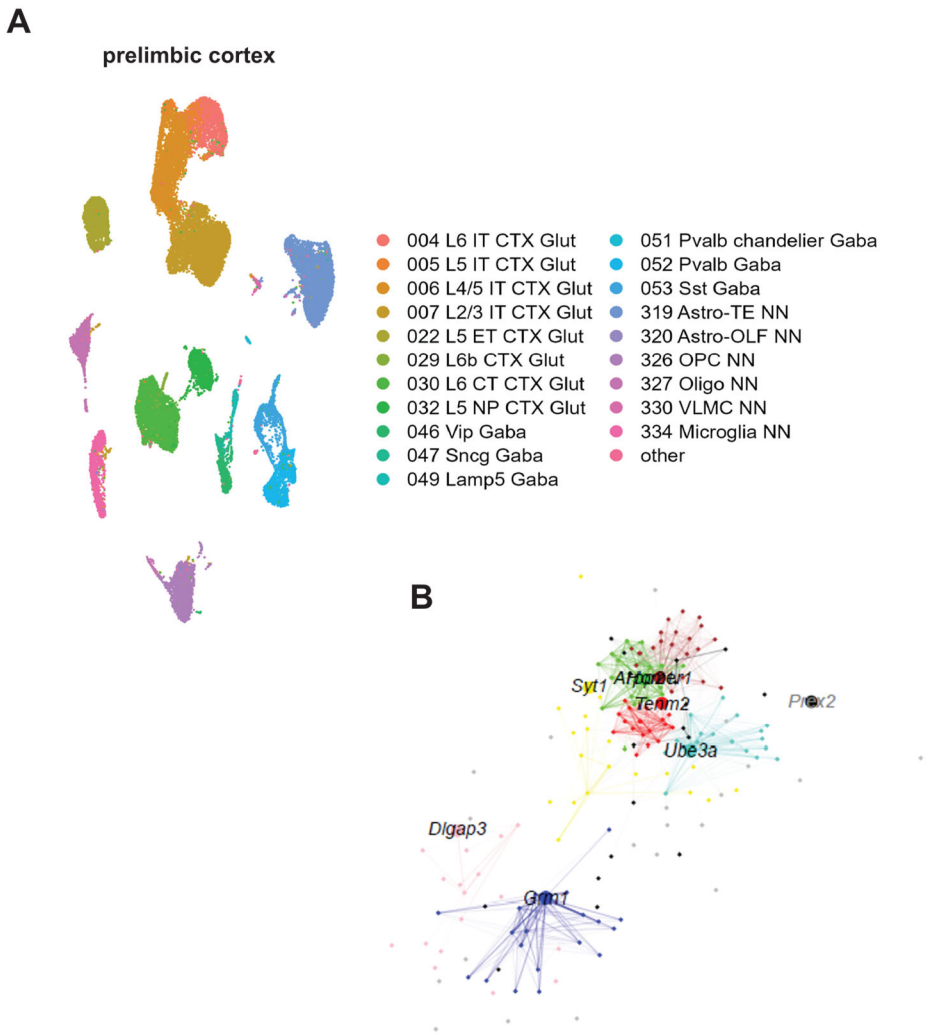

Figure 9: Summary of prelimbic cortex snRNAseq dataset. (A) UMAP depicting integrated data from each sample, labeled by Allen cell type. (B) WGCNA network plot. Each module is labeled with its highest kME hub gene.

Mapping inhibited neurons throughout PL in high and low risk rats: When neurons become inhibited, their metabolic activity also declines, leading to accumulation of phosphorylated metabolic proteins. This phenomenon led to the development and validation of phosphorylated pyruvate dehydrogenase (pPDH) as a marker of neuronal inhibition, with initial studies demonstrating an inverse correlation between pPDH levels and action potentials and broad induction of pPDH brain-wide after isoflurane treatment.[129] We sought to apply this approach to characterize neuronal activity after heroin self-administration by staining for pPDH with fluorescent immunohistochemistry. Preliminary data collected in seven rats with varying SA histories demonstrated pPDH immunolabeling in pyramidal cell bodies of only one subject (the only one of the seven to receive a "high-risk" LPA label, despite moderate heroin intake in other rats, Figure 10F.) pPDH putative neuron counts were significantly correlated with progressive ratio responding in PL, but not in NAc core or shell (Figure 10F.) More complete profiling of rats across the addiction spectrum is needed to determine whether this indicates true evidence of persistent pyramidal neuron inhibition in mPFC during protracted withdrawal.

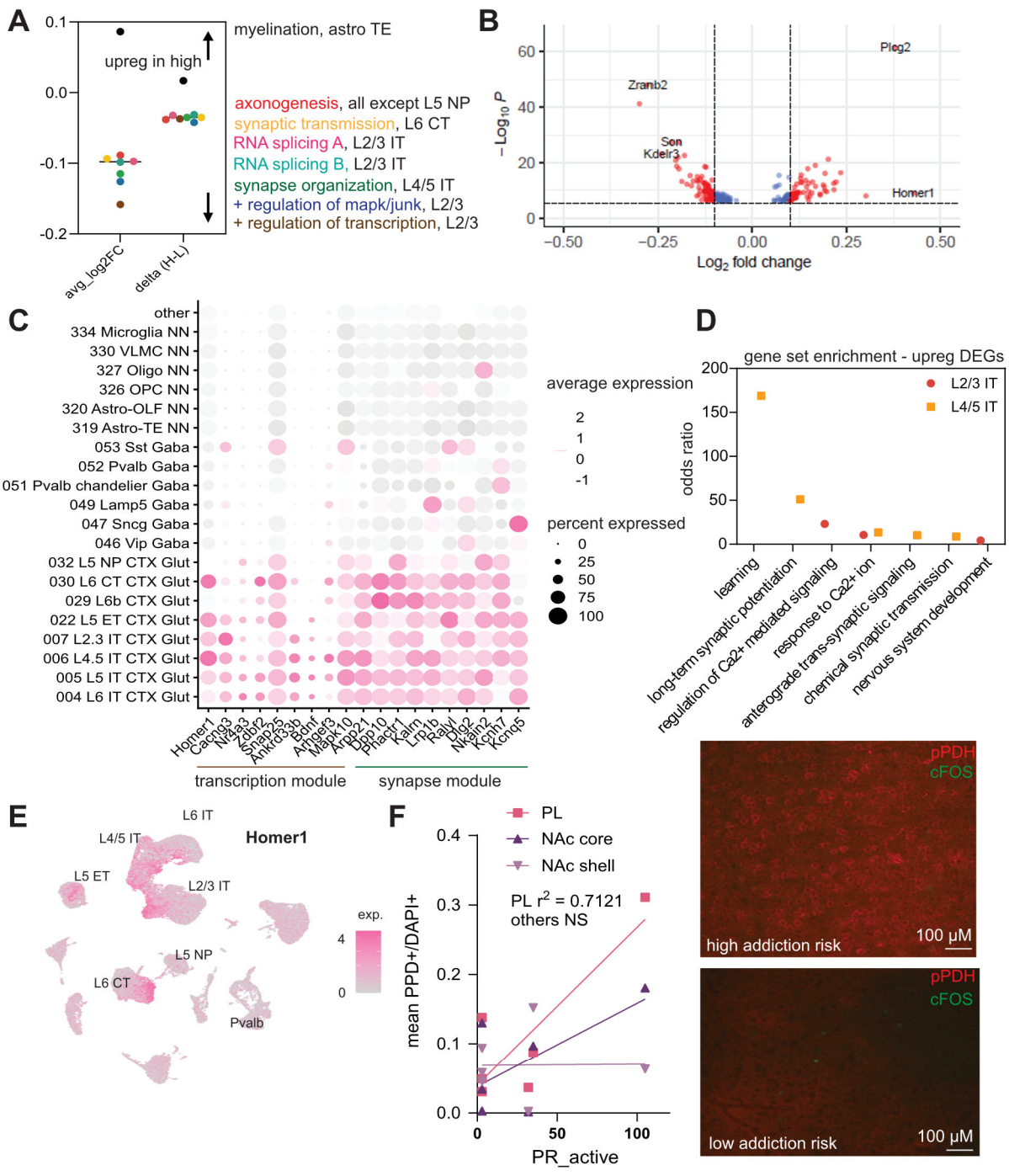
A
upreg in high
myelination, astro TE
axonogenesis, all except L5 NP
synaptic transmission, L6 CT
RNA splicing A, L2/3 IT
RNA splicing B, L2/3 IT
synapse organization, L4/5 IT
+ regulation of mapk/junk, L2/3
+ regulation of transcription, L2/3
avg_log2FC
delta (H-L)
B
Plcg2
Zranb2
Son
Kdelr3
Homer1
Log2 fold change
C
other
334 Microglia NN
330 VLMC NN
327 Oligo NN
326 OPC NN
320 Astro-OLF NN
319 Astro-TE NN
053 Sst Gaba
052 Pvalb Gaba
051 Pvalb chandelier Gaba
049 Lamp5 Gaba
047 Sncg Gaba
046 Vip Gaba
032 L5 NP CTX Glut
030 L6 CT CTX Glut
029 L6b CTX Glut
022 L5 ET CTX Glut
007 L2.3 IT CTX Glut
006 L4.5 IT CTX Glut
005 L5 IT CTX Glut
004 L6 IT CTX Glut
Homer1
Cacng3
Nr4a3
Zdbf2
Snap25
Ankrd36b
Bdnf
Arhgef3
Mapk10
Arpp21
Dpp10
Phactr1
Kalrn
Lrp1b
Ralyl
Dlg2
Nrgn
Kcnh7
Kcnq5
transcription module
synapse module
average expression
percent expressed
D
gene set enrichment - upreg DEGs
L2/3 IT
L4/5 IT
odds ratio
learning
long-term synaptic potentiation
regulation of Ca2+ mediated signaling
response to Ca2+ ion
anterograde trans-synaptic signaling
chemical synaptic transmission
nervous system development
E
L6 IT
L4/5 IT
Homer1
L5 ET
L2/3 IT
L5 NP
L6 CT
Pvalb
exp.
F
PL
NAc core
NAc shell
PL r2 = 0.7121
others NS
mean PPD+/DAPI+
PR_active
pPDH
cFOS
high addiction risk
100 µM
low addiction risk

Figure 10: PL IT neuron transcriptional activation co-occurs with evidence of ET neuron silencing in high addiction risk rats. (A) Differentially expressed correlated gene modules (each color represents a different module.) Labels reflect significant gene set enrichment terms for each module, and the cell type that they are primarily expressed in. (B) Volcano plot depicting DEGs (high addiction risk vs. low addiction risk) from L2/3 IT neurons. (C) Dot plot summarizing expression of high kME "hub genes" from two correlated gene modules. (D) Odds ratio of selected gene ontology terms with p_val_adj < 0.05 from gene set enrichment analysis (Enrichr) of upregulated DEGs for L2/3 and L4/5 IT neurons. (E) Normalized expression levels of Homer1 throughout PL. (F) Quantification of pPDH+ pyramidal cell bodies in rats with varying heroin use levels, with representative images from prelimbic cortex shown on right. No significant colocalization was noted between cFOS+ and pPDH+ neurons.

Cross-species integration to validate and further characterize mPFC cell type labels: A topic of considerable debate among behavioral neuroscientists is the extent to which mouse and rat PFC is homologous to the much larger, much more developed PFC found in primates. Detailed discussion of the evolution of PFC (and the validity of studying rodent PFC at all) is outside the scope of this work, however, we were curious to assess the extent of cross-species conservation in PFC cell types between mouse and rat (especially as we are using mouse cell type labels for downstream analysis.) To accomplish this, we utilized a publicly available mouse scRNAseq dataset, which sequenced PFC samples from mice after maintenance cocaine treatment, acute cocaine withdrawal, and chronic cocaine withdrawal (with corresponding saline groups.)[130] Raw data was processed through our snRNAseq pipeline and integrated together with the rat samples. Evaluating success or failure of integration is somewhat qualitative: samples that do not integrate will cluster separately, while samples that integrate well form homogenously intermixed clusters (as was the case with our rat samples.) The rat-mouse integration was an intermediate case, in which most clusters

contained both rat and mouse cells, but with readily apparent polarization in their gene expression patterns (Figure 11A.) Cells positively IDed as neurons were barcoded, subsetted, and re-integrated to improve our ability to detect variation in neuronal clusters (Figure 11 B, C.) Most Allen cell types were represented by a single cluster, except for L2/3 IT neurons, L4/5 IT neurons, and an activated cluster of unclear identity ("Mixed_Fos", which was composed primarily of cells from the mouse saline group, and excluded rat nuclei.) L4/5 neurons were split into a rat-enriched cluster marked by *Rorb* and a mouse-enriched cluster marked by *Etv1*. L2/3 neurons displayed a similar split, but instead of rat-enriched, the L2/3 *Glis3* cluster was only composed of rat neurons. This cluster also contained the *Homer1*+ L2/3 neurons that likely drove much of the high addiction risk DEG phenotype in those cells. Low numbers of rat nuclei were found in the mouse L2/3 IT cluster, marked by *Lamp5*. Discrepancies in numbers of cells per cell type when integrating samples (especially cross-species) are not usual, and can reflect technical differences (i.e. whole cell vs. single nuclei collection, varying dissection boundaries, etc.) However, given the low number of distinct cell types in PL, the lack of any mouse cells in the *Glis3* cluster is unusual. If these cells represent a nonconserved sub-celltype, the results may not generalize back to mice. *Glis3* itself is a transcription factor previously implicated as a schizophrenia risk-conferring gene variant, which has additionally been shown to be highly expressed in human PFC pyramidal neurons, particularly L4.[131] Additional characterization is necessary to determine whether L2/3 IT *Glis3*+ neurons have functional properties in common with human PFC *Glis3*+ neurons.

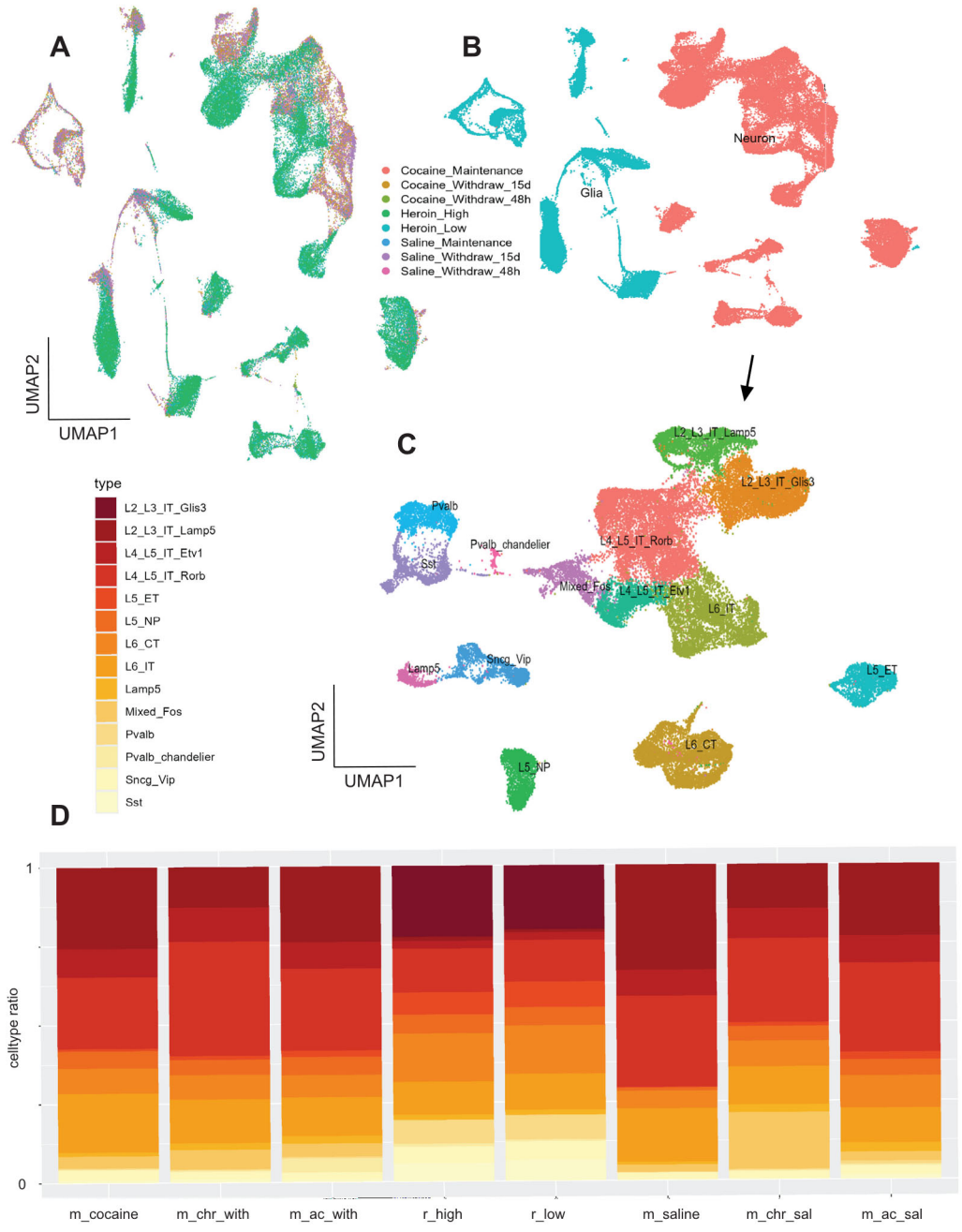

Figure 11: Cross-species integration of mouse and rat mPFC snRNAseq datasets. (A) UMAP depicting integration of rat and mouse data, color-coded by sample type. (B) Categorization of each cell as either neuron or glia. (C) Re-clustered neurons, labeled with their common denominator likely identity, determined via Allen labels and upregulated marker genes. (D) Relative proportion of each cell type and sub-cell type within each sample. R = rat, M = mouse.

Section IV: Nucleus accumbens neurons are robustly altered between high and low addiction risk groups, while ventral pallidal neurons remain quiescent

Consensus basal ganglia framework provides cell type labels for NAc and VP: Principal neuronal cell types identified in NAc tissue samples included D1 and D2 MSNs, GABAergic neurons of the extended amygdala/BNST, and Drd1/3-expressing neurons of the olfactory tubercle. For clarity, D1 and D2 MSNs belonging to the primary cluster for each type are referred to as canonical. Aside from this main group, three MSN subtypes were also delineated by the consensus framework. Forming their own separate cluster (with some D1+D2 MSNs interspersed) were dorsal striatum D2 "StrioMat Hybrid" MSNs, which expressed D2 and a novel marker, *Thsd7b*. These neurons appeared transcriptionally distinct from the main D2 MSN population and displayed minimal high:low differences in gene expression. Intriguingly, they were the only cluster in the dataset to significantly express a steroid hormone receptor (*Pgr*, Figure 13). We hoped to assess enrichment of female-derived neurons in this cluster but found that only a handful of neurons across the dataset expressed any sex-linked genes (searched for *Xist* as well as all annotated Y chromosome genes), a known limitation of snRNAseq. Next were ventral striatum D1 NUDAP ("Neurochemically Unique Domains in the Accumbens and Putamen")[132] neurons, which are found in both NAc and VP samples and display the highest *Oprm1* expression level of all NAc cell types (Figure 13.) Finally, intermixed with the StrioMat and NUDAP subtypes, and with canonical D1 and D2 MSNs, were D1+D2+ double positive "hybrid" MSNs. These neurons were found uniformly throughout the canonical D1, D2, and StrioMat clusters, but only the D1+D2+ neurons clustering near NUDAP neurons were polarized enough to form their own subcluster. This sub-subgroup expresses *Chst9* and receives a Chst9 Gaba mouse-derived label. The apparent transcriptional heterogeneity of these double-positive neurons complicates statistical comparison and likely contributes to the low number of high:low DEGs found in this subgroup. To assess whether this

cluster displayed a unique transcriptional response in protracted withdrawal, we tested for DEGs within Chst9 Gaba neurons as their own cluster in both NAc and VP but observed few high:low differences. GABAergic interneurons, including SST+, cholinergic, and VIP+ neurons were also present in the NAc dataset, but in very low numbers.

Neurons from ventral pallidum tissue samples were considerably more diverse than those found in NAc samples. Canonical D1 and D2 MSNs found in these samples are likely to be due to contamination during dissection, while D1 NUDAP neurons are known to extend from NAc to VP. The exact anatomic borders of VP are a topic of debate and were historically delineated with staining for Substance P+ fibers, which we have adopted as criteria for defining VP cell types. The Allen framework labels putative VP cell types as "SI," or substantia innominata, which contains and extends beyond the region labeled "ventral pallidum" in the Paxinos and Watson rat atlas.[133] Many GABAergic cell types with low numbers of neurons were present in the VP samples, most expressing some combination of SST, Lhx6, and Lhx8. Of these, one consensus cell type ("GPe-NDB-SI Lhx6-Lhx8-Gbx1 Gaba") was both a "true" VP cell type and present in sufficient numbers to facilitate statistical comparison between high and low groups. A medium-sized cluster of glutamatergic cells are also found within VP and are selectively marked by the *Skor1* gene. Thus, despite VP's wide diversity, only three Allen consensus cell types from these tissue samples were present in sufficient numbers to facilitate statistical comparison: D1 NUDAP MSNs, Lhx6-Lhx8-Gbx1 GABA, and Skor1 Glut.

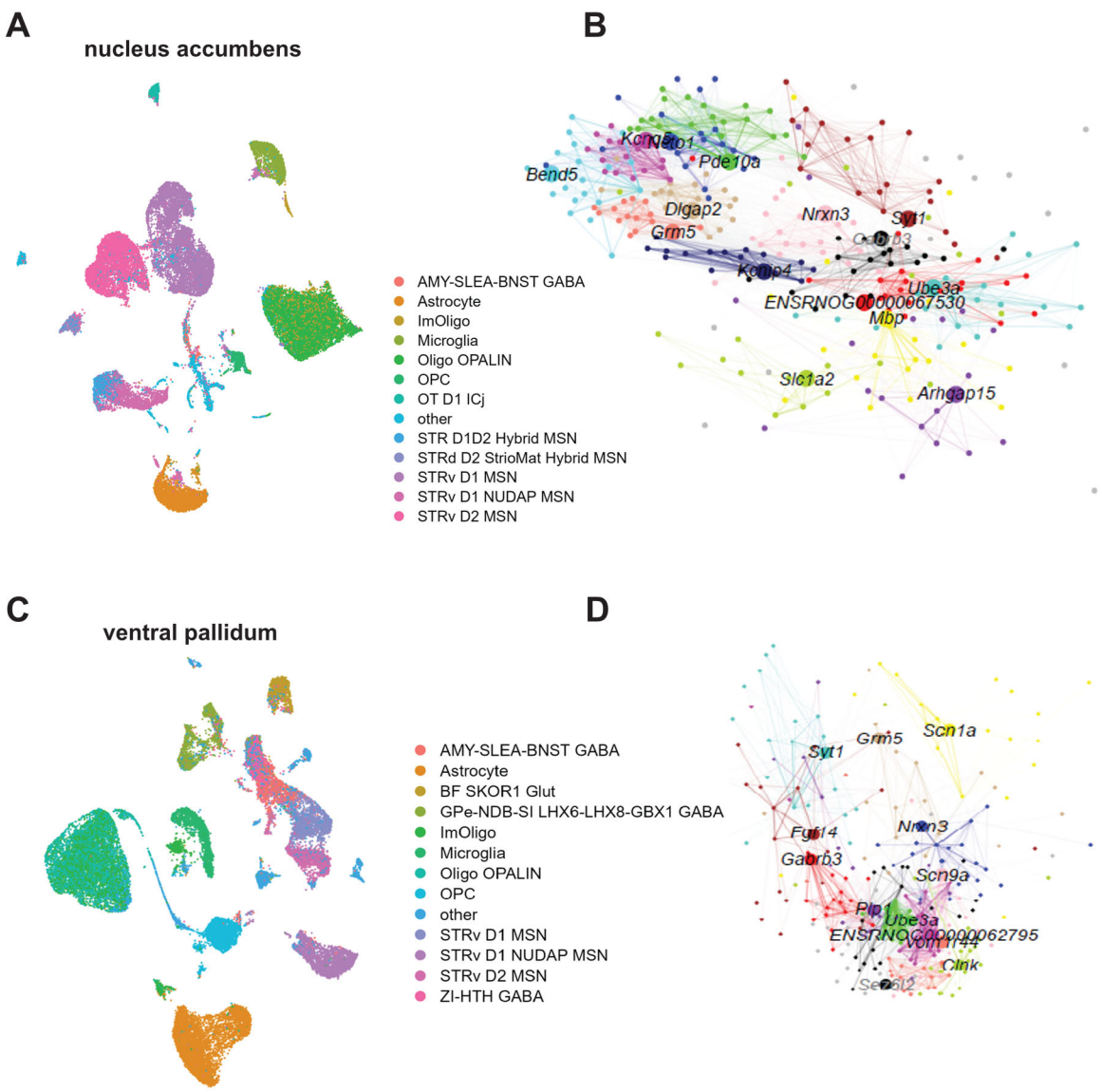

Figure 12: Summary of NAc and VP snRNAseq datasets. (A, C) UMAP depicting integrated data from each sample, labeled by Allen basal ganglia consensus framework cell type. (B, D) WGCNA network plot for NAc (B) and VP (D). Each module is labeled with its highest kME hub gene.

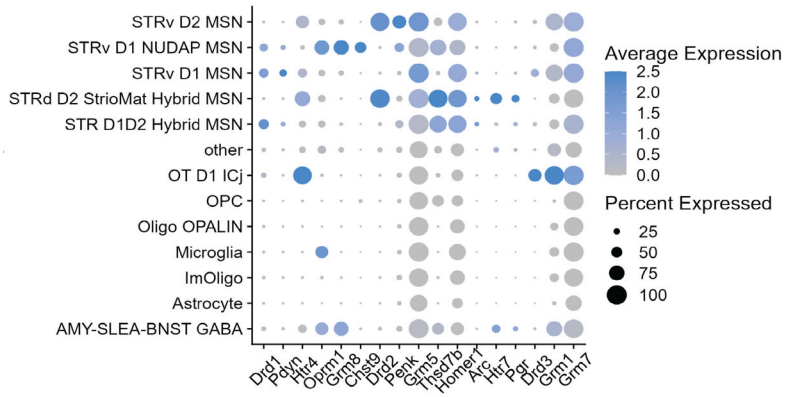

Figure 13: Expression of cell type markers and other genes of interest in NAc.

Transcriptional state of NAc neurons varies by addiction risk group and cell type: The most perturbed cell type in NAc were oligodendrocytes, with immature oligodendrocytes and OPCs following behind in 3rd and 6th (Figure 8C.) Gene set enrichment analysis of oligo DEGs did not provide a clear picture of the altered molecular pathways, but examination of WCGNA gene modules revealed two modules with oligodendrocyte-biased expression and upregulation in high-risk animals. The first module was related to "CNS development", with hub genes showing very strong expression in oligodendrocytes and more moderate expression in immature oligodendrocytes (Figure 14A). Myelin basic protein (*Mbp*), a highly expressed structural component of myelin, was the top hub gene for this module, suggesting a possible enhancement of local pro-myelination activity in high addiction risk rats. Increased myelination and *Mbp* levels in the NAc have been previously observed after chronic, voluntary EtOH consumption.[134] The other upregulated oligodendrocyte module, "protein/RNA complex assembly," was less cohesive in its gene set enrichment, possibly indicative of a cell stress phenotype in the oligodendrocytes of high-risk rats. Together, these findings suggest that myelination may be enhanced in the NAc of high-risk animals during protracted withdrawal, but not without some degree of subsequent co-occurring transcriptional

dysregulation. Increased activity (in neurons and glia) can be associated with metabolic cell stress, and distinguishing the two from snRNAseq data alone is challenging. In general, we find that large numbers of DEGs without an overarching functional correlate or theme are often indicators of cell stress. A true signature of correlated gene expression may be hidden within this list, which is one of the rationales for our use of dataset-wide WGCNA. Shorter DEG lists with greater molecular pathway cohesiveness are more likely to reflect healthy cells. However, cell stress alone (especially considering our stringent QC standards) is not a rationale to discard DEGs or modules, as characterizing which neurons are more likely to enter a state of metabolic stress during protracted withdrawal is not without value. One factor that may be contributing to these specific findings is a relative enrichment of oligodendrocytes in one high NAc sample (Supplemental Figure 1) This mismatch was only present for oligodendrocytes, not OPCs, immature oligodendrocytes, or any other cell type, making it difficult to determine whether it results from biological or technical variation. Follow up experiments assessing oligodendrocyte number and myelin quantity in NAc during protracted heroin withdrawal would clarify this question.

The most highly upregulated gene module in high addiction risk rats was related to "synapse pruning" and nearly exclusively expressed in microglia (Figure 14A). As in PL, NAc microglia uniformly expressed the *Oprm1* receptor. Long-lasting dysregulation of microglia has been observed in animals exposed to perinatal opioids[135], but specific links between opioid exposure and enhanced synaptic pruning have not previously been observed. To validate and further explore these findings, we plan to conduct IHC targeting Iba1 in the NAc, with the goal of characterizing the relative number, morphology, and inferred activation state of microglia after heroin SA and withdrawal. A small population of putative microglia were found to express MSN marker genes, increasing our suspicion that these microglia may be involved in active phagocytosis of MSN synapses. The combination of enhanced myelination and synaptic pruning in high-risk rats is an interesting one, as

both could be characterized as synaptic strengtheners, solidifying drug experiences into "memory" in reward circuits (i.e., one possible mechanism for incubation of craving in NAc.)

Following oligodendrocytes in the relative perturbation rank list were canonical D2 MSNs. These neurons are defined by their high baseline *Penk* expression (Figure 13) and were found to upregulate both *Penk* and *Oprm1* in the high addiction risk group (Figure 14C). Thus, the receptivity of these neurons to opioids (endogenous or exogenous), and their downstream endogenous opioid release are both increased in protracted withdrawal from heroin. Also upregulated in D2 neurons from high-risk rats was the 5-HT receptor *Htr2b*, a G_q-coupled GPCR. Although we did not observe any significant increase in dorsal raphe cFOS during protracted withdrawal, activation of serotonergic neurons has been reported as correlated with acute withdrawal from heroin in mice.[136] Very recent work has highlighted the importance of Htr2a/c signaling in bidirectionally co-regulating D2 MSN activity together with DA in cocaine reward,[137] however, Htr2b receptors specifically are implicated in amplifying synaptic depression in response to DA rather than counteracting it.[138] As a result, the dual upregulation of *Oprm1* and *Htr2b* suggests a pro-inhibitory phenotype for D2 MSNs in high-risk rats, which is also illustrated by the results of correlated gene module DME testing. Four modules were identified as biased towards D2 MSNs: "synaptic vesicle exocytosis," "glutamatergic synaptic transmission," "axonogenesis," and "synapse assembly." All were downregulated in high addiction risk animals dataset-wide, characterizing the high-risk NAc as both presynaptically and postsynaptically silenced. Further supporting this characterization was the relatively low expression of IEGs across the NAc: roughly 3% of NAc neurons were classified as activated, with no difference in the number of activated neurons between low and high-risk groups. *Homer1* was preferentially expressed in D1+D2+ and StrioMat MSNs but was not found to be altered between high and low rats. This is consistent with our whole brain cFOS findings, in which

there was no significant difference in NAc cFOS when high and low risk animals were pooled into binary groups.

The "synapse assembly" module was best represented by the hub gene *Grm5*, encoded mGluR5, which was previously discussed due to its upregulation in PL (in concert with Homer1.) In striatum, this directionality is reversed, and *Grm5* is slightly downregulated in both D1 and D2 MSNs (Figure 14C.) The related module for "glutamatergic synaptic transmission" was represented by *Syt1*, the same hub gene for the "synaptic transmission" module in PL. *Syt1* is also a DEG in both D1 and D2, showing a similar pattern of change as *Grm5* (Figure 14C.) Synthesis of all findings from PL thus far support a theory of hypo-activity, which would result in a decrease in PFC-NAc glutamatergic drive onto NAc MSNs. Although both D1s and D2s downregulate *Grm5*, only D2s have increased expression of *Oprm1* and *Htr2b* in high rats, presumably further silencing them. This inhibitory cascade could be propagated further downstream by increased transcription of and subsequent release of Penk in VP, where MOR is abundant.

In contrast to D2 MSNs, canonical D1 MSNs were the least-perturbed in the dataset. However, they did preferentially express one module related to "GABA/5-HT synaptic transmission," which again was downregulated in high-risk rats. Genes found here were somewhat diverse, with hub genes including the potassium channel *Kcnq5*, NMDAR *Grin2b*, and GABA A receptor subunit *Gabra4*. Right above D1 MSNs in the perturbation list was the much smaller subgroup of D1 NUDAP MSNs. These neurons show the highest baseline *Oprm1* expression and the highest induction of *Oprm1* in high addiction risk rats in the NAc samples (Figure 14C.) They additionally upregulate *Gad1*, possibly enhancing downstream inhibitory tone. It is not clear from the literature whether D1 NUDAP MSNs differ from canonical D1 MSNs in their likelihood to innervate VTA, VP, or both. Follow up experiments to determine (a) where these neurons project

and (b) what the functional consequences of their activation/inactivation are would shed light on their potential relative contribution to synaptic alterations observed during protracted opioid withdrawal.

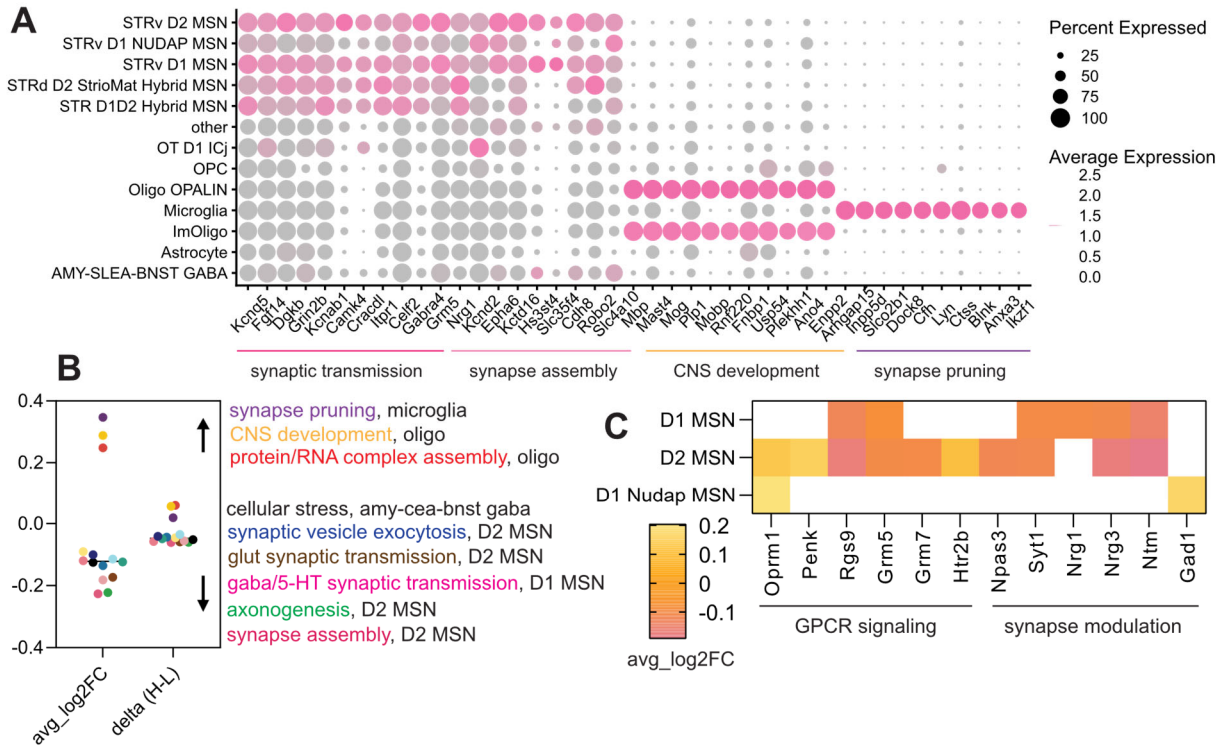

Figure 14: WGCNA illustrates upregulated glial activation and downregulated synaptic transmission gene expression pathways in the NAc of high-risk rats. (A) Expression of genes with top-10 kME scores for four modules across cell types. (B) Fold change and % expression change of each differentially expressed gene module. Modules are labeled with the most relevant GO theme and the cell type with the highest expression levels. (C) DEGs of interest from D1, D2, and D1 NUDAP MSNs.

Ventral pallidal neuronal diversity precludes characterization of high:low transcriptional differences: Many neurons in VP tissue samples were categorized as extended amygdala/BNST GABA neurons, which likely drove much of the correlated gene expression observed in the 13

identified gene modules (Figure 12D.) Once again, *Grm5* emerged as a hub gene and a DEG in this population, displaying a 0.188 $\log_2$ FC in high-risk rats, and accompanied by a 0.212 increase in *Homer1*. However, unlike NAc, the gene set module including *Grm5* did not show differential expression between high and low risk rats (modules with differential expression are summarized in Figure 15.) In both NAc and VP, neurons categorized as AMY-BNST displayed a cell-stress related gene signature with differential expression in high-risk rats, suggesting that future specific exploration of these neurons in opioid withdrawal may be warranted. This pattern was best captured by a "mitochondrial respiratory chain complex" module, which was expressed in both "true" VP neurons (Lhx6-Lhx8 SI) and extended amygdala cell. One DEG of interest in Lhx6-Lhx8 SI neurons was *Shank3* (-0.187 $\log_2$ FC), a structural protein on postsynaptic densities. Despite high basal levels of *Oprm1* expression in VP cell types, no change was found in this gene or its counterpart *Oprk1* in VP, in contrast to NAc where high-risk animals displayed *Oprm1* upregulation in both D2 and D1 NUDAP MSNs. If *Oprm1* expression were enhanced in high-risk animals in all neurons that express it robustly, one could conclude that opioid exposure alone might be driving an allostatic increase. The cell-type specificity of the observed changes in *Oprm1* induction instead indicate that other intra-cellular processes, presumably unique to each MSN subtype, are acting to modulate the receptor's expression.

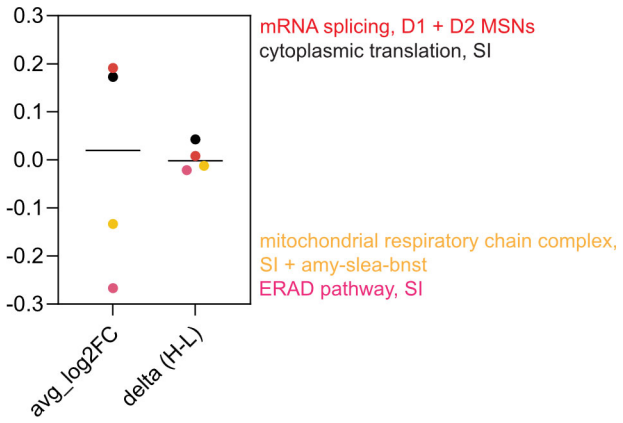

Figure 15: Differential expression of gene modules in VP cell types.

Both the most populous and the most perturbed cell types in VP were glia (astrocyte > immature oligos > microglia.) Although several modules were identified with glia-like expression patterns (ex. hub gene *Plp1*, crucial in myelination), none were differentially expressed between high and low risk animals. One unexpected finding from all three regions was the specificity in glial responses observed: for example, although microglia were present in all regions in substantial numbers, only in NAc was a correlated gene expression signature related to synaptic pruning detected. Differences in numbers and types of neurons displaying an inflammatory stress-like phenotype also support an argument for region and cell-type specific induction of glial activation during protracting opioid withdrawal.

Cross-species integration to further characterize NAc and VP cell types: As with PL, we sought out a high-quality mouse NAc snRNAseq dataset to integrate with our rat data. The selected dataset captured NAc from 11 adult mice, with no experimental manipulation.[139] To maximize our ability to compare cell types, we added two naïve control rat NAc samples that were collected for David Ottenheimer's paper on ventral pallidum transcriptional heterogeneity. After initial integration

steps, putative neurons were identified, subsetted, and re-clustered (Figure 16B.) Major cell types were unchanged between mouse and rat, although neurons from rat samples segregated into a greater number of subclusters, which may indicate increased transcriptional diversity, a more generous tissue sampling technique, or both (Figure 16C).

D1 MSNs displayed the greatest degree of transcriptional heterogeneity across mouse and rat samples. Rat-derived D1 MSNs were best labeled with *Pdyn*, unlike mouse-derived, who were better defined by the D1 marker gene *Ebf1*. A transitionary cluster between rat D1 MSNs and extended amygdala GABAergic neurons was selectively marked by the 5-HT receptor *Htr4*. As above, these extended amygdala-like cells were generally too diverse to be defined by one or two marker genes. Both mouse and rat contained likely contaminating VP-like cell types, including one cluster was marked by *Dscam* and another marked by *Lhx6*. Among D1 NUDAP/D1D2 double positive neurons, mouse-derived neurons were marked by *Pcp4*, while rat-derived neurons were marked by *Erbb4*. The novel D2 *Thsd7b* subcluster was largely absent from mouse samples, which could be due to a species difference or to differences in NAc dissection strategy. Other rare NAc or NAc-adjacent celltypes including Drd3 neurons, SST+ interneurons, and cholinergic interneurons were better-appreciated in this large dataset, with no apparent difference between rat and mouse.

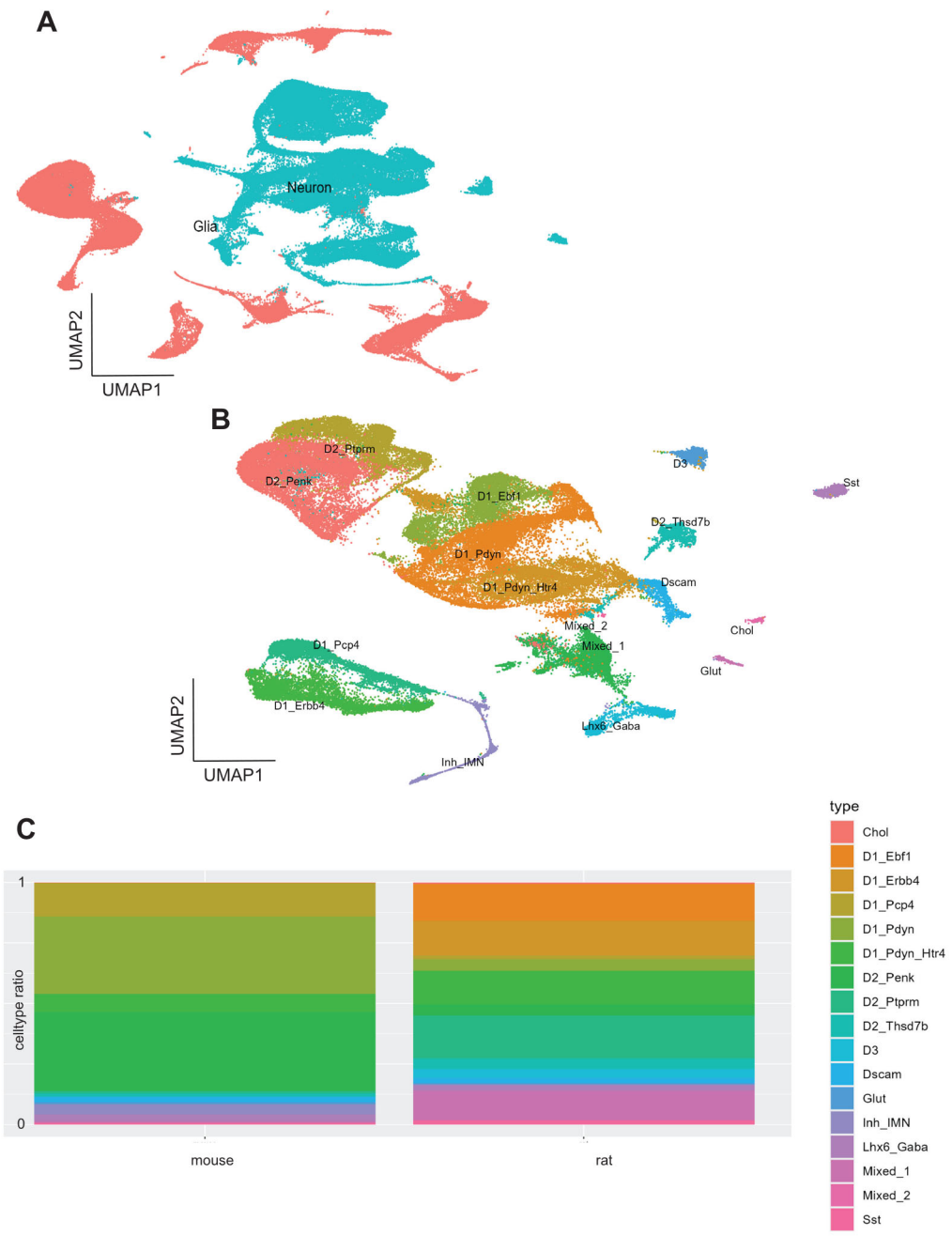

Figure 16: Cross-species integration highlights relative diversity of rat NAc over mouse. (A) UMAP depicting all cells after integration, n = 63,323. (B) Neuronal subclusters, labeled by marker gene when applicable. (C) Relative distribution of identified cell types in mouse and rat samples.

For cross-species analysis of VP, we utilized a mouse dataset collected by Stuber lab postdoc David Ottenheimer, which assessed the effect of high-fat diet upon VP cell types and addressed cross-species heterogeneity by comparing naïve mouse and rat VP samples.[99] Repeating the same approach, we utilized Allen mouse labels and Seurat's FindMarkers function to identify marker genes for each neuron cluster. Notably, rat and mouse data integrated near-perfectly (Figure 17B), which may be indicative of enhanced inter-species homogeneity in VP compared to NAc and PL. We noted that the diverse extended amygdala/BNST cell types were possible to capture with one or two marker genes: *Dach1* for an MSN-like cluster, *Dscam/Esr1* for what looks like striatal-pallidum transitional cells, and an *Ebf1+/Drd1-* cluster within the larger *Dscam/Esr1* group (Figure 17C.) Among *Lhx8+* GABAergic neurons that are more likely to reflect true VP cell types, three markers selectively labeled specific clusters: *Zfhx3*, *Alk*, and *Gpc5*. Putative interneurons either expressed *Sst* or *Tcf4*. Re-assessment of DEGs within these cluster assignments, rather than using the diverse Allen labels, failed to produce an increase in the number of DEGs identified. This was not very surprising, given that the cluster ID and composition of "true" VP cell types (Sema5a Gaba, Chst9 Gaba, Skor1 Glut, and Lhx8 Gaba) remained consistent with either approach. However, it was helpful to determine that the lack of VP DEGs was not solely due to the increased parcellation of the dataset compared to PL and NAc: when striatal-pallidal neurons were collapsed together into a *Dscam/Esr1* mega-cluster, they still failed to display addiction-risk correlated changes in gene expression. Thus, we can conclude that the VP and VP-adjacent cells characterized here are more defined by their transcriptional diversity than by the addiction risk group of the rat they originated from.

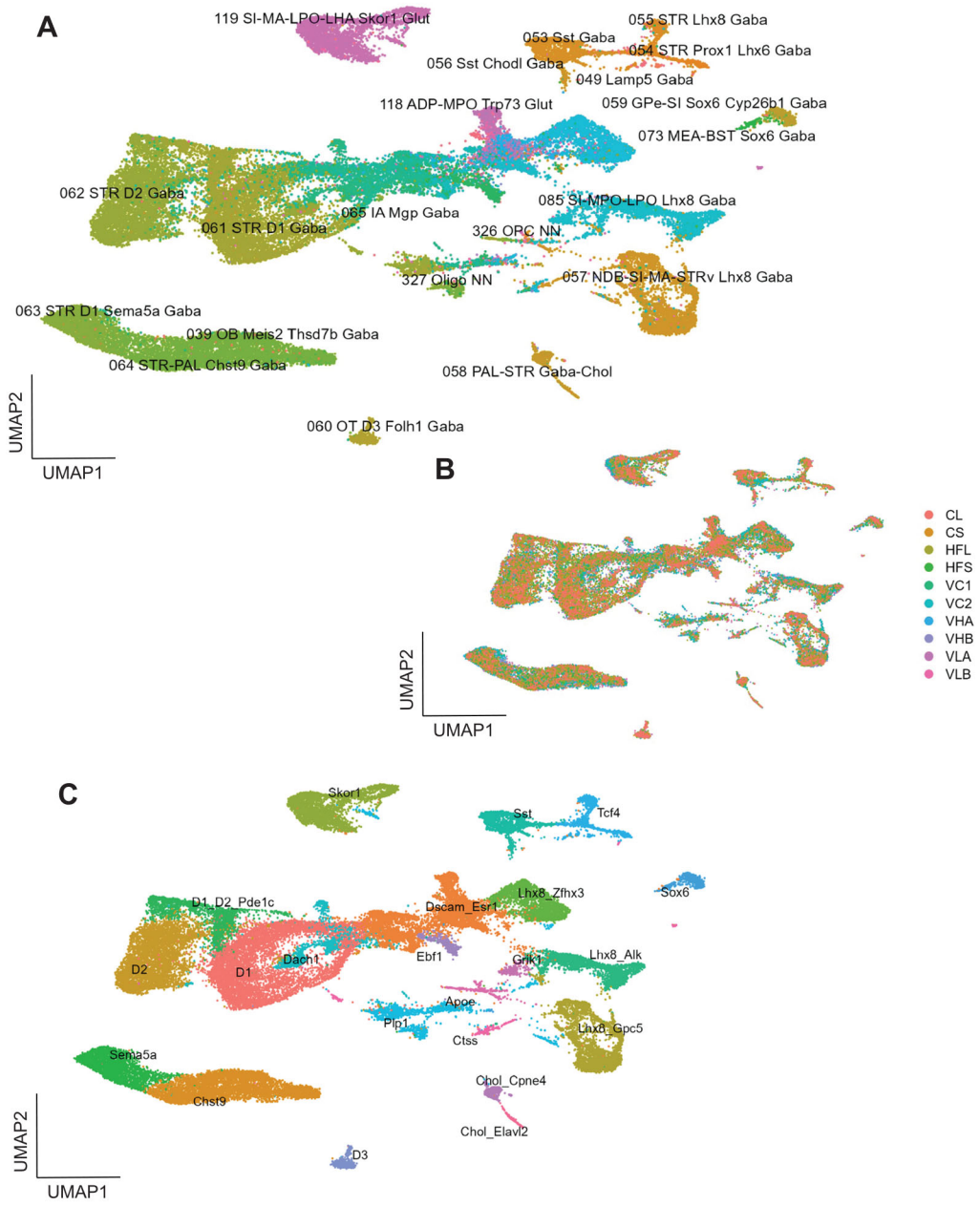

Figure 17: Cross-species integration provides novel cell type markers for VP GABAergic subpopulations. (A) Allen cell type labels for all neurons in dataset. (B) Distribution of neurons from each group, "CL, CS, HFL, and HFS" are mouse, remainder are rat. (C) Clusters re-labeled by putative cell type.

Section V: Summary

Specific investigation of the expression pattern of individual cells in the PL, NAc, and VP of high and low addiction-risk rats has revealed a distinct pattern of widespread downregulation of activity and synaptic-transmission related genes in PL and NAc, with VP comparatively unchanged. However, an important exception to this rule was found in PL L2/3 and L4/5 IT neurons, subsets of which were found to specifically upregulate the IEG *Homer1* in high addiction risk rats, along with other genes associated with enhanced LTP and Ca^{2+} signaling. A subcluster of L2/3 IT neurons marked by the transcription factor *Glis3* was found to be unique to rat samples, suggesting that transcriptional diversity may differ between the two species in medial PFC. Histological examination of PL for evidence of neuronal silencing via pPDH immunoreactivity revealed a significant relationship between addiction risk metrics and pPDH positivity rate in PL, but not NAc core or shell. Taken together, this data supports a phenotype of hypoactivity for PL neurons, which could theoretically be exacerbated by hyper-active IT neurons innervating local interneurons. Compared to pyramidal neurons, PL interneurons were comparatively less altered between high and low risk rats, but Pvalb interneurons showed the highest rates of change in expression patterns (especially the rare Pvalb chandelier cell type.)

In the NAc, D2 MSNs appeared more transcriptionally homogenous than D1 MSNs, and were the most altered cell type between high and low addiction risk rats. A subcluster of D1/D2 hybrid MSNs was found to express the novel marker *Thsd7b*, and was the only neuronal cluster found to have significant expression of a hormone receptor (*Pgr*.) Across NAc neurons, gene set analysis revealed downregulation of synaptic transmission-related genes, but these signatures differed between the two major cell types. One common feature between the two cell types was the significant downregulation of the metabotropic glutamate receptor 5 gene, *Grm5*, which was also a

hub gene for a downregulated synaptic transmission module. Both D1 and D2 MSNs receive strong glutamatergic input from a variety of sources (mPFC/PL, ventral hippocampus, PVT, BLA.) Decreases in mGluR5 expression alone would most likely be pro-inhibitory for both cell types, which corresponds with the other loss-of-activity-like gene set expression changes. Enhanced expression of *Oprm1* was observed in D2 MSNs of high-risk rats, likely further exacerbating a pro-inhibitory phenotype in those neurons in response to endogenous or exogenous opioids. Intriguingly, microglia in high-risk rats were found to upregulate a gene set related to synaptic pruning. Differences in DEG induction were observed in glia across the dataset, suggesting that local inflammatory changes induced by opioid use and withdrawal are region and cell-type specific. Although we are limited in our ability to make firm conclusions regarding causality and functional consequences of these gene expression changes, this wide-scale study has illuminated several potential avenues of future investigation. To test the relevance of these findings in maladaptive opioid use, we conducted a cell-type specific manipulation of a highly expressed gene that displayed robust between-group differences, mGluR5. Preliminary results from this study are described in the following chapter.

Chapter Four: Assessing the effect of cell-type-specific mGluR5 knockout upon addiction risk trajectory after protracted withdrawal

i. Rationale, experimental design, methods, and hypotheses

Rationale:

Big-data experiments, such as the one described above, can yield many potential avenues of further exploration. Our goal in conducting these large-scale studies is to utilize the information collected to generate testable hypotheses. Selecting cell types and genes for manipulation is not a simple process: focusing on only those that are already known to play a role in opioid addiction may be a safer choice but is less likely to produce novel findings. Conversely, choosing an overlooked cell type and/or gene could be highly novel, or could instead result in a wild goose chase if these targets do not meaningfully contribute to opioid-taking behaviors.

Keeping these risks in mind, we conducted a literature search on all DEGs that met certain criteria for further investigation: either upregulated or downregulated in at least one cell type in high-risk rats and included in or functionally related to a WGCNA gene set. This process identified one gene of particular interest: the metabotropic glutamate receptor 5, or mGluR5, a G_q coupled GPCR that localizes to post-synaptic densities, which is known to interact with the (highly expressed in high-risk rats) IEG Homer1.[140] Although mGluR5 itself is pro-excitatory, co-induction with Homer1 has been reported to result in removal of mGluR5 from the postsynaptic membrane in a pro-homeostatic, activity-regulating mechanism.[141] (More recent studies specifically localize mGluR5 to "peri-synaptic nanodomains", rather than the synapse itself.[142]) As a reminder, we observe modest decreases in *Grm5* expression in both D1 and D2 MSNs in high-risk rats, but addiction-risk dependent changes in *Homer1* were restricted to PL (where *Grm5* is also highly expressed.) In the dorsal root ganglion, mGluR5 interacts with NMDARs to contribute to opioid-induced

hyperalgesia[143] and is associated with induction of ERK signaling and cFOS expression in neuropathic pain.[144] Similarly, in the medium spiny neurons of the NAc, mGluR5 activation potentiates NMDA-evoked responses[145], modulating both D1 and D2 MSNs into a pro-excitatory state. However, there is also evidence of cell-type specific alterations in mGluR signaling, with similar end results between cell types: mGluR5 and D1R co-activation induces ERK, in a PKC-dependent pathway,[146] while mGluR5 and A2AR (specific to D2 MSNs) activation was found to induce both ERK and cFOS.[147] In a hypothetical situation where glutamate is stable and dopamine is enhanced, we could reasonably expect D1Rs to be relatively more potentiated than D2Rs, due to the additive effect of D1R and mGluR5 activation when compared to A2AR and mGluR5 activation, which would still need to overcome D2R-induced inhibition.

Considerable evidence exists to support a role for mGluR5 pharmacological antagonism in reducing drug self-administration. The noncompetitive antagonist MPEP was found to reduce both alcohol seeking and reinstatement after chronic alcohol self-administration[148], but interestingly was found to potentiate CPP to multiple substances, including heroin.[148] The more-selective antagonist MTEP was found to reduce morphine self-administration in mice, as well as cue-induced drug seeking.[149] Intra-accumbal delivery of MPEP modestly reduced responding for cocaine, with additional reports of suspected anhedonic-like behavior in response to the drug.[150] However, a study assessing effects of MTEP on methamphetamine self-administration reported decreased drug intake, but stable food intake at escalating doses of the antagonist, which does not support the induction of a pro-anhedonic state by mGluR5 antagonism. Clinical trials assessing the utility of mGluR5 antagonists in depression and nicotine use disorder have occurred, but no results are easily accessible. However, a recent clinical trial tested a mGluR5 negative allosteric modulator (mavoglurant) in subjects with cocaine use disorder, and reported a robust decrease in the number of cocaine use days over many weeks, with limited incidence of negative side effects.[151] This result

provides the first clear evidence that modulation of mGluRs in humans can support drug abstinence. To further expand our knowledge of the role of these receptors in maladaptive opioid use, we next sought to test whether cell-type-specific manipulation of mGluR5 was sufficient to alter opioid self-administration behavior. For initial experiments, we selected D1 MSNs for manipulation, hypothesizing that selective knockdown of mGluR5 expression in these neurons would attenuate addiction risk phenotypes.

Experimental design and methods:

Behavioral methods were as described in Chapter Two, with the following modifications. Rats underwent seven days of heroin self-administration during the pre-test period, followed by progressive ratio test #1. Utilizing latent profile analysis as previously described, each rat was classified as either low or high addiction risk and assigned to receive either the experimental virus (AAV1-DIO-Grm5-SACas9, titer of $1.75x10^{12}$ GC/mL, 1:5 dilution) or the corresponding control (AAV1-DIO-sgROSA.) CRISPR or control viruses were mixed 1:1 with a D1 MSN-specific enhancer virus expressing Cre recombinase (AiP13779 - pAAV-AiE0779m_3xC2-minBG-iCre(R297T)-BGHpA.)[152] 1 μL of the viral mixture (500 nL 1:5 diluted CRISPR/control, 500 nL 1:25 diluted enhancer virus) was delivered bilaterally to the NAc core and shell of each animal at the following coordinates: 1.3, 1.5, -7. After a three-week incubation period, rats were re-introduced to heroin intermittent self-administration for seven additional days, after which they underwent progressive ratio test #2, eleven days of extinction, and a cued-reinstatement test. Brains were flash-frozen 1-2 days following cued-reinstatement for validation of *Grm5* knockdown, which is ongoing. We additionally have conducted separate validation experiments in non-behavioral cohorts to assess the firing patterns of MSNs +/- *Grm5* knockdown, collection and analysis of this data is also in progress.

Hypotheses:

During the pre-test self-administration period, we expected rats to separate into low and high addiction risk groups as previously described. Following delivery and expression of the *Grm5* CRISPR or control viruses, we hypothesized that high addiction risk rats would be more likely to show a behavioral effect due to loss of mGluR5-mediated pro-excitatory signaling in D1 MSNs. Thus, we predicted that high-risk rats would display signs of attenuated heroin escalation after knockdown, while low-risk rats were more likely to remain unaffected.

ii. Results

As previously shown in Chapter Two, high and low addiction risk rats differ not only in their rates of self-administration, but in their behavioral trajectories over time: high-risk rats display escalation during the intermittent self-administration period, go through acute withdrawal after cessation of self-administration, and then enter a state of protracted withdrawal. In contrast, low-risk rats (despite taking some heroin) do not engage in escalation and are unlikely to display signs of withdrawal. Considering this, it is not surprising that both CRISPR and control animals display continued escalation of their heroin intake after intervention, as both groups contained high-risk rats that presumably went through withdrawal during the incubation period (Figure 18B.) Surprisingly, a subset of low risk rats in both groups displayed an abrupt switch in their behavior during the post-test period to a high-risk phenotype (Figure 18E.) These switches happened more frequently in the control group than in the CRISPR group, suggesting that the *Grm5* knockdown may have exerted a protective effect. To further explore this, we calculated within-animal z-scores of each behavioral metric, allowing us to account for each animal's varying addiction-risk trajectory and specifically interrogate the potential effect of the intervention upon risk state. By testing for a significant linear relationship across z scores in the pre-KO and post-KO periods, we could assess whether each rat

was displaying signs of amelioration, worsening, or no change in their addiction risk phenotype. Following the intervention, rats who received the mGluR5 CRISPR showed an immediate spike in their excess pressing and infusions (Figure 18A, B), which was followed by a downward trend, resulting in an overall less positive slope compared to the control group. In seeking, control animals displayed no linear relationship, implying that their seeking remained consistent over time (Figure 18C.) In contrast, KO animals displayed a weak negative linear relationship, indicating an overall decrease in seeking in the post-KO period compared to pre-KO. Control animals displayed a negative linear relationship in extinction responding (active lever presses during extinction), while KO animals had no linear relationship. Analysis of pre and post KO addiction metric with PCA (Figure 18 G, H) revealed a cluster of high-risk KO animals most defined by their pre-KO addiction metrics, whereas control animals were more represented by post-KO metrics (except one control animal) or by the exploratory metric (foodtray.)

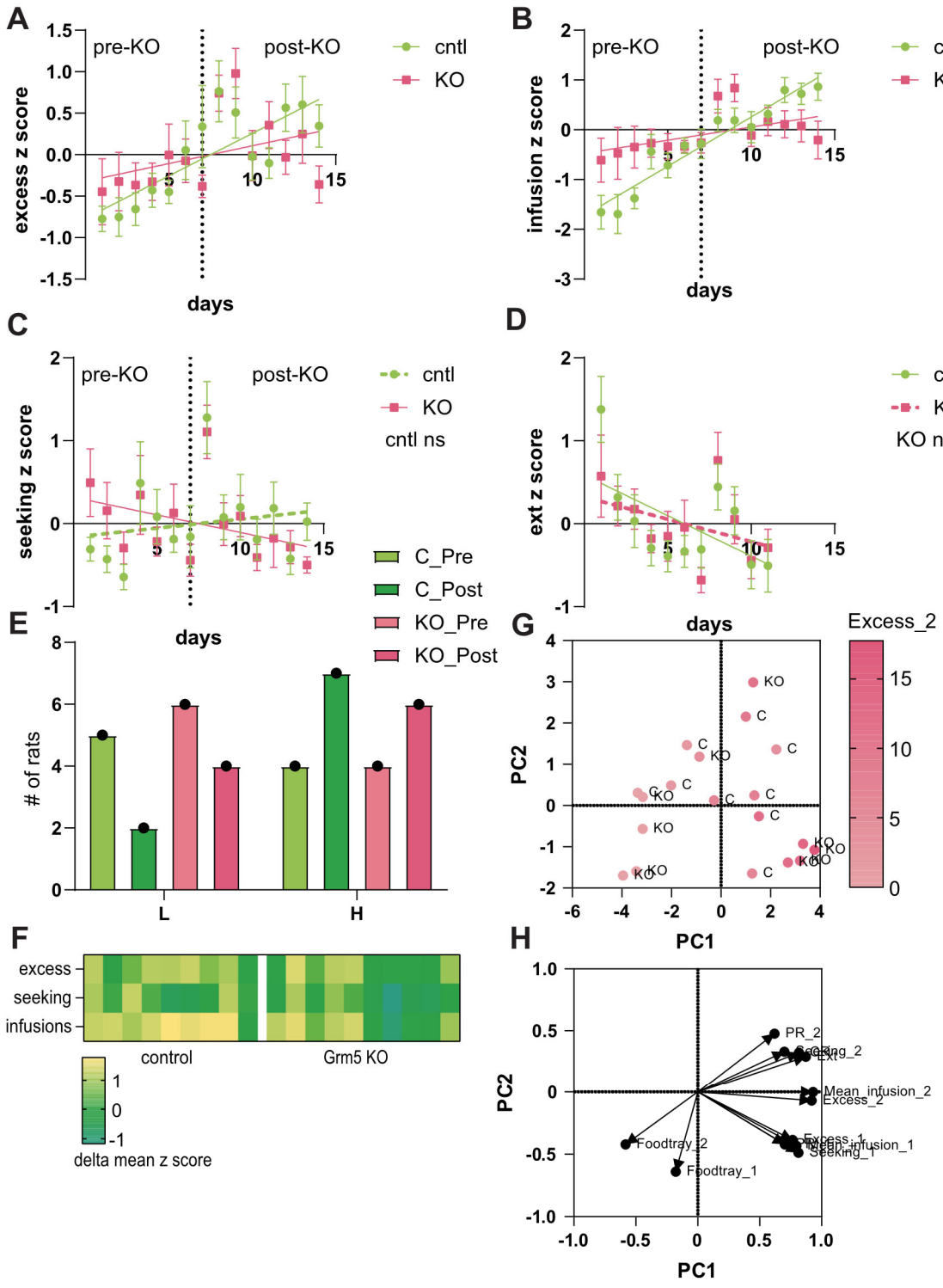
A
pre-KO
post-KO
cntl
KO
excess z score
days
B
infusion z score
C
seeking z score
cntl ns
C_Pre
C_Post
KO_Pre
KO_Post
D
ext z score
KO ns
E
# of rats
L
H
F
excess
seeking
infusions
control
Grm5 KO
delta mean z score
G
PC2
PC1
Excess_2
H
PR_2
Mean_infusion_2
Excess_2
Foodtray_2
Foodtray_1

Figure 18: Rats display an attenuated addiction risk phenotype after mGluR5 knockdown in D1 MSNs. (A-D) Z-scored behavioral metrics before and after intervention. (E) Number of rats in low and high-risk groups before and after intervention. (F) Delta z-scores (post – pre) for excess presses, seeking presses, and infusions. (G-H) PCA on pre (1) and post (2) addiction metrics reveals clustering of KO animals with pre-intervention addiction metrics, and control animals toward polarized post-intervention metrics.

iii. Summary

Behavioral analysis of video collected during this experiment is ongoing, which we expect to broaden our understanding of the effect of the intervention upon locomotion and drug or withdrawal-induced behavioral sensitization. Crucial validation experiments to confirm the selectivity of the D1 enhancer virus, extent of knockdown/knockout of mGluR5 in targeting neurons and characterize the firing patterns of MSNs +/- intervention are also in progress. Preliminary analysis of the behavioral data collected across this experiment indicates that animals that were high-risk before KO display a modestly attenuated addiction phenotype post-KO, and animals that were low-risk before KO appear less likely to undergo a low to high transition in their addiction phenotype. If the mGluR5 manipulation reduces excitability of D1 MSNs in response to glutamate, we would expect relatively more activation of D2 MSNs by glutamate, which may reduce opioid reward and disrupt normal learning processes (perhaps contributing to the persistence of KO animals in active lever pressing during extinction.) Evaluating the effect of mGluR5 KO in D2 MSNs is a natural future direction in this work and is likely the experiment that we would choose to undertake next. Another option for manipulation would be prelimbic cell types, especially L5 ET and Pvalb neurons, who may be the targets of contralateral hyperactive IT neurons in high-risk rats.

Discussion and conclusions

The broad goal of this work was to utilize a translational rodent model of OUD to facilitate two large-scale studies: first, comparing low and high addiction risk rats brain-wide in withdrawal and after "relapse," and second, comparing low and high addiction risk rats at the gene-expression level during protracted withdrawal. Here, we have sought to document the results of these experiments completely, and to describe hypothesis-based follow-up experiments that are ongoing. The most novel and surprising finding from the whole brain cFOS experiment was the marked loss of intra-cortical and parahippocampal activity correlations in the high-risk group. One region, mediofrontal cortex, displayed complete loss of correlation, indicating that cFOS z-scores within this group no longer had any relationship with z-scores in any other region. snRNA sequencing in prelimbic cortex, a subregion of mediofrontal cortex, revealed that L2/3 and L4/5 IT neurons were the most transcriptionally perturbed by far. However, dataset-wide, correlated gene sets (including those related to neuronal activity) tended to be downregulated in high addiction risk rats. Quantification of likely-hypoactive neurons with pPDH supported this finding, with pPDH positivity rates increasing with progressive ratio responding in PL, but not in the NAc core or shell. Identification of IT neurons, who project more locally than ET or CT neurons, as the most perturbed presents the possibility that disruption of function in these neurons could be contributing to the lack of correlated intracortical cFOS in high-risk rats. In the NAc, canonical D1 and D2 MSNs displayed broadly similar gene expression patterns, with relatively more DEGs detected in the homogenous D2 MSNs than the heterogenous D1 MSNs. Rare MSN celltypes, including D2 StrioMat, D1/D2 hybrid, and D1 NUDAP, tended to be quiescent (except for an upregulation of *Oprm1* in D1 NUDAP MSNs of high-risk rats), as did diverse cell types in the VP. Lack of differential gene expression detected in this experiment by no means implies that these cell types do not contribute to heroin escalation and withdrawal. Cross-species integration of our rat datasets with

mouse has facilitated the identification of novel markers for these rare cell types, which could be employed to perform targeted follow up experiments. In all three regions, glia displayed striking but varying patterns of gene expression change in high addiction risk rats, with the most compelling alteration being the induction of synaptic pruning-related genes in NAc microglia. Further work is in progress to validate these findings, but for now we can conclude that our sequencing data strongly supports dysregulation of glia as one of the most salient gene expression phenotypes during protracted withdrawal from heroin.

Two priorities predominate for our future work. First, although our snRNAseq dataset is wide-ranging and high quality, it of course lacks information about the spatial location of each perturbed and non-perturbed cell in each region. In PL, the layer specificity of cell types gives us some idea where to look, but in NAc and VP little is known about the spatial heterogeneity of the neurons we sequenced, especially in rare cell types. To address this gap, we plan to conduct *in situ* hybridization experiments targeting novel cell type markers and other genes of interest in NAc and VP. However, this approach will not allow us to discover previously unappreciated cell type markers. Thus, to do this we hope to conduct sequencing-based spatial transcriptomic assays in the PL and NAc of high and low-risk rats, both to validate our snRNAseq findings and map out putative activated and inhibited neurons at high resolution. Second, by selecting the protracted withdrawal timepoint (8+ days after last heroin session) to do our studies, we remain blind to alterations that are occurring during escalation and shortly after, during physiologic opioid withdrawal. *In vivo* imaging of MSN activity with GCaMP, coupled with a dopamine sensor, would provide much needed information about how MSN activity is differentially regulated by DA during escalation and withdrawal. We have previously attempted this using D1 MSN enhancers, DIO-GCaMP, and red GRAB-DA, in conjunction with GRIN lenses and 1p miniscopes, but have not yet produced high-quality recordings during self-administration.

Finally, we have summarized preliminary data collected during a functional manipulation of *Grm5* expression during heroin self-administration. As previously described, follow up studies evaluating the effect of mGluR5 KO upon other cell types would naturally be of interest. In prelimbic cortex, L4/5 IT neurons emerged as perhaps the most functionally perturbed cell type (L2/3 IT neurons showed more DEGs, but also more signs of cellular stress), making them an intriguing candidate for future manipulation. To simply test their contribution to episodes of relapse, we could deliver Cre-dependent G_i DREADDs to the PL, in conjunction with a L4/5 IT-specific enhancer virus expressing Cre and inject CNO an hour before cue-induced reinstatement. If these neurons play an important role in the observed dysregulation of mediofrontal cortex in withdrawal, we would hypothesize that their silencing would attenuate reinstatement responding (and vice versa with a G_q DREADD.)

In addition to the systems neuroscience work described above, we have utilized cutting-edge statistical approaches to analyze, categorize, and make predictions about each rat's addiction risk state. By doing so, we have come to appreciate the wide spectrum of addiction risk behaviors that can be observed in rodents. This spectrum has considerable value to our work, as it underlies much of the proposed translatability of these studies to a varied population of diverse humans. However, it also necessitates rigorous, robust, and high-throughput science, which is challenging and costly to execute well. Relatively common psychiatric conditions, like opioid use disorder, are unlikely to converge upon a singular brain region, cell type, or specific gene as a putative "key" to unlocking addiction. Here, we have cast some very wide nets and have been rewarded with many new pieces of incremental knowledge, as well as some surprising and novel findings that have generated new hypotheses. By continuing to test and revise our working theories about how cortical, striatal, pallidal, and midbrain regions interact to produce addiction-like behaviors, we hope to arrive at an improved understanding of the neural mechanisms underlying opioid use disorder.

Supplementary information:

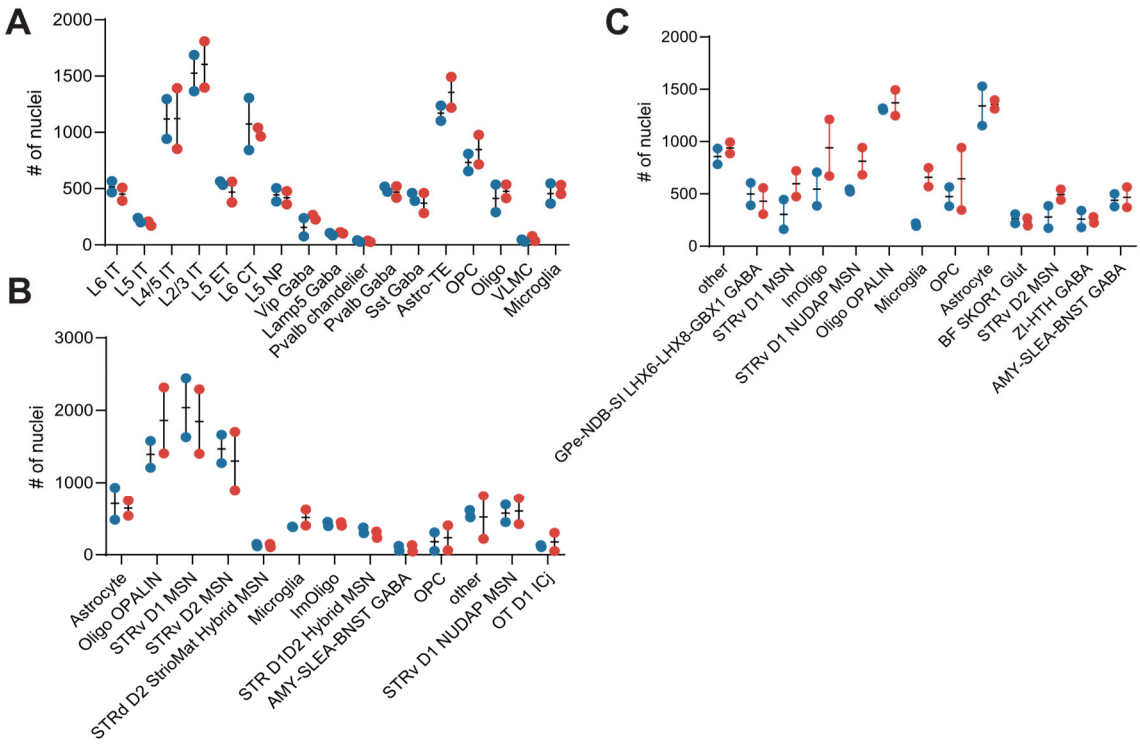

Supplementary Figure 1: Counts within each cell type, for each region (A, prelimbic, B, nucleus accumbens, C, ventral pallidum) sequenced, in high (red) and low (blue) addiction risk pooled samples.

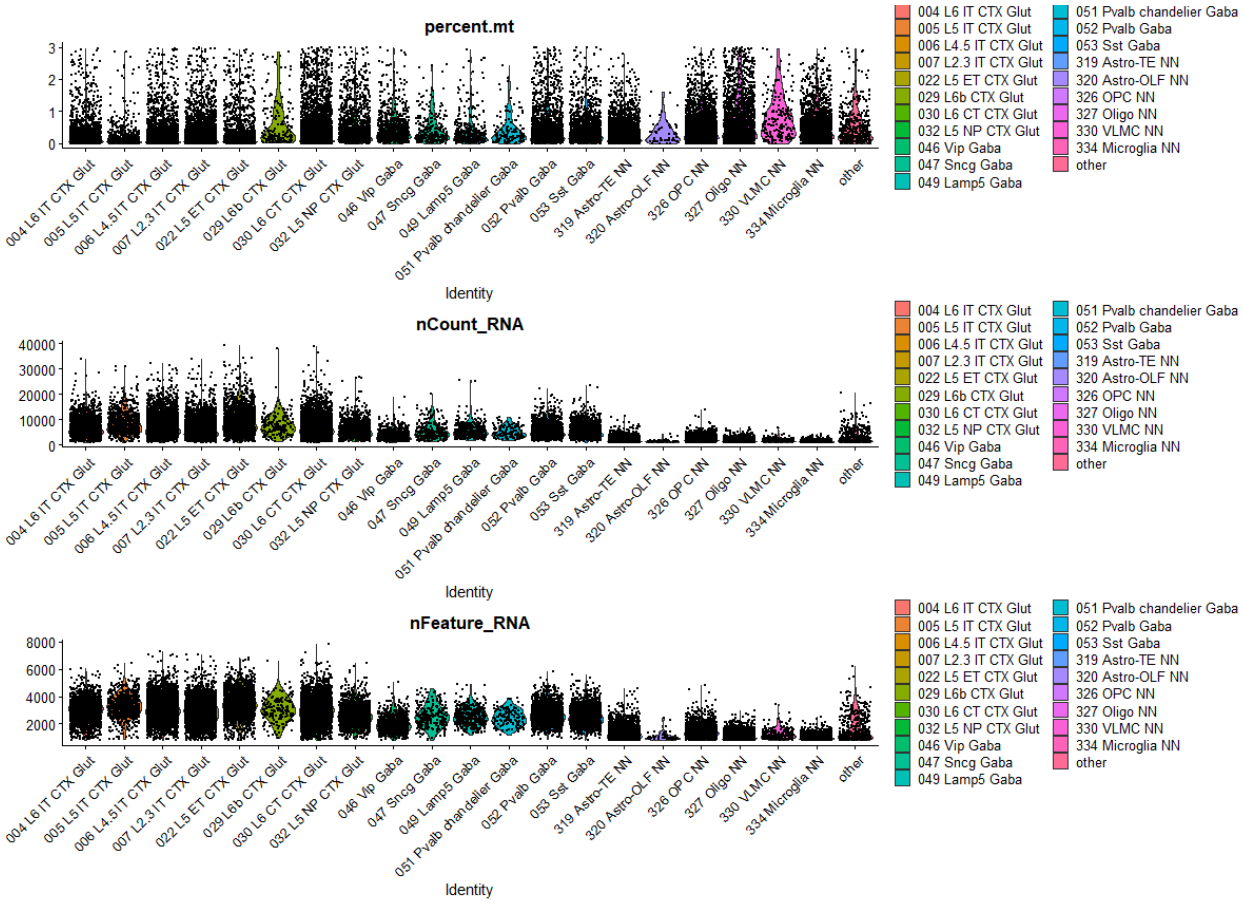

Supplementary Figure 2: Quality control metrics for prelimbic cortex.

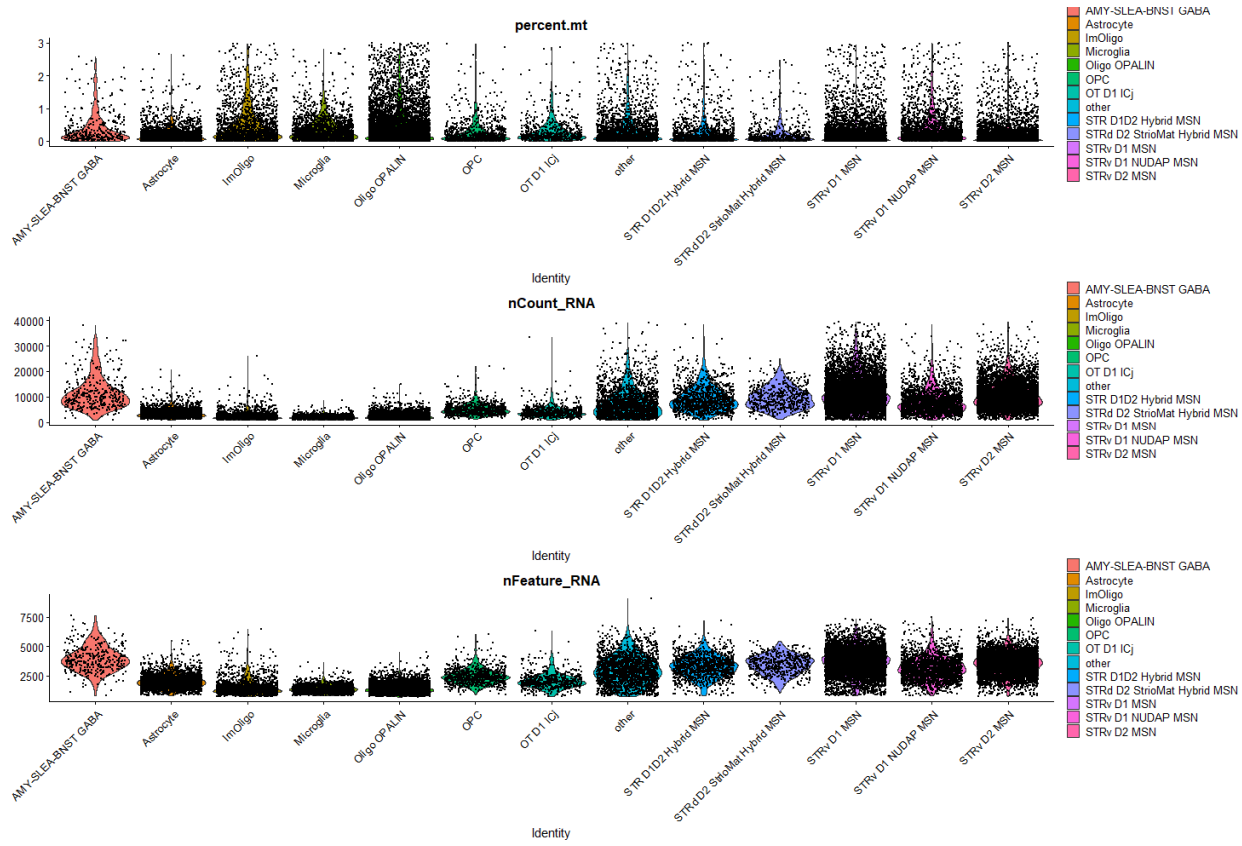

Supplementary Figure 2: Quality control metrics for nucleus accumbens.

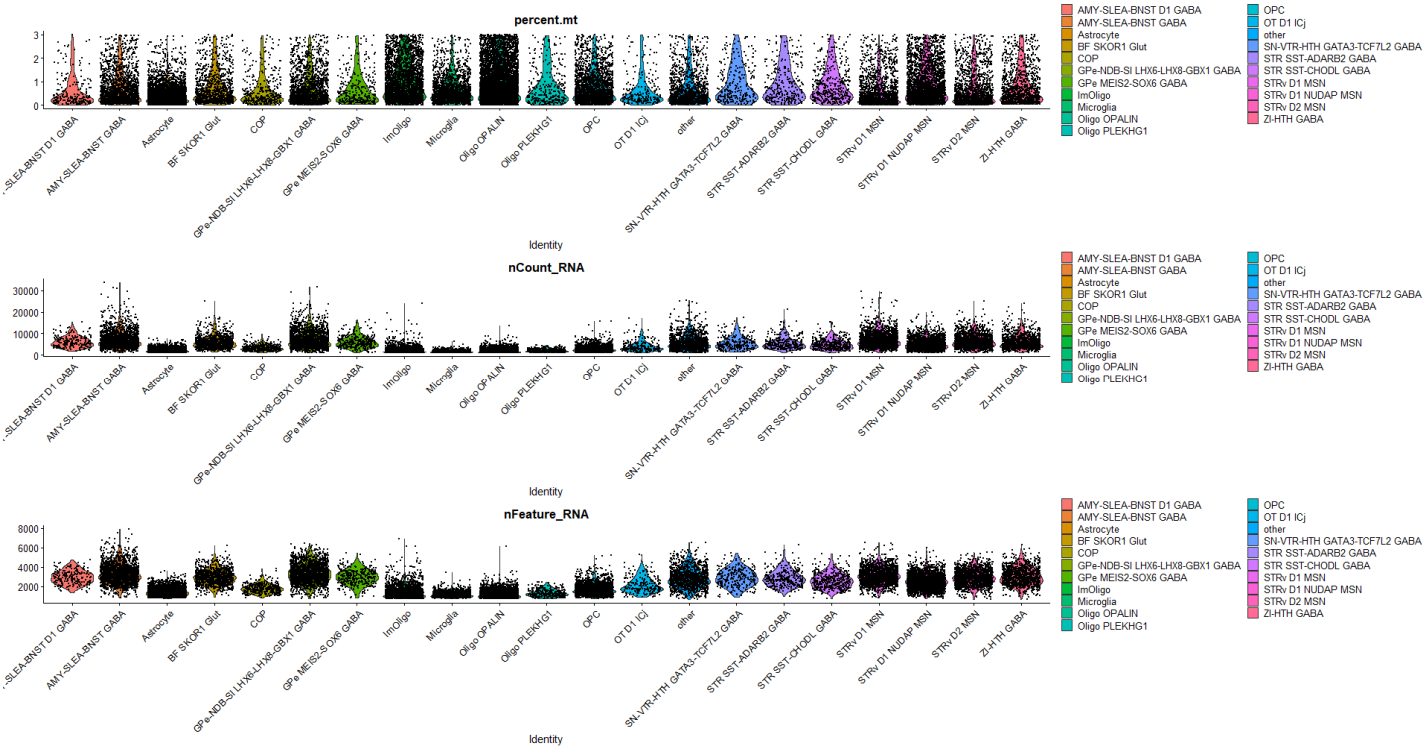

Supplementary Figure 3: Quality control metrics for ventral pallidum.

Index of abbreviations:

OB: Olfactory bulb

Sub: Subiculum

CA1: Cornu ammonis 1

CA2: Cornu ammonis 2

CA3: Cornu ammonis 3

DG: Dentate gyrus

PrC: Postrhinal cortex

Presub: Presubiculum

Parasub: Parsubiculum

PeriC: Perirhinal cortex

EntoC: Entorhinal cortex

PiriC: Piriform cortex

CR: Cingulate region

RsC: Retrosplenial cortex

IR: Insular region

OfC: Orbitofrontal cortex

MfC: Mediofrontal cortex

MC: Motor cortex

SSC: Primary somatosensory cortex

PPC: Posterior parietal cortex

VC: Visual cortex

TAC: Temporal association cortex

AC: Auditory cortex

EndoN: Endopiriform nucleus

Amy: Amygdaloid area unspecified

CP: Caudate putamen

NAcC: Nucleus accumbens core

NAcSh: Nucleus accumbens shell

VS: Ventral striatal region unspecified

GPe: Globus pallidus externus

EntoN: Entopeduncular nucleus

VP: Ventral pallidum

BF: Basal forebrain region

BNST: Bed nucleus of the stria terminalis

SR: Septal region

StN: Subthalamic nuclei

ZI: Zona incerta

LHb: Lateral habenular nucleus

MHb: Medial habenular nucleus

NSM: Nucleus of the stria medullaris

PG: Pineal gland

ANDT: Anterior nuclei of the dorsal thalamus

DCDT: Dorsal-caudal midline group of the dorsal thalamus

VDT: Ventral nuclei of the dorsal thalamus

ILDT: Intralaminar nuclei of the dorsal thalamus

LPDT: Lateral posterior (pulvinar) complex of the dorsal thalamus

LDDT: Laterodorsal thalamic nuclei of the dorsal thalamus

DLGN: Dorsal lateral geniculate nucleus

Hypo: Hypothalamus

IC: Inferior colliculus

SC: Superior colliculus

SN: Substantia nigra

VTA: Ventral tegmental area

PPN: Peripeduncular nucleus

IPN: Interpeduncular nucleus

PAG: Periaqueductal gray

PN: Pontine nuclei

Cb: Cerebellum

References:

(1) Booth, M. *Opium, a History*; Simon and Schuster, 1996.
(2) Macht, D. The History of Opium and Some of Its Preparations and Alkaloids. *JAMA* **1915**, *LXIV* (6), 477–481.
(3) Jennings, E. M.; Okine, B. N.; Roche, M.; Finn, D. P. Stress-Induced Hyperalgesia. *Prog. Neurobiol.* **2014**, *121*, 1–18. https://doi.org/10.1016/j.pneurobio.2014.06.003.
(4) Leknes, S.; Eikemo, M.; Løseth, G. Understanding Individual Variability in Opioid Responses: A Call to Arms. *Addict. Biol.* **2024**, *29* (6), e13418. https://doi.org/10.1111/adb.13418.
(5) Markou, A.; Kosten, T. R.; Koob, G. F. Neurobiological Similarities in Depression and Drug Dependence: A Self-Medication Hypothesis. *Neuropsychopharmacol. Off. Publ. Am. Coll. Neuropsychopharmacol.* **1998**, *18* (3), 135–174. https://doi.org/10.1016/S0893-133X(97)00113-9.
(6) Khantzian, E. J. The Self-Medication Hypothesis of Addictive Disorders: Focus on Heroin and Cocaine Dependence. *Am. J. Psychiatry* **1985**, *142* (11), 1259–1264. https://doi.org/10.1176/ajp.142.11.1259.
(7) Strang, J.; Volkow, N. D.; Degenhardt, L.; Hickman, M.; Johnson, K.; Koob, G. F.; Marshall, B. D. L.; Tyndall, M.; Walsh, S. L. Opioid Use Disorder. *Nat. Rev. Dis. Primer* **2020**, *6* (1), 3. https://doi.org/10.1038/s41572-019-0137-5.
(8) Singh, D. *Naltrexone*; StatPearls, 2023.
(9) Langendam, M. W.; van Brussel, G. H.; Coutinho, R. A.; van Ameijden, E. J. The Impact of Harm-Reduction-Based Methadone Treatment on Mortality among Heroin Users. *Am. J. Public Health* **2001**, *91* (5), 774–780. https://doi.org/10.2105/ajph.91.5.774.
(10) Johnson, S. W.; North, R. A. Opioids Excite Dopamine Neurons by Hyperpolarization of Local Interneurons. *J. Neurosci. Off. J. Soc. Neurosci.* **1992**, *12* (2), 483–488. https://doi.org/10.1523/JNEUROSCI.12-02-00483.1992.
(11) Beier, K. T.; Steinberg, E. E.; DeLoach, K. E.; Xie, S.; Miyamichi, K.; Schwarz, L.; Gao, X. J.; Kremer, E. J.; Malenka, R. C.; Luo, L. Circuit Architecture of VTA Dopamine Neurons Revealed by Systematic Input-Output Mapping. *Cell* **2015**, *162* (3), 622–634. https://doi.org/10.1016/j.cell.2015.07.015.
(12) Zhuang, Y.; Xu, P.; Mao, C.; Wang, L.; Krumm, B.; Zhou, X. E.; Huang, S.; Liu, H.; Cheng, X.; Huang, X.-P.; Shen, D.-D.; Xu, T.; Liu, Y.-F.; Wang, Y.; Guo, J.; Jiang, Y.; Jiang, H.; Melcher, K.; Roth, B. L.; Zhang, Y.; Zhang, C.; Xu, H. E. Structural Insights into the Human D1 and D2 Dopamine Receptor Signaling Complexes. *Cell* **2021**, *184* (4), 931-942.e18. https://doi.org/10.1016/j.cell.2021.01.027.
(13) Kravitz, A. V.; Freeze, B. S.; Parker, P. R. L.; Kay, K.; Thwin, M. T.; Deisseroth, K.; Kreitzer, A. C. Regulation of Parkinsonian Motor Behaviours by Optogenetic Control of Basal Ganglia Circuitry. *Nature* **2010**, *466* (7306), 622–626. https://doi.org/10.1038/nature09159.
(14) Danjo, T.; Yoshimi, K.; Funabiki, K.; Yawata, S.; Nakanishi, S. Aversive Behavior Induced by Optogenetic Inactivation of Ventral Tegmental Area Dopamine Neurons Is Mediated by Dopamine D2 Receptors in the Nucleus Accumbens. *Proc. Natl. Acad. Sci. U. S. A.* **2014**, *111* (17), 6455–6460. https://doi.org/10.1073/pnas.1404323111.
(15) Cole, S. L.; Robinson, M. J. F.; Berridge, K. C. Optogenetic Self-Stimulation in the Nucleus Accumbens: D1 Reward versus D2 Ambivalence. *PLOS ONE* **2018**, *13* (11), e0207694. https://doi.org/10.1371/journal.pone.0207694.
(16) Zachry, J. E.; Kutlu, M. G.; Yoon, H. J.; Leonard, M. Z.; Chevée, M.; Patel, D. D.; Gaidici, A.; Kondev, V.; Thibeault, K. C.; Bethi, R.; Tat, J.; Melugin, P. R.; Isiktas, A. U.; Joffe, M. E.; Cai, D. J.; Conn, P. J.; Grueter, B. A.; Calipari, E. S. D1 and D2 Medium Spiny Neurons in the

Nucleus Accumbens Core Have Distinct and Valence-Independent Roles in Learning. *Neuron* **2024**, *112* (5), 835-849.e7. https://doi.org/10.1016/j.neuron.2023.11.023.
(17) Domingues, A. V.; Carvalho, T. T. A.; Martins, G. J.; Correia, R.; Coimbra, B.; Bastos-Gonçalves, R.; Wezik, M.; Gaspar, R.; Pinto, L.; Sousa, N.; Costa, R. M.; Soares-Cunha, C.; Rodrigues, A. J. Dynamic Representation of Appetitive and Aversive Stimuli in Nucleus Accumbens Shell D1- and D2-Medium Spiny Neurons. *Nat. Commun.* **2025**, *16* (1), 59. https://doi.org/10.1038/s41467-024-55269-9.
(18) Zhu, Y.; Wienecke, C. F. R.; Nachtrab, G.; Chen, X. A Thalamic Input to the Nucleus Accumbens Mediates Opiate Dependence. *Nature* **2016**, *530* (7589), 219–222. https://doi.org/10.1038/nature16954.
(19) Yang, H.; de Jong, J. W.; Tak, Y.; Peck, J.; Bateup, H. S.; Lammel, S. Nucleus Accumbens Subnuclei Regulate Motivated Behavior via Direct Inhibition and Disinhibition of VTA Dopamine Subpopulations. *Neuron* **2018**, *97* (2), 434-449.e4. https://doi.org/10.1016/j.neuron.2017.12.022.
(20) Bromberg-Martin, E. S.; Matsumoto, M.; Hikosaka, O. Dopamine in Motivational Control: Rewarding, Aversive, and Alerting. *Neuron* **2010**, *68* (5), 815–834. https://doi.org/10.1016/j.neuron.2010.11.022.
(21) Glimcher, P. W. Understanding Dopamine and Reinforcement Learning: The Dopamine Reward Prediction Error Hypothesis. *Proc. Natl. Acad. Sci.* **2011**, *108* (supplement_3), 15647–15654. https://doi.org/10.1073/pnas.1014269108.
(22) Smith, K. S.; Tindell, A. J.; Aldridge, J. W.; Berridge, K. C. Ventral Pallidum Roles in Reward and Motivation. *Behav. Brain Res.* **2009**, *196* (2), 155–167. https://doi.org/10.1016/j.bbr.2008.09.038.
(23) Root, D. H.; Melendez, R. I.; Zaborszky, L.; Napier, T. C. The Ventral Pallidum: Subregion-Specific Functional Anatomy and Roles in Motivated Behaviors. *Prog. Neurobiol.* **2015**, *130*, 29–70. https://doi.org/10.1016/j.pneurobio.2015.03.005.
(24) Smith, K. S.; Berridge, K. C. The Ventral Pallidum and Hedonic Reward: Neurochemical Maps of Sucrose "Liking" and Food Intake. *J. Neurosci. Off. J. Soc. Neurosci.* **2005**, *25* (38), 8637–8649. https://doi.org/10.1523/JNEUROSCI.1902-05.2005.
(25) Hnasko, T. S.; Sotak, B. N.; Palmiter, R. D. Morphine Reward in Dopamine-Deficient Mice. *Nature* **2005**, *438* (7069), 854–857. https://doi.org/10.1038/nature04172.
(26) Zheng, R.; Chen, Y.; Zhang, J.; Liu, Q.; Zheng, Y.; Wang, Z. Prelimbic Cortex Is Involved in the Regulation of Morphine-Induced Conditioned Place Preference in Both Resistant and Sensitive Mice. *Sci. Rep.* **2025**, *15* (1), 5596. https://doi.org/10.1038/s41598-025-87084-7.
(27) Jiang, C.; Wang, X.; Le, Q.; Liu, P.; Liu, C.; Wang, Z.; He, G.; Zheng, P.; Wang, F.; Ma, L. Morphine Coordinates SST and PV Interneurons in the Prelimbic Cortex to Disinhibit Pyramidal Neurons and Enhance Reward. *Mol. Psychiatry* **2021**, *26* (4), 1178–1193. https://doi.org/10.1038/s41380-019-0480-7.
(28) De Jaeger, X.; Bishop, S. F.; Ahmad, T.; Lyons, D.; Ng, G. A.; Laviolette, S. R. The Effects of AMPA Receptor Blockade in the Prelimbic Cortex on Systemic and Ventral Tegmental Area Opiate Reward Sensitivity. *Psychopharmacology (Berl.)* **2013**, *225* (3), 687–695. https://doi.org/10.1007/s00213-012-2852-4.
(29) Trantham-Davidson, H.; Neely, L. C.; Lavin, A.; Seamans, J. K. Mechanisms Underlying Differential D1 versus D2 Dopamine Receptor Regulation of Inhibition in Prefrontal Cortex. *J. Neurosci. Off. J. Soc. Neurosci.* **2004**, *24* (47), 10652–10659. https://doi.org/10.1523/JNEUROSCI.3179-04.2004.

(30) Xu, T.-X.; Yao, W.-D. D1 and D2 Dopamine Receptors in Separate Circuits Cooperate to Drive Associative Long-Term Potentiation in the Prefrontal Cortex. *Proc. Natl. Acad. Sci. U. S. A.* **2010**, *107* (37), 16366–16371. https://doi.org/10.1073/pnas.1004108107.
(31) Gipson, C. D.; Dunn, K. E.; Bull, A.; Ulangkaya, H.; Hossain, A. Establishing Preclinical Withdrawal Syndrome Symptomatology Following Heroin Self-Administration in Male and Female Rats. *Exp. Clin. Psychopharmacol.* **2021**, *29* (6), 636–649. https://doi.org/10.1037/pha0000375.
(32) Bonci, A.; Williams, J. T. Increased Probability of GABA Release during Withdrawal from Morphine. *J. Neurosci. Off. J. Soc. Neurosci.* **1997**, *17* (2), 796–803. https://doi.org/10.1523/JNEUROSCI.17-02-00796.1997.
(33) Welsch, L.; Bailly, J.; Darcq, E.; Kieffer, B. L. The Negative Affect of Protracted Opioid Abstinence: Progress and Perspectives From Rodent Models. *Biol. Psychiatry* **2020**, *87* (1), 54–63. https://doi.org/10.1016/j.biopsych.2019.07.027.
(34) Zhu, Y.; Wang, K.; Ma, T.; Ji, Y.; Lou, Y.; Fu, X.; Lu, Y.; Liu, Y.; Dang, W.; Zhang, Q.; Yin, F.; Wang, K.; Yu, B.; Zhang, H.; Lai, J.; Wang, Y. Nucleus Accumbens D1/D2 Circuits Control Opioid Withdrawal Symptoms in Mice. *J. Clin. Invest.* **2023**, *133* (18), e163266. https://doi.org/10.1172/JCI163266.
(35) Fox, M. E.; Wulff, A. B.; Franco, D.; Choi, E. Y.; Calarco, C. A.; Engeln, M.; Turner, M. D.; Chandra, R.; Rhodes, V. M.; Thompson, S. M.; Ament, S. A.; Lobo, M. K. Adaptations in Nucleus Accumbens Neuron Subtypes Mediate Negative Affective Behaviors in Fentanyl Abstinence. *Biol. Psychiatry* **2023**, *93* (6), 489–501. https://doi.org/10.1016/j.biopsych.2022.08.023.
(36) Kaufling, J.; Aston-Jones, G. Persistent Adaptations in Afferents to Ventral Tegmental Dopamine Neurons after Opiate Withdrawal. *J. Neurosci.* **2015**, *35* (28), 10290–10303. https://doi.org/10.1523/JNEUROSCI.0715-15.2015.
(37) Pomrenze, M. B.; Cardozo Pinto, D. F.; Neumann, P. A.; Llorach, P.; Tucciarone, J. M.; Morishita, W.; Eshel, N.; Heifets, B. D.; Malenka, R. C. Modulation of 5-HT Release by Dynorphin Mediates Social Deficits during Opioid Withdrawal. *Neuron* **2022**, *110* (24), 4125-4143.e6. https://doi.org/10.1016/j.neuron.2022.09.024.
(38) Grimm, J. W.; Hope, B. T.; Wise, R. A.; Shaham, Y. Neuroadaptation. Incubation of Cocaine Craving after Withdrawal. *Nature* **2001**, *412* (6843), 141–142. https://doi.org/10.1038/35084134.
(39) Bergeria, C. L.; Gipson, C. D.; Smith, K. E.; Stoops, W. W.; Strickland, J. C. Opioid Craving Does Not Incubate over Time in Inpatient or Outpatient Treatment Studies: Is the Preclinical Incubation of Craving Model Lost in Translation? *Neurosci. Biobehav. Rev.* **2024**, *160*, 105618. https://doi.org/10.1016/j.neubiorev.2024.105618.
(40) Altshuler, R. D.; Garcia, K. T.; Li, X. Incubation of Oxycodone Craving Following Adult-Onset and Adolescent-Onset Oxycodone Self-Administration in Male Rats. *Front. Behav. Neurosci.* **2021**, *15*, 697509. https://doi.org/10.3389/fnbeh.2021.697509.
(41) Fredriksson, I.; Shaham, Y. A Novel Rat Model of Potentiated Incubation of Opioid Craving after Abstinence Induced by Adverse Consequences of Drug Seeking. *Neuropsychopharmacol. Off. Publ. Am. Coll. Neuropsychopharmacol.* **2024**, *49* (1), 311–312. https://doi.org/10.1038/s41386-023-01623-2.
(42) Li, Q.; Li, Z.; Li, W.; Zhang, Y.; Wang, Y.; Zhu, J.; Chen, J.; Li, Y.; Yan, X.; Ye, J.; Li, L.; Wang, W.; Liu, Y. Disrupted Default Mode Network and Basal Craving in Male Heroin-Dependent Individuals: A Resting-State fMRI Study. *J. Clin. Psychiatry* **2016**, *77* (10), e1211–e1217. https://doi.org/10.4088/JCP.15m09965.

(43) Lin, H.-C.; Wang, P.-W.; Wu, H.-C.; Ko, C.-H.; Yang, Y.-H.; Yen, C.-F. Altered Gray Matter Volume and Disrupted Functional Connectivity of Dorsolateral Prefrontal Cortex in Men with Heroin Dependence. *Psychiatry Clin. Neurosci.* **2018**, *72* (6), 435–444. https://doi.org/10.1111/pcn.12655.
(44) Ma, N.; Liu, Y.; Li, N.; Wang, C.-X.; Zhang, H.; Jiang, X.-F.; Xu, H.-S.; Fu, X.-M.; Hu, X.; Zhang, D.-R. Addiction Related Alteration in Resting-State Brain Connectivity. *NeuroImage* **2010**, *49* (1), 738–744. https://doi.org/10.1016/j.neuroimage.2009.08.037.
(45) Li, Q.; Liu, J.; Wang, W.; Wang, Y.; Li, W.; Chen, J.; Zhu, J.; Yan, X.; Li, Y.; Li, Z.; Ye, J.; Wang, W. Disrupted Coupling of Large-Scale Networks Is Associated with Relapse Behaviour in Heroin-Dependent Men. *J. Psychiatry Neurosci. JPN* **2018**, *43* (1), 48–57. https://doi.org/10.1503/jpn.170011.
(46) McNamara, R.; Dalley, J. W.; Robbins, T. W.; Everitt, B. J.; Belin, D. Trait-like Impulsivity Does Not Predict Escalation of Heroin Self-Administration in the Rat. *Psychopharmacology (Berl.)* **2010**, *212* (4), 453–464. https://doi.org/10.1007/s00213-010-1974-9.
(47) Volkow, N. D.; Fowler, J. S.; Wang, G. J.; Baler, R.; Telang, F. Imaging Dopamine's Role in Drug Abuse and Addiction. *Neuropharmacology* **2009**, *56 Suppl 1* (Suppl 1), 3–8. https://doi.org/10.1016/j.neuropharm.2008.05.022.
(48) Shi, Z.; Li, X.; Todaro, D. R.; Cao, W.; Lynch, K. G.; Detre, J. A.; Loughead, J.; Langleben, D. D.; Wiers, C. E. Medial Prefrontal Neuroplasticity during Extended-Release Naltrexone Treatment of Opioid Use Disorder - a Longitudinal Structural Magnetic Resonance Imaging Study. *Transl. Psychiatry* **2024**, *14* (1), 360. https://doi.org/10.1038/s41398-024-03061-0.
(49) Paniccia, J. E.; Vollmer, K. M.; Green, L. M.; Grant, R. I.; Winston, K. T.; Buchmaier, S.; Westphal, A. M.; Clarke, R. E.; Doncheck, E. M.; Bordieanu, B.; Manusky, L. M.; Martino, M. R.; Ward, A. L.; Rinker, J. A.; McGinty, J. F.; Scofield, M. D.; Otis, J. M. Restoration of a Paraventricular Thalamo-Accumbal Behavioral Suppression Circuit Prevents Reinstatement of Heroin Seeking. *Neuron* **2024**, *112* (5), 772-785.e9. https://doi.org/10.1016/j.neuron.2023.11.024.
(50) Jones-Tabah, J.; Mohammad, H.; Paulus, E. G.; Clarke, P. B. S.; Hébert, T. E. The Signaling and Pharmacology of the Dopamine D1 Receptor. *Front. Cell. Neurosci.* **2021**, *15*, 806618. https://doi.org/10.3389/fncel.2021.806618.
(51) Grecksch, G.; Just, S.; Pierstorff, C.; Imhof, A.-K.; Glück, L.; Doll, C.; Lupp, A.; Becker, A.; Koch, T.; Stumm, R.; Höllt, V.; Schulz, S. Analgesic Tolerance to High-Efficacy Agonists But Not to Morphine Is Diminished in Phosphorylation-Deficient S375A μ-Opioid Receptor Knock-In Mice. *J. Neurosci.* **2011**, *31* (39), 13890–13896. https://doi.org/10.1523/JNEUROSCI.2304-11.2011.
(52) Zachariou, V.; Georgescu, D.; Sanchez, N.; Rahman, Z.; DiLeone, R.; Berton, O.; Neve, R. L.; Sim-Selley, L. J.; Selley, D. E.; Gold, S. J.; Nestler, E. J. Essential Role for RGS9 in Opiate Action. *Proc. Natl. Acad. Sci. U. S. A.* **2003**, *100* (23), 13656–13661. https://doi.org/10.1073/pnas.2232594100.
(53) Polter, A. M.; Barcomb, K.; Chen, R. W.; Dingess, P. M.; Graziane, N. M.; Brown, T. E.; Kauer, J. A. Constitutive Activation of Kappa Opioid Receptors at Ventral Tegmental Area Inhibitory Synapses Following Acute Stress. *eLife* **2017**, *6*, e23785. https://doi.org/10.7554/eLife.23785.
(54) Nikoshkov, A.; Drakenberg, K.; Wang, X.; Horvath, M. Cs.; Keller, E.; Hurd, Y. L. Opioid Neuropeptide Genotypes in Relation to Heroin Abuse: Dopamine Tone Contributes to Reversed Mesolimbic Proenkephalin Expression. *Proc. Natl. Acad. Sci.* **2008**, *105* (2), 786–791. https://doi.org/10.1073/pnas.0710902105.

(55) Comings, D. E.; Blake, H.; Dietz, G.; Gade-Andavolu, R.; Legro, R. S.; Saucier, G.; Johnson, P.; Verde, R.; MacMurray, J. P. The Proenkephalin Gene (PENK) and Opioid Dependence. *Neuroreport* **1999**, *10* (5), 1133–1135. https://doi.org/10.1097/00001756-199904060-00042.
(56) Muschamp, J. W.; Carlezon, W. A. Roles of Nucleus Accumbens CREB and Dynorphin in Dysregulation of Motivation. *Cold Spring Harb. Perspect. Med.* **2013**, *3* (2), a012005. https://doi.org/10.1101/cshperspect.a012005.
(57) Shaw-Lutchman, T. Z.; Barrot, M.; Wallace, T.; Gilden, L.; Zachariou, V.; Impey, S.; Duman, R. S.; Storm, D.; Nestler, E. J. Regional and Cellular Mapping of cAMP Response Element-Mediated Transcription during Naltrexone-Precipitated Morphine Withdrawal. *J. Neurosci.* **2002**, *22* (9), 3663–3672. https://doi.org/10.1523/JNEUROSCI.22-09-03663.2002.
(58) Sheng, M.; Greenberg, M. E. The Regulation and Function of C-Fos and Other Immediate Early Genes in the Nervous System. *Neuron* **1990**, *4* (4), 477–485. https://doi.org/10.1016/0896-6273(90)90106-p.
(59) Korb, E.; Finkbeiner, S. Arc in Synaptic Plasticity: From Gene to Behavior. *Trends Neurosci.* **2011**, *34* (11), 591–598. https://doi.org/10.1016/j.tins.2011.08.007.
(60) Nestler, E. J.; Barrot, M.; Self, D. W. ΔFosB: A Sustained Molecular Switch for Addiction. *Proc. Natl. Acad. Sci.* **2001**, *98* (20), 11042–11046. https://doi.org/10.1073/pnas.191352698.
(61) Lobo, M. K.; Zaman, S.; Damez-Werno, D. M.; Koo, J. W.; Bagot, R. C.; DiNieri, J. A.; Nugent, A.; Finkel, E.; Chaudhury, D.; Chandra, R.; Riberio, E.; Rabkin, J.; Mouzon, E.; Cachope, R.; Cheer, J. F.; Han, M.-H.; Dietz, D. M.; Self, D. W.; Hurd, Y. L.; Vialou, V.; Nestler, E. J. ΔFosB Induction in Striatal Medium Spiny Neuron Subtypes in Response to Chronic Pharmacological, Emotional, and Optogenetic Stimuli. *J. Neurosci. Off. J. Soc. Neurosci.* **2013**, *33* (47), 18381–18395. https://doi.org/10.1523/JNEUROSCI.1875-13.2013.
(62) Nestler, E. J. Is There a Common Molecular Pathway for Addiction? *Nat. Neurosci.* **2005**, *8* (11), 1445–1449. https://doi.org/10.1038/nn1578.
(63) Kauer, J. A.; Malenka, R. C. Synaptic Plasticity and Addiction. *Nat. Rev. Neurosci.* **2007**, *8* (11), 844–858. https://doi.org/10.1038/nrn2234.
(64) Zachariou, V.; Bolanos, C. A.; Selley, D. E.; Theobald, D.; Cassidy, M. P.; Kelz, M. B.; Shaw-Lutchman, T.; Berton, O.; Sim-Selley, L. J.; Dileone, R. J.; Kumar, A.; Nestler, E. J. An Essential Role for DeltaFosB in the Nucleus Accumbens in Morphine Action. *Nat. Neurosci.* **2006**, *9* (2), 205–211. https://doi.org/10.1038/nn1636.
(65) Brown, J. R.; Ye, H.; Bronson, R. T.; Dikkes, P.; Greenberg, M. E. A Defect in Nurturing in Mice Lacking the Immediate Early Gene fosB. *Cell* **1996**, *86* (2), 297–309. https://doi.org/10.1016/s0092-8674(00)80101-4.
(66) Sklair-Tavron, L.; Shi, W. X.; Lane, S. B.; Harris, H. W.; Bunney, B. S.; Nestler, E. J. Chronic Morphine Induces Visible Changes in the Morphology of Mesolimbic Dopamine Neurons. *Proc. Natl. Acad. Sci.* **1996**, *93* (20), 11202–11207. https://doi.org/10.1073/pnas.93.20.11202.
(67) Huang, Y.; Ceceli, A. O.; Kronberg, G.; King, S.; Malaker, P.; Parvaz, M. A.; Alia-Klein, N.; Garland, E. L.; Goldstein, R. Z. Association of Cortico-Striatal Engagement During Cue Reactivity, Reappraisal, and Savoring of Drug and Non-Drug Stimuli With Craving in Heroin Addiction. *Am. J. Psychiatry* **2024**, *181* (2), 153–165. https://doi.org/10.1176/appi.ajp.20220759.
(68) Berrettini, W. A Brief Review of the Genetics and Pharmacogenetics of Opioid Use Disorders. *Dialogues Clin. Neurosci.* **2017**, *19* (3), 229–236. https://doi.org/10.31887/DCNS.2017.19.3/wberrettini.
(69) Kuhn, B. N.; Cannella, N.; Chitre, A. S.; Nguyen, K.-M. H.; Cohen, K.; Chen, D.; Peng, B.; Ziegler, K. S.; Lin, B.; Johnson, B. B.; Missfeldt Sanches, T.; Crow, A. D.; Lunerti, V.; Gupta, A.; Dereschewitz, E.; Soverchia, L.; Hopkins, J. L.; Roberts, A. T.; Ubaldi, M.; Abdulmalek, S.; Kinen, A.; Hardiman, G.; Chung, D.; Polesskaya, O.; Solberg Woods, L. C.; Ciccocioppo, R.;

Kalivas, P. W.; Palmer, A. A. Genome-Wide Association Study Reveals Multiple Loci for Nociception and Opioid Consumption Behaviors Associated with Heroin Vulnerability in Outbred Rats. *Mol. Psychiatry* **2025**, *30* (8), 3363–3375. https://doi.org/10.1038/s41380-025-02922-4.

(70) Zhou, Z.; Karlsson, C.; Liang, T.; Xiong, W.; Kimura, M.; Tapocik, J. D.; Yuan, Q.; Barbier, E.; Feng, A.; Flanigan, M.; Augier, E.; Enoch, M.-A.; Hodgkinson, C. A.; Shen, P.-H.; Lovinger, D. M.; Edenberg, H. J.; Heilig, M.; Goldman, D. Loss of Metabotropic Glutamate Receptor 2 Escalates Alcohol Consumption. *Proc. Natl. Acad. Sci. U. S. A.* **2013**, *110* (42), 16963–16968. https://doi.org/10.1073/pnas.1309839110.

(71) Godynyuk, E.; Bluitt, M. N.; Tooley, J. R.; Kravitz, A. V.; Creed, M. C. An Open-Source, Automated Home-Cage Sipper Device for Monitoring Liquid Ingestive Behavior in Rodents. *eneuro* **2019**, *6* (5), ENEURO.0292-19.2019. https://doi.org/10.1523/ENEURO.0292-19.2019.

(72) Nath, C.; Gupta, M. B.; Patnaik, G. K.; Dhawan, K. N. Morphine-Induced Straub Tail Response: Mediated by Central Mu2-Opioid Receptor. *Eur. J. Pharmacol.* **1994**, *263* (1–2), 203–205. https://doi.org/10.1016/0014-2999(94)90543-6.

(73) Nishida, K. S.; Park, T. Y.; Lee, B. H.; Ursano, R. J.; Choi, K. H. Individual Differences in Initial Morphine Sensitivity as a Predictor for the Development of Opiate Addiction in Rats. *Behav. Brain Res.* **2016**, *313*, 315–323. https://doi.org/10.1016/j.bbr.2016.07.038.

(74) Wanigasekera, V.; Lee, M. C.; Rogers, R.; Kong, Y.; Leknes, S.; Andersson, J.; Tracey, I. Baseline Reward Circuitry Activity and Trait Reward Responsiveness Predict Expression of Opioid Analgesia in Healthy Subjects. *Proc. Natl. Acad. Sci.* **2012**, *109* (43), 17705–17710. https://doi.org/10.1073/pnas.1120201109.

(75) Swain, Y.; Muelken, P.; LeSage, M. G.; Gewirtz, J. C.; Harris, A. C. Locomotor Activity Does Not Predict Individual Differences in Morphine Self-Administration in Rats. *Pharmacol. Biochem. Behav.* **2018**, *166*, 48–56. https://doi.org/10.1016/j.pbb.2018.01.008.

(76) Ambrosio, E.; Goldberg, S. R.; Elmer, G. I. Behavior Genetic Investigation of the Relationship between Spontaneous Locomotor Activity and the Acquisition of Morphine Self-Administration Behavior. *Behav. Pharmacol.* **1995**, *6* (3), 229–237.

(77) Kosten, T. A.; Ball, S. A.; Rounsaville, B. J. A Sibling Study of Sensation Seeking and Opiate Addiction. *J. Nerv. Ment. Dis.* **1994**, *182* (5), 284–289. https://doi.org/10.1097/00005053-199405000-00006.

(78) Marino, E. N.; Rosen, K. D.; Gutierrez, A.; Eckmann, M.; Ramamurthy, S.; Potter, J. S. Impulsivity but Not Sensation Seeking Is Associated with Opioid Analgesic Misuse Risk in Patients with Chronic Pain. *Addict. Behav.* **2013**, *38* (5), 2154–2157. https://doi.org/10.1016/j.addbeh.2013.01.020.

(79) Swain, Y.; Muelken, P.; Skansberg, A.; Lanzdorf, D.; Haave, Z.; LeSage, M. G.; Gewirtz, J. C.; Harris, A. C. Higher Anhedonia during Withdrawal from Initial Opioid Exposure Is Protective against Subsequent Opioid Self-Administration in Rats. *Psychopharmacology (Berl.)* **2020**, *237* (8), 2279–2291. https://doi.org/10.1007/s00213-020-05532-w.

(80) Holtz, N. A.; Radke, A. K.; Zlebnik, N. E.; Harris, A. C.; Carroll, M. E. Intracranial Self-Stimulation Reward Thresholds during Morphine Withdrawal in Rats Bred for High (HiS) and Low (LoS) Saccharin Intake. *Brain Res.* **2015**, *1602*, 119–126. https://doi.org/10.1016/j.brainres.2015.01.004.

(81) Radke, A. K.; Holtz, N. A.; Gewirtz, J. C.; Carroll, M. E. Reduced Emotional Signs of Opiate Withdrawal in Rats Selectively Bred for Low (LoS) versus High (HiS) Saccharin Intake. *Psychopharmacology (Berl.)* **2013**, *227* (1), 117–126. https://doi.org/10.1007/s00213-012-2945-0.

(82) O'Neal, T. J.; Nooney, M. N.; Thien, K.; Ferguson, S. M. Chemogenetic Modulation of Accumbens Direct or Indirect Pathways Bidirectionally Alters Reinstatement of Heroin-Seeking

in High- but Not Low-Risk Rats. *Neuropsychopharmacol. Off. Publ. Am. Coll. Neuropsychopharmacol.* **2020**, *45* (8), 1251–1262. https://doi.org/10.1038/s41386-019-0571-9.
(83) Latent Profile Analysis Basics, 2022. https://sscc.wisc.edu/sscc/pubs/MPlus/Basics/Latent_Profile_Analysis.html.
(84) Pereira, T. D.; Tabris, N.; Matsliah, A.; Turner, D. M.; Li, J.; Ravindranath, S.; Papadoyannis, E. S.; Normand, E.; Deutsch, D. S.; Wang, Z. Y.; McKenzie-Smith, G. C.; Mitelut, C. C.; Castro, M. D.; D'Uva, J.; Kislin, M.; Sanes, D. H.; Kocher, S. D.; Wang, S. S.-H.; Falkner, A. L.; Shaevitz, J. W.; Murthy, M. SLEAP: A Deep Learning System for Multi-Animal Pose Tracking. *Nat. Methods* **2022**, *19* (4), 486–495. https://doi.org/10.1038/s41592-022-01426-1.
(85) Weinreb, C.; Pearl, J. E.; Lin, S.; Osman, M. A. M.; Zhang, L.; Annapragada, S.; Conlin, E.; Hoffmann, R.; Makowska, S.; Gillis, W. F.; Jay, M.; Ye, S.; Mathis, A.; Mathis, M. W.; Pereira, T.; Linderman, S. W.; Datta, S. R. Keypoint-MoSeq: Parsing Behavior by Linking Point Tracking to Pose Dynamics. *Nat. Methods* **2024**, *21* (7), 1329–1339. https://doi.org/10.1038/s41592-024-02318-2.
(86) Renier, N.; Wu, Z.; Simon, D. J.; Yang, J.; Ariel, P.; Tessier-Lavigne, M. iDISCO: A Simple, Rapid Method to Immunolabel Large Tissue Samples for Volume Imaging. *Cell* **2014**, *159* (4), 896–910. https://doi.org/10.1016/j.cell.2014.10.010.
(87) Kleven, H.; Bjerke, I. E.; Clascá, F.; Groenewegen, H. J.; Bjaalie, J. G.; Leergaard, T. B. Waxholm Space Atlas of the Rat Brain: A 3D Atlas Supporting Data Analysis and Integration. *Nat. Methods* **2023**, *20* (11), 1822–1829. https://doi.org/10.1038/s41592-023-02034-3.
(88) Renier, N.; Adams, E. L.; Kirst, C.; Wu, Z.; Azevedo, R.; Kohl, J.; Autry, A. E.; Kadiri, L.; Umadevi Venkataraju, K.; Zhou, Y.; Wang, V. X.; Tang, C. Y.; Olsen, O.; Dulac, C.; Osten, P.; Tessier-Lavigne, M. Mapping of Brain Activity by Automated Volume Analysis of Immediate Early Genes. *Cell* **2016**, *165* (7), 1789–1802. https://doi.org/10.1016/j.cell.2016.05.007.
(89) Berg, S.; Kutra, D.; Kroeger, T.; Straehle, C. N.; Kausler, B. X.; Haubold, C.; Schiegg, M.; Ales, J.; Beier, T.; Rudy, M.; Eren, K.; Cervantes, J. I.; Xu, B.; Beuttenmueller, F.; Wolny, A.; Zhang, C.; Koethe, U.; Hamprecht, F. A.; Kreshuk, A. Ilastik: Interactive Machine Learning for (Bio)Image Analysis. *Nat. Methods* **2019**, *16* (12), 1226–1232. https://doi.org/10.1038/s41592-019-0582-9.
(90) Ciscato, M.; Chouvaeff, M.; Mourot, A. Nicotinic Receptors in the Medial Habenula to Interpeduncular Nucleus Pathway: Modulators of Reward, Aversion and Emotion. *Eur. J. Neurosci.* **2025**, *62* (11), e70352. https://doi.org/10.1111/ejn.70352.
(91) Handa, T.; Sugiyama, T.; Islam, T.; Johansen, J. P.; Yanagawa, Y.; McHugh, T. J.; Okamoto, H. The Neural Pathway from the Superior Subpart of the Medial Habenula to the Interpeduncular Nucleus Suppresses Anxiety. *Mol. Psychiatry* **2025**, *30* (8), 3752–3764. https://doi.org/10.1038/s41380-025-02964-8.
(92) Xie, L.; Wu, H.; Chen, Q.; Xu, F.; Li, H.; Xu, Q.; Jiao, C.; Sun, L.; Ullah, R.; Chen, X. Divergent Modulation of Pain and Anxiety by GABAergic Neurons in the Ventrolateral Periaqueductal Gray and Dorsal Raphe. *Neuropsychopharmacology* **2023**, *48* (10), 1509–1519. https://doi.org/10.1038/s41386-022-01520-0.
(93) Li, C.; Sugam, J. A.; Lowery-Gionta, E. G.; McElligott, Z. A.; McCall, N. M.; Lopez, A. J.; McKlveen, J. M.; Pleil, K. E.; Kash, T. L. Mu Opioid Receptor Modulation of Dopamine Neurons in the Periaqueductal Gray/Dorsal Raphe: A Role in Regulation of Pain. *Neuropsychopharmacology* **2016**, *41* (8), 2122–2132. https://doi.org/10.1038/npp.2016.12.
(94) Cruz, A. M.; Spencer, H. F.; Kim, T. H.; Jhou, T. C.; Smith, R. J. Prelimbic Cortical Projections to Rostromedial Tegmental Nucleus Play a Suppressive Role in Cue-Induced Reinstatement of Cocaine Seeking. *Neuropsychopharmacology* **2021**, *46* (8), 1399–1406. https://doi.org/10.1038/s41386-020-00909-z.

(95) Hashikawa, Y.; Hashikawa, K.; Rossi, M. A.; Basiri, M. L.; Liu, Y.; Johnston, N. L.; Ahmad, O. R.; Stuber, G. D. Transcriptional and Spatial Resolution of Cell Types in the Mammalian Habenula. *Neuron* **2020**, *106* (5), 743-758.e5. https://doi.org/10.1016/j.neuron.2020.03.011.
(96) Rossi, M. A.; Basiri, M. L.; Liu, Y.; Hashikawa, Y.; Hashikawa, K.; Fenno, L. E.; Kim, Y. S.; Ramakrishnan, C.; Deisseroth, K.; Stuber, G. D. Transcriptional and Functional Divergence in Lateral Hypothalamic Glutamate Neurons Projecting to the Lateral Habenula and Ventral Tegmental Area. *Neuron* **2021**, *109* (23), 3823-3837.e6. https://doi.org/10.1016/j.neuron.2021.09.020.
(97) Pauli, J. L.; Chen, J. Y.; Basiri, M. L.; Park, S.; Carter, M. E.; Sanz, E.; McKnight, G. S.; Stuber, G. D.; Palmiter, R. D. Molecular and Anatomical Characterization of Parabrachial Neurons and Their Axonal Projections. *eLife* **2022**, *11*, e81868. https://doi.org/10.7554/eLife.81868.
(98) Simon, R. C.; Fleming, W. T.; Briones, B. A.; Trzeciak, M.; Senthilkumar, P.; Ishii, K. K.; Hjort, M. M.; Martin, M. M.; Hashikawa, K.; Sanders, A. D.; Golden, S. A.; Stuber, G. D. Opioid-Driven Disruption of the Septum Reveals a Role for Neurotensin-Expressing Neurons in Withdrawal. *Neuron* **2025**, *113* (14), 2325-2343.e9. https://doi.org/10.1016/j.neuron.2025.04.024.
(99) Ottenheimer, D. J.; Simon, R. C.; Briones, B. A.; Burke, C. T.; Bowen, A. J.; Ferguson, S. M.; Stuber, G. D. Single-Cell Sequencing of Rodent Ventral Pallidum Reveals Diverse Neuronal Subtypes with Noncanonical Interregional Continuity. *Sci. Adv.* **2025**, *11* (49), eadp3059. https://doi.org/10.1126/sciadv.adp3059.
(100) Avey, D.; Sankararaman, S.; Yim, A. K. Y.; Barve, R.; Milbrandt, J.; Mitra, R. D. Single-Cell RNA-Seq Uncovers a Robust Transcriptional Response to Morphine by Glia. *Cell Rep.* **2018**, *24* (13), 3619-3629.e4. https://doi.org/10.1016/j.celrep.2018.08.080.
(101) Valentinova, K.; Tchenio, A.; Trusel, M.; Clerke, J. A.; Lalive, A. L.; Tzanoulinou, S.; Matera, A.; Moutkine, I.; Maroteaux, L.; Paolicelli, R. C.; Volterra, A.; Bellone, C.; Mameli, M. Morphine Withdrawal Recruits Lateral Habenula Cytokine Signaling to Reduce Synaptic Excitation and Sociability. *Nat. Neurosci.* **2019**, *22* (7), 1053–1056. https://doi.org/10.1038/s41593-019-0421-4.
(102) Zhu, Y.; Yan, P.; Wang, R.; Lai, J.; Tang, H.; Xiao, X.; Yu, R.; Bao, X.; Zhu, F.; Wang, K.; Lu, Y.; Dang, J.; Zhu, C.; Zhang, R.; Dang, W.; Zhang, B.; Fu, Q.; Zhang, Q.; Kang, C.; Chen, Y.; Chen, X.; Liang, Q.; Wang, K. Opioid-Induced Fragile-like Regulatory T Cells Contribute to Withdrawal. *Cell* **2023**, *186* (3), 591-606.e23. https://doi.org/10.1016/j.cell.2022.12.030.
(103) Qiu, Y.; Jiang, G.; Su, H.; Lv, X.; Zhang, X.; Tian, J.; Zhuo, F. Progressive White Matter Microstructure Damage in Male Chronic Heroin Dependent Individuals: A DTI and TBSS Study. *PloS One* **2013**, *8* (5), e63212. https://doi.org/10.1371/journal.pone.0063212.
(104) Liu, H.; Li, L.; Hao, Y.; Cao, D.; Xu, L.; Rohrbaugh, R.; Xue, Z.; Hao, W.; Shan, B.; Liu, Z. Disrupted White Matter Integrity in Heroin Dependence: A Controlled Study Utilizing Diffusion Tensor Imaging. *Am. J. Drug Alcohol Abuse* **2008**, *34* (5), 562–575. https://doi.org/10.1080/00952990802295238.
(105) Li, W.; Li, Q.; Zhu, J.; Qin, Y.; Zheng, Y.; Chang, H.; Zhang, D.; Wang, H.; Wang, L.; Wang, Y.; Wang, W. White Matter Impairment in Chronic Heroin Dependence: A Quantitative DTI Study. *Brain Res.* **2013**, *1531*, 58–64. https://doi.org/10.1016/j.brainres.2013.07.036.
(106) De Jong, T. V.; Pan, Y.; Rastas, P.; Munro, D.; Tutaj, M.; Akil, H.; Benner, C.; Chen, D.; Chitre, A. S.; Chow, W.; Colonna, V.; Dalgard, C. L.; Demos, W. M.; Doris, P. A.; Garrison, E.; Geurts, A. M.; Gunturkun, H. M.; Guryev, V.; Hourlier, T.; Howe, K.; Huang, J.; Kalbfleisch, T.; Kim, P.; Li, L.; Mahaffey, S.; Martin, F. J.; Mohammadi, P.; Ozel, A. B.; Polesskaya, O.; Pravenec, M.; Prins, P.; Sebat, J.; Smith, J. R.; Solberg Woods, L. C.; Tabakoff, B.; Tracey, A.; Uliano-Silva, M.; Villani, F.; Wang, H.; Sharp, B. M.; Telese, F.; Jiang, Z.; Saba, L.; Wang, X.; Murphy, T. D.; Palmer, A. A.; Kwitek, A. E.; Dwinell, M. R.; Williams, R. W.; Li, J. Z.; Chen, H.

A Revamped Rat Reference Genome Improves the Discovery of Genetic Diversity in Laboratory Rats. *Cell Genomics* **2024**, *4* (4), 100527. https://doi.org/10.1016/j.xgen.2024.100527.

(107) Hafemeister, C.; Satija, R. Normalization and Variance Stabilization of Single-Cell RNA-Seq Data Using Regularized Negative Binomial Regression. *Genome Biol.* **2019**, *20* (1), 296. https://doi.org/10.1186/s13059-019-1874-1.

(108) Yao, Z.; van Velthoven, C. T. J.; Kunst, M.; Zhang, M.; McMillen, D.; Lee, C.; Jung, W.; Goldy, J.; Abdelhak, A.; Aitken, M.; Baker, K.; Baker, P.; Barkan, E.; Bertagnolli, D.; Bhandiwad, A.; Bielstein, C.; Bishwakarma, P.; Campos, J.; Carey, D.; Casper, T.; Chakka, A. B.; Chakrabarty, R.; Chavan, S.; Chen, M.; Clark, M.; Close, J.; Crichton, K.; Daniel, S.; DiValentin, P.; Dolbeare, T.; Ellingwood, L.; Fiabane, E.; Fliss, T.; Gee, J.; Gerstenberger, J.; Glandon, A.; Gloe, J.; Gould, J.; Gray, J.; Guilford, N.; Guzman, J.; Hirschstein, D.; Ho, W.; Hooper, M.; Huang, M.; Hupp, M.; Jin, K.; Kroll, M.; Lathia, K.; Leon, A.; Li, S.; Long, B.; Madigan, Z.; Malloy, J.; Malone, J.; Maltzer, Z.; Martin, N.; McCue, R.; McGinty, R.; Mei, N.; Melchor, J.; Meyerdierks, E.; Mollenkopf, T.; Moonsman, S.; Nguyen, T. N.; Otto, S.; Pham, T.; Rimorin, C.; Ruiz, A.; Sanchez, R.; Sawyer, L.; Shapovalova, N.; Shepard, N.; Slaughterbeck, C.; Sulc, J.; Tieu, M.; Torkelson, A.; Tung, H.; Valera Cuevas, N.; Vance, S.; Wadhwani, K.; Ward, K.; Levi, B.; Farrell, C.; Young, R.; Staats, B.; Wang, M.-Q. M.; Thompson, C. L.; Mufti, S.; Pagan, C. M.; Kruse, L.; Dee, N.; Sunkin, S. M.; Esposito, L.; Hawrylycz, M. J.; Waters, J.; Ng, L.; Smith, K.; Tasic, B.; Zhuang, X.; Zeng, H. A High-Resolution Transcriptomic and Spatial Atlas of Cell Types in the Whole Mouse Brain. *Nature* **2023**, *624* (7991), 317–332. https://doi.org/10.1038/s41586-023-06812-z.

(109) Yang, L.; Fang, L. Z.; Lynch, M. R.; Xu, C. S.; Hahm, H. J.; Zhang, Y.; Heitmeier, M. R.; Costa, V. D.; Samineni, V. K.; Creed, M. C. Transcriptomic Landscape of Mammalian Ventral Pallidum at Single-Cell Resolution. *Sci. Adv.* **2024**, *10* (50), eadq6017. https://doi.org/10.1126/sciadv.adq6017.

(110) Johansen, N. J.; Fu, Y.; Schmitz, M.; Dubuc, A.; Kempynck, N.; Wirthlin, M.; Garcia, A. D.; Hewitt, M.; Turner, M. A.; Seeman, S. C.; Long, B.; Liu, X.-P.; Dan, S.; DeBerardine, M.; Kapen, I.; Yanny, A. M.; Avola, A.; Barlow, S. T.; Bertagnolli, D.; Bhandiwad, A.; Budzillo, A.; Caballero, V. E. N.; Caceres, L.; Casper, T.; Chakka, A. B.; Chakrabarty, R.; Clark, M.; Daniel, S.; Eggermont, J.; Ferrer, R.; French, L.; Gloe, J.; Goldy, J.; Guilford, N.; Guzman, J.; Hirschstein, D.; Ho, W.; James, K.; Jones, D. L.; Jungert, M.; Kannan, M.; Kedzierska, K. Z.; Kroes, T.; Leytze, M.; Manning, A.; McCue, R.; Morrison, C.; Nguy, B.; Otto, S.; Pena, N.; Pham, T.; Phillips, E.; Rajagopal, A.; Rimorin, C.; Rivera, A. D.; Rocha, D.; Sanchez, R.; Schau, G.; Schembri, J.; Shapovalova, N. V.; Sherman, J.; Thijssen, J.; Tieu, M.; Torkelson, A.; Tran, A.; Vieth, A.; Wang, Y.; Yuan, D.; Close, J.; Daigle, T. L.; Dalley, R.; Dee, N.; Ding, S.-L.; Fiabane, E.; Gouwens, N.; Huynh, G.; Lee, B. R.; Levi, B. P.; McMillen, D.; Miller, J. A.; Mollenkopf, T.; Ng, L.; Ray, P. L.; Sobieski, C.; Sorensen, S. A.; Yao, Z.; Yazdani, F.; Freiwald, W.; Lelieveldt, B.; Kalmbach, B.; Keene, C. D.; Gillis, J.; Osumi-Sutherland, D.; Ting, J. T.; Zeng, H.; Smith, K.; Krienen, F. M.; Hodge, R. D.; Lein, E. S.; Bakken, T. E. Cross-Species Consensus Atlas of the Primate Basal Ganglia. Neuroscience December 16, 2025. https://doi.org/10.64898/2025.12.15.694496.

(111) Morabito, S.; Reese, F.; Rahimzadeh, N.; Miyoshi, E.; Swarup, V. hdWGCNA Identifies Co-Expression Networks in High-Dimensional Transcriptomics Data. *Cell Rep. Methods* **2023**, *3* (6), 100498. https://doi.org/10.1016/j.crmeth.2023.100498.

(112) Korsunsky, I.; Millard, N.; Fan, J.; Slowikowski, K.; Zhang, F.; Wei, K.; Baglaenko, Y.; Brenner, M.; Loh, P.; Raychaudhuri, S. Fast, Sensitive and Accurate Integration of Single-Cell Data with Harmony. *Nat. Methods* **2019**, *16* (12), 1289–1296. https://doi.org/10.1038/s41592-019-0619-0.

(113) Babiczky, Á.; Matyas, F. Molecular Characteristics and Laminar Distribution of Prefrontal Neurons Projecting to the Mesolimbic System. *eLife* **2022**, *11*, e78813. https://doi.org/10.7554/eLife.78813.
(114) Bhattacherjee, A.; Zhang, C.; Watson, B. R.; Djekidel, M. N.; Moffitt, J. R.; Zhang, Y. Spatial Transcriptomics Reveals the Distinct Organization of Mouse Prefrontal Cortex and Neuronal Subtypes Regulating Chronic Pain. *Nat. Neurosci.* **2023**, *26* (11), 1880–1893. https://doi.org/10.1038/s41593-023-01455-9.
(115) Bae, J. W.; Jeong, H.; Yoon, Y. J.; Bae, C. M.; Lee, H.; Paik, S.-B.; Jung, M. W. Parallel Processing of Working Memory and Temporal Information by Distinct Types of Cortical Projection Neurons. *Nat. Commun.* **2021**, *12* (1), 4352. https://doi.org/10.1038/s41467-021-24565-z.
(116) Heindorf, M.; Arber, S.; Keller, G. B. Mouse Motor Cortex Coordinates the Behavioral Response to Unpredicted Sensory Feedback. *Neuron* **2018**, *99* (5), 1040-1054.e5. https://doi.org/10.1016/j.neuron.2018.07.046.
(117) Garcia, A. F.; Crummy, E. A.; Webb, I. G.; Nooney, M. N.; Ferguson, S. M. Distinct Populations of Cortical Pyramidal Neurons Mediate Drug Reward and Aversion. *Nat. Commun.* **2021**, *12* (1), 182. https://doi.org/10.1038/s41467-020-20526-0.
(118) Brakeman, P. R.; Lanahan, A. A.; O'Brien, R.; Roche, K.; Barnes, C. A.; Huganir, R. L.; Worley, P. F. Homer: A Protein That Selectively Binds Metabotropic Glutamate Receptors. *Nature* **1997**, *386* (6622), 284–288. https://doi.org/10.1038/386284a0.
(119) Sala, C.; Piëch, V.; Wilson, N. R.; Passafaro, M.; Liu, G.; Sheng, M. Regulation of Dendritic Spine Morphology and Synaptic Function by Shank and Homer. *Neuron* **2001**, *31* (1), 115–130. https://doi.org/10.1016/S0896-6273(01)00339-7.
(120) Gershon, Z.; Bonito-Oliva, A.; Kanke, M.; Terceros, A.; Rankin, G.; Fak, J.; Harada, Y.; Iannone, A. F.; Gebremedhin, M.; Fabella, B.; De Marco García, N. V.; Sethupathy, P.; Rajasethupathy, P. Genetic Mapping Identifies Homer1 as a Developmental Modifier of Attention. *Nat. Neurosci.* **2026**, *29* (3), 647–659. https://doi.org/10.1038/s41593-025-02155-2.
(121) Chinen, J. Spectrum of Clinical Phenotypes of PLCG2 Gene Variants: Just PLAID. *J. Allergy Clin. Immunol.* **2024**, *153* (5), 1260–1261. https://doi.org/10.1016/j.jaci.2024.02.007.
(122) Kammermeier, P. J.; Worley, P. F. Homer 1a Uncouples Metabotropic Glutamate Receptor 5 from Postsynaptic Effectors. *Proc. Natl. Acad. Sci.* **2007**, *104* (14), 6055–6060. https://doi.org/10.1073/pnas.0608991104.
(123) Lemke, J. R.; Eoli, A.; Krey, I.; Popp, B.; Strehlow, V.; Wittekind, D. A.; Vuorinen, A.-L.; Aldhalaan, H. M.; Baer, S.; De Saint Martin, A.; Hammer, T. B.; Herman, I.; Hornemann, F.; Ingebrigtsen, T.; Lederer, D.; Lesca, G.; Marafie, D.; Mathot, M.; Rosenfeld, J. A.; Møller, R. S.; Schelhaas, H. J.; Stillman, C.; Orsini, A.; Patel, A. D.; Piard, J.; Veggiotti, P.; Vlaskamp, D. R. M.; Weckhuysen, S.; Traynelis, S. F.; Benke, T. A.; Heyne, H. O.; Syrbe, S. GRIN2A Null Variants Confer a High Risk for Early-Onset Schizophrenia and Other Mental Disorders and Potentially Enable Precision Therapy. *Mol. Psychiatry* **2026**, *31* (1), 374–382. https://doi.org/10.1038/s41380-025-03279-4.
(124) Berman, D. M.; Wilkie, T. M.; Gilman, A. G. GAIP and RGS4 Are GTPase-Activating Proteins for the Gi Subfamily of G Protein α Subunits. *Cell* **1996**, *86* (3), 445–452. https://doi.org/10.1016/S0092-8674(00)80117-8.
(125) Prasad, K. M. R.; Chowdari, K. V.; Nimgaonkar, V. L.; Talkowski, M. E.; Lewis, D. A.; Keshavan, M. S. Genetic Polymorphisms of the RGS4 and Dorsolateral Prefrontal Cortex Morphometry among First Episode Schizophrenia Patients. *Mol. Psychiatry* **2005**, *10* (2), 213–219. https://doi.org/10.1038/sj.mp.4001562.

(126) Jeong, M.; Baek, S.; Wang, Q.; Yao, L.; Lee, E. J.; Marroquin Rivera, A.; Lee, J. J.; Jang, H.; Bambah-Mukku, D.; Mun, C. H.-S.; Boesen, T.; Nanda, S.; Ku, C. R.; Dong, H.; Labonté, B.; Paik, S.-B.; Lim, B. K. Distinct Interneuronal Dynamics Selectively Gate Target-Specific Cortical Projections in Drug Seeking. *Neuron* **2026**, S0896627326000024. https://doi.org/10.1016/j.neuron.2026.01.002.

(127) Barbier, E.; Barchiesi, R.; Domi, A.; Chanthongdee, K.; Domi, E.; Augier, G.; Augier, E.; Xu, L.; Adermark, L.; Heilig, M. Downregulation of Synaptotagmin 1 in the Prelimbic Cortex Drives Alcohol-Associated Behaviors in Rats. *Biol. Psychiatry* **2021**, *89* (4), 398–406. https://doi.org/10.1016/j.biopsych.2020.08.027.

(128) Rehfeld, F.; Maticzka, D.; Grosser, S.; Knauff, P.; Eravci, M.; Vida, I.; Backofen, R.; Wulczyn, F. G. The RNA-Binding Protein ARPP21 Controls Dendritic Branching by Functionally Opposing the miRNA It Hosts. *Nat. Commun.* **2018**, *9* (1), 1235. https://doi.org/10.1038/s41467-018-03681-3.

(129) Yang, D.; Wang, Y.; Qi, T.; Zhang, X.; Shen, L.; Ma, J.; Pang, Z.; Lal, N. K.; McClatchy, D. B.; Seradj, S. H.; Leung, V. H.; Wang, K.; Xie, Y.; Polli, F. S.; Maximov, A.; Gonzalez, O. C.; de Lecea, L.; Cline, H. T.; Augustine, V.; Yates, J. R.; Ye, L. Phosphorylation of Pyruvate Dehydrogenase Inversely Associates with Neuronal Activity. *Neuron* **2024**, *112* (6), 959-971.e8. https://doi.org/10.1016/j.neuron.2023.12.015.

(130) Bhattacherjee, A.; Djekidel, M. N.; Chen, R.; Chen, W.; Tuesta, L. M.; Zhang, Y. Cell Type-Specific Transcriptional Programs in Mouse Prefrontal Cortex during Adolescence and Addiction. *Nat. Commun.* **2019**, *10* (1), 4169. https://doi.org/10.1038/s41467-019-12054-3.

(131) Zhang, J.; Li, M.; Wang, M.; Sun, Y.; Yin, C.; Yang, S.; Wang, B.; Liu, Z.; Wang, W.; Liu, M.; Zhao, Y.; Zhou, X.; Cai, L.; Zhong, S.; Wang, X.; Wu, Q. Single-Cell Spatiotemporal Transcriptomic and Chromatin Accessibility Profiling in Developing Postnatal Human and Macaque Prefrontal Cortex. *Nat. Neurosci.* **2026**, *29* (3), 746–758. https://doi.org/10.1038/s41593-025-02150-7.

(132) He, J.; Kleyman, M.; Chen, J.; Alikaya, A.; Rothenhoefer, K. M.; Ozturk, B. E.; Wirthlin, M.; Bostan, A. C.; Fish, K.; Byrne, L. C.; Pfenning, A. R.; Stauffer, W. R. Transcriptional and Anatomical Diversity of Medium Spiny Neurons in the Primate Striatum. *Curr. Biol. CB* **2021**, *31* (24), 5473-5486.e6. https://doi.org/10.1016/j.cub.2021.10.015.

(133) Paxinos AO (BA, M. A. *The Rat Brain in Stereotaxic Coordinates*, 7th ed.; Elsevier Science & Technology: Chantilly, 2013.

(134) Liran, M.; Fischer, I.; Elboim, M.; Rahamim, N.; Gordon, T.; Urshansky, N.; Assaf, Y.; Barak, B.; Barak, S. Long-Term Excessive Alcohol Consumption Enhances Myelination in the Mouse Nucleus Accumbens. *J. Neurosci.* **2025**, *45* (14), e0280242025. https://doi.org/10.1523/JNEUROSCI.0280-24.2025.

(135) Smith, B. L.; Guzman, T. A.; Brendle, A. H.; Laaker, C. J.; Ford, A.; Hiltz, A. R.; Zhao, J.; Setchell, K. D. R.; Reyes, T. M. Perinatal Morphine Exposure Leads to Sex-Dependent Executive Function Deficits and Microglial Changes in Mice. *eneuro* **2022**, *9* (5), ENEURO.0238-22.2022. https://doi.org/10.1523/ENEURO.0238-22.2022.

(136) Alvarez-Bagnarol, Y.; Marchette, R. C. N.; Francis, C.; Morales, M.; Vendruscolo, L. F. Neuronal Correlates of Hyperalgesia and Somatic Signs of Heroin Withdrawal in Male and Female Mice. *eneuro* **2022**, *9* (4), ENEURO.0106-22.2022. https://doi.org/10.1523/ENEURO.0106-22.2022.

(137) Cardozo Pinto, D. F.; Guo, M. Y.; Pomrenze, M. B.; Morishita, W.; Li, M. X.; Zweifel, L. S.; Eshel, N.; Malenka, R. C. Dopamine and Serotonin Inversely Modulate D2 Medium Spiny Neurons to Regulate Cocaine Reward. *Nat. Commun.* **2026**. https://doi.org/10.1038/s41467-026-70519-8.

(138) Burke, D. A.; Alvarez, V. A. Serotonin Receptors Contribute to Dopamine Depression of Lateral Inhibition in the Nucleus Accumbens. *Cell Rep.* **2022**, *39* (6), 110795. https://doi.org/10.1016/j.celrep.2022.110795.
(139) Chen, R.; Blosser, T. R.; Djekidel, M. N.; Hao, J.; Bhattacherjee, A.; Chen, W.; Tuesta, L. M.; Zhuang, X.; Zhang, Y. Decoding Molecular and Cellular Heterogeneity of Mouse Nucleus Accumbens. *Nat. Neurosci.* **2021**, *24* (12), 1757–1771. https://doi.org/10.1038/s41593-021-00938-x.
(140) Brakeman, P. R.; Lanahan, A. A.; O'Brien, R.; Roche, K.; Barnes, C. A.; Huganir, R. L.; Worley, P. F. Homer: A Protein That Selectively Binds Metabotropic Glutamate Receptors. *Nature* **1997**, *386* (6622), 284–288. https://doi.org/10.1038/386284a0.
(141) Kammermeier, P. J.; Worley, P. F. Homer 1a Uncouples Metabotropic Glutamate Receptor 5 from Postsynaptic Effectors. *Proc. Natl. Acad. Sci.* **2007**, *104* (14), 6055–6060. https://doi.org/10.1073/pnas.0608991104.
(142) Scheefhals, N.; Westra, M.; MacGillavry, H. D. mGluR5 Is Transiently Confined in Perisynaptic Nanodomains to Shape Synaptic Function. *Nat. Commun.* **2023**, *14* (1), 244. https://doi.org/10.1038/s41467-022-35680-w.
(143) Jin, D.; Chen, H.; Zhou, M.-H.; Chen, S.-R.; Pan, H.-L. mGluR5 from Primary Sensory Neurons Promotes Opioid-Induced Hyperalgesia and Tolerance by Interacting with and Potentiating Synaptic NMDA Receptors. *J. Neurosci. Off. J. Soc. Neurosci.* **2023**, *43* (31), 5593–5607. https://doi.org/10.1523/JNEUROSCI.0601-23.2023.
(144) Vincent, K.; Cornea, V. M.; Jong, Y.-J. I.; Laferrière, A.; Kumar, N.; Mickeviciute, A.; Fung, J. S. T.; Bandegi, P.; Ribeiro-da-Silva, A.; O'Malley, K. L.; Coderre, T. J. Intracellular mGluR5 Plays a Critical Role in Neuropathic Pain. *Nat. Commun.* **2016**, *7* (1), 10604. https://doi.org/10.1038/ncomms10604.
(145) Pisani, A.; Gubellini, P.; Bonsi, P.; Conquet, F.; Picconi, B.; Centonze, D.; Bernardi, G.; Calabresi, P. Metabotropic Glutamate Receptor 5 Mediates the Potentiation of N-Methyl-D-Aspartate Responses in Medium Spiny Striatal Neurons. *Neuroscience* **2001**, *106* (3), 579–587. https://doi.org/10.1016/S0306-4522(01)00297-4.
(146) Voulalas, P. J.; Holtzclaw, L.; Wolstenholme, J.; Russell, J. T.; Hyman, S. E. Metabotropic Glutamate Receptors and Dopamine Receptors Cooperate to Enhance Extracellular Signal-Regulated Kinase Phosphorylation in Striatal Neurons. *J. Neurosci. Off. J. Soc. Neurosci.* **2005**, *25* (15), 3763–3773. https://doi.org/10.1523/JNEUROSCI.4574-04.2005.
(147) Ferré, S.; Karcz-Kubicha, M.; Hope, B. T.; Popoli, P.; Burgueño, J.; Gutiérrez, M. A.; Casadó, V.; Fuxe, K.; Goldberg, S. R.; Lluis, C.; Franco, R.; Ciruela, F. Synergistic Interaction between Adenosine A2A and Glutamate mGlu5 Receptors: Implications for Striatal Neuronal Function. *Proc. Natl. Acad. Sci. U. S. A.* **2002**, *99* (18), 11940–11945. https://doi.org/10.1073/pnas.172393799.
(148) Bäckström, P.; Bachteler, D.; Koch, S.; Hyytiä, P.; Spanagel, R. mGluR5 Antagonist MPEP Reduces Ethanol-Seeking and Relapse Behavior. *Neuropsychopharmacology* **2004**, *29* (5), 921–928. https://doi.org/10.1038/sj.npp.1300381.
(149) Brown, R. M.; Stagnitti, M. R.; Duncan, J. R.; Lawrence, A. J. The mGlu5 Receptor Antagonist MTEP Attenuates Opiate Self-Administration and Cue-Induced Opiate-Seeking Behaviour in Mice. *Drug Alcohol Depend.* **2012**, *123* (1–3), 264–268. https://doi.org/10.1016/j.drugalcdep.2011.11.002.
(150) Bäckström, P.; Hyytiä, P. Involvement of AMPA/Kainate, NMDA, and mGlu5 Receptors in the Nucleus Accumbens Core in Cue-Induced Reinstatement of Cocaine Seeking in Rats. *Psychopharmacology (Berl.)* **2007**, *192* (4), 571–580. https://doi.org/10.1007/s00213-007-0753-8.

(151) Gomez-Mancilla, B.; Dürsteler, K. M.; Vogel, M.; Herdener, M.; Torrens, M.; Gálvez, B. P.; Gual, A.; Corral, R. M.; Kuper, E. I.; Mosca, D. L.; Dumitras, S.; Pezous, N.; Berkheimer, M.; Walker, E.; Gasparini, F.; Cha, J.-H.; Dolmetsch, R. Mavoglurant Reduces Cocaine Use in Patients with Cocaine Use Disorder in a Phase 2 Clinical Trial. *Sci. Transl. Med.* **2025**, *17* (792), eadi4505. https://doi.org/10.1126/scitranslmed.adi4505.

(152) Hunker, A. C.; Wirthlin, M. E.; Gill, G.; Johansen, N. J.; Hooper, M.; Omstead, V.; Vargas, S.; Lerma, M. N.; Taskin, N.; Weed, N.; Laird, W. D.; Bishaw, Y. M.; Bendrick, J. L.; Gore, B. B.; Ben-Simon, Y.; Opitz-Araya, X.; Martinez, R. A.; Way, S. W.; Thyagarajan, B.; Otto, S.; Sanchez, R. E. A.; Alexander, J. R.; Amaya, A.; Amster, A.; Arbuckle, J.; Ayala, A.; Baker, P. M.; Barcelli, T.; Barta, S.; Bertagnolli, D.; Bielstein, C.; Bishwakarma, P.; Bowlus, J.; Boyer, G.; Brouner, K.; Casian, B.; Casper, T.; Chakka, A. B.; Chakrabarty, R.; Chong, P.; Clark, M.; Colbert, K.; Daniel, S.; Dawe, T.; Departee, M.; DiValentin, P.; Donadio, N. P.; Dotson, N. I.; Dwivedi, D.; Egdorf, T.; Fliss, T.; Gary, A.; Goldy, J.; Grasso, C.; Groce, E. L.; Gudsnuk, K.; Han, W.; Haradon, Z.; Hastings, S.; Helback, O.; Ho, W. V.; Huang, C.; Johnson, T.; Jones, D. L.; Juneau, Z.; Kenney, J.; Leibly, M.; Li, S.; Liang, E.; Loeffler, H.; Lusk, N. A.; Madigan, Z.; Malloy, J.; Malone, J.; McCue, R.; Melchor, J.; Mich, J. K.; Moosman, S.; Morin, E.; Naidoo, R.; Newman, D.; Ngo, K.; Nguyen, K.; Oster, A. L.; Ouellette, B.; Oyama, A. A.; Pena, N.; Pham, T.; Phillips, E.; Pom, C.; Potekhina, L.; Ransford, S.; Ray, P. L.; Reding, M.; Rette, D. F.; Reynoldson, C.; Rimorin, C.; Sigler, A. R.; Rocha, D. B.; Ronellenfitch, K.; Ruiz, A.; Sawyer, L.; Sevigny, J. P.; Shapovalova, N. V.; Shepard, N.; Shulga, L.; Soliman, S.; Staats, B.; Taormina, M. J.; Tieu, M.; Wang, Y.; Wilkes, J.; Wood, T.; Zhou, T.; Williford, A.; Dee, N.; Mollenkopf, T.; Ng, L.; Esposito, L.; Kalmbach, B. E.; Yao, S.; Ariza, J.; Collman, F.; Mufti, S.; Smith, K.; Waters, J.; Ersing, I.; Patrick, M.; Zeng, H.; Lein, E. S.; Kojima, Y.; Horwitz, G.; Owen, S. F.; Levi, B. P.; Daigle, T. L.; Tasic, B.; Bakken, T. E.; Ting, J. T. Enhancer AAV Toolbox for Accessing and Perturbing Striatal Cell Types and Circuits. *Neuron* **2025**, *113* (10), 1507-1524.e17. https://doi.org/10.1016/j.neuron.2025.04.035.